2018

Application Of Geophysical And Geochronological Methods To Sedimentologic And Stratigraphic Problems In The Lower Cambrian Monkton Formation: Northwestern Vermont

Henry C. Maguire
University of Vermont

APPLICATION OF GEOPHYSICAL AND GEOCHRONOLOGICAL METHODS TO SEDIMENTOLOGIC AND STRATIGRAPHIC PROBLEMS IN THE LOWER CAMBRIAN MONKTON FORMATION: NORTHWESTERN VERMONT

A Thesis Presented

by

Henry C. Maguire IV

to

The Faculty of the Graduate College

of

The University of Vermont

In Partial Fulfillment of the Requirements
for the Degree of Master of Science
Specializing in Geology

October, 2018

Defense Date: June 15, 2018
Thesis Examination Committee:

Charlotte J. Mehrtens, Ph.D., Advisor
Britt A. Holmén, Ph.D., Chairperson
Laura E. Webb, Ph.D.
Jon Kim, Ph.D.
Cynthia J. Forehand, Ph.D., Dean of the Graduate College

ABSTRACT

The Monkton Formation of the western shelf stratigraphic sequence in Vermont (VT) is identified as a Lower Cambrian regressive sandstone unit containing parasequences recording tidal flat progradation. Previous workers identified cycles believed to represent parasequences in a portion of a 1034' deep geothermal well drilled at Champlain College in Burlington, Vermont. For this study, both outcrop and well geophysical surveys were completed to better identify gamma emission curves and relative values for parasequences and select lithologies that are indicators of bathymetry and sea level. After using physical stratigraphic techniques to assemble a composite stratigraphic section for the Monkton Formation, analysis of the gamma emission curve and relative gamma values resulted in the identification and characterization of parasequences and select lithologies within the Monkton. Interpretation of bathymetry-sensitive lithologies along with parasequence architecture and thickness trends reveals three distinctive intervals over the thickness of the Monkton. It is recognized that the succession of these intervals represents an overall decreasing rate in accommodation space generation through Monkton deposition.

Previous workers have suggested that biostratigraphic relationships of the Monkton Formation to the Potsdam Group in New York (NY) suggest that that they would be at least partially correlative. To further refine age relationships and constrain and compare the provenance of the Vermont stratigraphy locally and regionally, zircon samples were collected from the Monkton and the overlying Danby Formations and radiometric age determinations were completed by laser ablation–inductively coupled plasma mass spectrometry (LA-ICPMS) at University of Arizona Laserchron Center. Zircon age probability distribution curves show two dominate age peaks between 1.05-1.09 Ga and 1.15-1.18 Ga for the Monkton and Danby suggesting either a continuity of provenance through the Cambrian or the cycling of the Monkton's sand. The 1.05-1.09 Ga age range corresponds to rocks generated during the Ottawan Orogeny while the 1.15-1.18 Ga range is associated with the Shawinigan Orogeny and anorthosite-mangerite-charnockite-granite (AMCG) plutonism. Dominant age peaks in the Vermont samples between 1.15-1.18 Ga are similar to the 1.16 Ga age peak reported by other workers from the Altona and Ausable Formations of the Potsdam Group of New York. The shared dominant age peak and close proximity of the Vermont and New York stratigraphy may suggest a primarily shared provenance.

ACKNOWLEDGMENTS

First and foremost, I would like to thank my Advisor Char Mehrtens. I really count myself lucky to have been able to work with you and cannot thank you enough for making this such a wonderful graduate experience. I am incredibly grateful for the guidance from my committee of Laura Webb, Jon Kim and Britt Holmén. I would like to thank a cast of people, including Edwin Romanowicz, Jeffrey Chiarenzelli, Dan Jones and Jody Smith, who were integral to the many aspects of this study. Finally, I would like to acknowledge the late Bruce Selleck, who so generously lent the geophysical equipment that was used in this study.

I would also like to thank my fellow graduate students, 2018 Philadelphia Eagles, cats, family, and friends for their help, motivation and support throughout this process.

TABLE OF CONTENTS

ACKNOWLEDGMENTS ..... **ii**
LIST OF TABLES ..... **v**
LIST OF FIGURES ..... **vi**
LIST OF APPENDICES ..... **viii**
CHAPTER 1: LITERATURE REVIEW **1**
1.1. Introduction 1
1.2. Geologic Setting 1
1.3 Sequence Stratigraphy 4
1.3.1. Background 4
1.3.2. Sea Level 6
1.3.3. Key Concepts in sequence stratigraphy 9
1.3.4. System Tracts 11
1.3.5. Parasequences 12
1.4. Vermont/New York Stratigraphic Relationships 13
1.5. Monkton Sedimentology/Stratigraphy 16
1.5.1 Cambrian Continental Shelves 16
1.5.2 Tide-Dominated Environments 18
1.5.3. Peritidal Carbonate Environments 19
1.5.3. Clastic Carbonate Mixing 20
1.5.4. Tidal Flat Progradation 21
CHAPTER 2: ZIRCON **25**
2.1. Introduction 25
2.2. Background 25
2.2.1 U-Pb Geochronology 25
2.2.2 Tectonic History 27
2.3. Methods 31
2.3.1. Detrital Zircon Sampling and Processing 31
2.3.2 Geochronological Data Processing 32
2.4. Results 33
2.5. Discussion 34

Summary 37
CHAPTER 3: ARTICLE FOR JOURNAL SUBMISSION..... 57
3.1. Abstract 57
3.2. Introduction 58
3.3. Geologic Setting 59
3.3. Monkton Formation 63
3.4. Survey Methods 66
3.4.1 Outcrop Survey 66
3.4.2 Well Survey 67
3.5. Data Processing Methods 70
3.5.1 Well Log Filtering 70
3.5.2. Outcrop Survey 71
3.5.3. Fleming Well 72
3.5.4 Champlain College Well 72
3.6. Results 73
3.7. Discussion 76
CHAPTER 3: BIBLIOGRAPHY 88
COMPREHENSIVE BIBLIOGRAPHY 92

LIST OF TABLES

CHAPTER 1: TABLES 54

Table 1.1: Summary of sea level cycles 54

CHAPTER 2: TABLES 55

Table 2.1: Results from Gehrels (2010a) AGE PICK 55

Table 2.2: Similarity results from Arizona Laserchron Center's OVERLAP-SIMILARITY PROGRAM 2010 56

CHAPTER 3: TABLES 87

Table 3.1: Summary of lithologies identified in outcrop and subsurface studies 87

LIST OF FIGURES

CHAPTER 1: FIGURES 39

Figure 1.1. Geologic overview map 39

Figure 1.2. Physiographic map 40

Figure 1.3. Generalized geological, structural and isopach map 41

Figure 1.4. Stratigraphic relationships 42

Figure 1.5. Paleogeographic reconstruction of the Laurentian Iapetus margin 43

Figure 1.6. Visual representation of shoreline depositional sequences 44

Figure 1.7. Summary of the three major parasequence stacking patterns 45

CHAPTER 2: FIGURES 46

Figure 2.1. Map of Grenville Province with major terranes 46

Figure 2.2. Generalized geologic map of the Adirondacks units 47

Figure 2.3. Simplified bedrock geologic map of Vermont showing 48

Figure 2.4. Normalized $^{206}Pb/^{207}Pb$ ages of detrital zircon age-relative probability distributions 49

Figure 2.5. U–Pb isotopic data 50

Figure 2.6. Post-ablation CL images 51

Figure 2.7. Potential source rocks of Grenville age 52

Figure 2.8. Detrital zircon population age group distributions of the Potsdam Group graph 53

CHAPTER 3: FIGURES 78

Figure 3.1. Stratigraphic columns and corresponding outcrop examples of Rahmanian's Type 1 and Type 2 parasequences 78

Figure 3.2. Outcrop photograph of lithofacies 79

Figure 3.3. Simplified bedrock geologic map of Vermont showing 80

Figure 3.4. Relationships between Monkton stratigraphic intervals from wells and outcrops 81

Figure 3.5. Expected relative gamma values for lithologies 82

Figure 3.6. Redstone Quarry stratigraphic column with outcrop survey gamma results 83

Figure 3.7. Interpretation of parasequence architecture through the composite Champlain and Fleming wells 85

Figure 3.8. Rate in sea level change curves for systems tracts model (A) and interpretation of sea level changes through Monkton deposition (B) 86

LIST OF APPENDICES

APPENDIX A: MONKTON U-Pb ANALYTICAL RESULTS 105
APPENDIX B: DANBY U-Pb ANALYTICAL RESULTS..... 117

CHAPTER 1: LITERATURE REVIEW

1.1. Introduction

The presence of meter-scale shallowing up cycles within the late Lower Cambrian Monkton Formation has been known for some time (Rahmanian, 1981). Though interpretations have been made about what these cycles mean in relationship to sea level, the lack of continuous outcrop make it difficult to identify larger scale trends in the formation. More recently, subsurface well-log data has allowed for the opportunity to investigate these larger scale trends. This chapter will address the topics essential in understanding the deposition of the Monkton Formation and how these cycles can be interpreted in light of the concepts of sequence stratigraphy. Topics that will be addressed include: (1) a geologic background on the formation of the shelf where the Monkton was deposited; (2) outline of key concepts in sequence stratigraphy needed to understand the cyclic deposition and how that relates to sea level ; (3) regional relationships between the Cambrian sedimentary sequences in Vermont and New York to understand previous work and interpretations and how they relate to the Monkton; and (4) specific information about the sedimentology and stratigraphy of the Monkton Formation.

1.2. Geologic Setting

Understanding the regional Precambrian tectonic history is useful when examining the sedimentary Monkton Formation of present day northwestern Vermont because the paleogeography established by Precambrian rifting constructed the basins in which these Cambrian units were deposited. Rift related basalts (e.g., Tibbit Hill Formation) were formed in modern Vermont and Southern Quebec at a triple junction

associated with the breakup of Rodina (Kumarapeli et al., 1989). Radiometric age determinations by Kumarapeli et al. (1989) of the Tibbit Hill Formation in northern Vermont (Figure 1.1) are between 615 and 554 Ma, dates which mark the formation of the Laurentian-Iapetus Ocean margin. More recent work by Li et al. (2013) integrates paleomagnetic, lithologic and geochronologic data to suggest that the breakup of Rodina was complete by 580 Ma.

Major paleogeographic features formed by rifting include the New York Promontory, Quebec Reentrant and the Ottawa-Bonnechere aulacogen (Figure 1.2). Two of the arms of the triple junction that rifted successfully formed Laurentian-Iapetus Ocean (Kumarapeli, 1981). Along this margin of Laurentia, northwest-striking transform faults offset northeast-striking rift segments including the (convex ocean-ward) New York Promontory and (convex land-ward) Quebec Reentrant features (Thomas, 1977). These two features are separated by a major transform fault named the Missisquoi Valley Transfer Zone (MVTZ) by Cherichetti et al. (1998). The failed third arm of the triple juncture forms the 55 km wide and 700 km long topographic low known as the Ottawa-Bonnechere aulacogen, extending northwest from Montreal to Sudbury (Kay, 1942; Kumarapeli, 1985; Kumarapeli, 1981). Kay (1942) recognized the extent of this northwest-trending feature by the identification of uniform trends in major faults and by its relationship to the Lake Ontario homocline, the northern border of the Allegheny synclinorium and block-faulted Madawaska Highlands of central Ontario.

The Ottawa Bonnechere-aulacogen, also referred to as the Ottawa Embayment in a stratigraphic study work Sanford and Arnott (2010), was host to a range of marginal-marine to marine sandstones and carbonates deposited during the Cambrian (Sanford, 2007; Sanford and Arnott, 2010). The Cambrian age Potsdam Group in New York is found primarily along the margin of the Ottawa Embayment and into the adjacent Montreal Basin (Figure 1.3). The Potsdam Group consists of, in ascending age, the Altona, Ausable and Keeseville Formations (Sanford and Arnott, 2010) (Figure 1.4). Brink (2015) interpreted the depositional environments of the Altona Formation and compared this unit to the Monkton Formation in Vermont. The paleogeographic depositional relationship along the Iapetus Margin between the Monkton and Altona is outlined in Figure 1.5. Brink's work will be discussed further in Chapter 2.

Along the Iapetus Ocean margin proper, a thermally subsiding, tectonically stable shelf formed following these rifting events (Bond, 1997). This Cambrian platform became the depositional setting for the Cambrian stratigraphic sequence in Western Vermont (Figure 1.4). The formations making up this Western Vermont Iapetus Shelf include, in ascending order, the Cheshire, Dunham, Monkton, Winooski and Danby Formations. These western shelf units are a sequence of alternating siliciclastic and carbonate deposits formed in a range of peritidal to shallow-subtidal environments (Dorsey and Stanley, 1983; Mehrtens et al., 1987; Rahmanian, 1981). However, as documented by Dorsey and Stanley (1983), the shelf passed along strike to the north into shale and breccia horizons that were deposited in the Franklin Basin (Shaw, 1958). The

Parker, Skeels Corners, Rugg Brook and Rockledge Formations represent these deposits (Mehrtens and Hadley, 1995; Mehrtens and Hillman, 1988).

The Cambrian sedimentary sequences in New York and Vermont have been affected by tectonic processes following deposition. Brink (2015) notes that much of the rift-related and post-rift sedimentary record in the Ottawa embayment has been deformed during later tectonic events; however, some stratigraphy in the aulacogen, such as the Potsdam Group, have remained relatively undeformed. The Cambrian stratigraphy in the Champlain Valley is also relatively undeformed even though it has been transported ~80 km to the west on the upper-plate of the Champlain Thrust (Stanley and Roy, 1987). Brink (2015) was able to make detailed sedimentological comparisons between the units deposited on the shelf and in the aulacogen because both were relatively undeformed.

1.3 Sequence Stratigraphy

1.3.1. Background

Palmer (1970) described the Cambrian stratigraphic sequence in western Vermont as alternating siliciclastic and carbonate deposits, observations that are best explained by concepts that form the basis of the field of sequence stratigraphy. Sequence stratigraphy is defined by Posamentier et al. (1988) as the study of rock relationships within a time-stratigraphic framework of repetitive, genetically related strata bounded by surfaces of erosion or no deposition, or their corelative conformities. Though sequence stratigraphy's origin is often associated with seismic stratigraphy of the 1970s, its beginnings can be traced back to previous work by Twenhofel (1939), Sloss (1949, 1963) and Fisher and

McGowen (1967). Their foundational work identified and described relationships between base level, sedimentation, unconformities and the depositional systems they were produced in (Catuneanu, 2002). The concept of base level, or the highest level which a sedimentary succession can be built, was first outlined by Twenhofel (1939) and later was described by Cross (1994) to represents the boundary between deposition and erosion. Sloss (1949) described a package of strata bound by unconformities as a "sequence" and went on (1963) to identify six sequences of Phanerozoic strata whose deposition was attributed to fluctuating sea level. These sequences form the depositional systems described by Fisher and McGowen (1967) as three-dimensional assemblages of lithofacies linked by depositional processes. The linkage between these depositional systems representing the subdivision of a sequence is termed a system tract by Brown and Fischer (1977).

Vail and his coworkers (1975 and 1977) authored seminal papers in the new field of seismic stratigraphy, but more importantly their work identified the driving force behind sequence formation. Using seismic data to identify unconformity-bound packages of strata in the subsurface of continental margins, these authors determined that regional unconformities were isochronous and the result of global eustatic processes occurring at different scales and frequencies. Later, Posamentier et al. (1988) and Van Wagoner et al. (1990) broadened the application and interpretation of sequence boundaries as chronostratigraphic surfaces, a revision which led to the beginning of modern sequence stratigraphy.

1.3.2. Sea Level

Changing sea level is often the driving process in sequence stratigraphy, so an understanding of how and why sea level changes is fundamental to the field. Changes in sea level can be broken into two types. Eustatic sea level changes are those that cause changes in the volume of the world oceans. Relative sea level changes are those that are observed with respect to a land-based reference frame or in other words land and ocean move relative to one another (Kemp et al., 2015; Miller et al., 2005). In a summary paper by Rovere et al. (2016), they suggested that, though these sea level changes are individual concepts, they not totally independent; a eustatic sea level rise can directly change relative sea level. Understanding the processes that change eustatic and relative sea level should help clarify their relationships.

According to Rovere and his coworkers (2016), tectono-, hydro- and glacio-eustasy are the primary processes effecting eustatic sea level. Tectono-eustasy affects the volume of the ocean basin itself. Wilson (1968) first described the cyclic tectonic movement resulting in the opening and closing of ocean basins, later to be termed "Wilson Cycles". The opening of an ocean basin occurs at mid-ocean ridges, where new oceanic crust is being formed and spreading apart. One might assume that the spreading and subsequent increasing of the volume of the basin would decrease eustatic sea level, however this is not always the case. The volume of the mid ocean ridges generated with sea floor spreading are considered a major factor in increasing eustatic sea level (Hays and Pitman III, 1973). The rate at which new crust is being formed at the mid ocean ridge and spreading versus the increase in the volume of the basin, are not always balanced. If

the new oceanic crust forming at the ridge outpaces the spreading rate (the ability to make the basin larger) then the new material displaces the water and there is a rise in eustatic sea level (Kominz, 2009). In contrast, if the opening of the basin is increasing volume at a greater rate than the mid-ocean ridge is filling it, there is a drop is eustatic sea level. In addition to new volcanic material filling into an oceanic basin, sediment deposition can also decrease volume. Eventually, plates will start to converge, the oceanic basin previously formed will close, decreasing basin volume, resulting in a eustatic sea level rise. A detailed description of the solid earth process in relation to sea level are summarized in Conrad (2013).

Rovere et al. (2016) describes glacio- and hydro-eustatic processes and their contribution to sea level. Glacio-eustasy describes the storage or release of water in glacial ice. If glacial ice is forming or melting then water will be removed or added to ocean volume, resulting in a decreasing or increasing eustatic sea level change respectively. Hydro-eustasy describes the effect on sea level when water is stored in snow, rivers, lakes and other reservoirs on a craton. The more water that is stored in these reservoirs, the lower the eustatic sea level.

In their summary, Rovere et al. (2016) also mention the climatic processes that affect ocean water volume. Increasing temperatures over geologic time will have a direct impact on water volume from thermal expansion. These authors explain that over 4 °C, heating causes greater molecule motion and expansion in water. These thermal changes can change the eustatic sea level in oceans with constant water and basin volume by

changing the water's density (Llovel et al., 2011). Rovere et al. (2016) suggested that over geologic time the amplitude, in terms of eustatic sea level change, from these thermal changes can be in the 10's of meters.

Processes that drive relative sea level change can be can be generally categorized into those related to isostatic responses, tectonics or mantle dynamics. Isostatic responses would include any process that would load a portion of the crust and create subsidence, but as a result, an isotropic response would result in uplift elsewhere. An example of this would be the formation of a volcano that would load the crust, causing subsidence and result in adjacent uplift (Moore, 1987). Glaciers can have the same effect when they are formed and the opposite response, uplift where the glacier was and proximal subsidence, when they melt and the load on the crust is removed (Farrell and Clark, 1976). Relative sea level can be impacted by tectonic forces along active margins (Dura et al., 2016). Vertical ground motion associated earthquake cycle tectonic deformation can occur resulting in the rise or fall of shoreline (Larsen et al., 2003). Tectonically driven uplift or subsidence, at a variety of frequencies and spatial scales, are considered one of the primary drivers of relative sea level changes (Rovere et al., 2016).

In addition to describing the processes that control sea level, the work of Rovere et al. (2016) also outlines the range in duration and scale of the processes that drive cycles in sea level change. Vail and Mitchum (1979) described the cyclic rise and fall of global sea level at varying magnitude and frequency through Phanerozoic time. A hierarchal system, assigning an order to sea level changes and associated processes, was

created by Mitchum and Van Wagoner (1990) to describe the variety in duration and scale. The hierarchal system from Mitchum and Van Wagoner (1990) is outlined in Table 1 and includes some of the commonly associated sea level processes and cycle orders. An understanding of the hierarchal system describing sea cycle is just the start of the terminology and background knowledge needed for the field of sequence stratigraphy.

1.3.3. Key Concepts in sequence stratigraphy

Catuneanu (2002) explains that the variable and wide range of "jargon" that cannot be standardized in sequence models can make understanding the field of sequence stratigraphy difficult. To reduce jargon, terms such as a "sequence" or "systems tract" are applied across a wide range of scales based on a hierarchal order. Additionally, there is still even disagreement, depending what model you use, in definitions as essential to the field as a "sequence". To better navigate the field of sequence stratigraphy some key components have been outlined or a comprehensive summary of this material can be found at the Society for Sedimentary Geology Strata (sepmstrata.org) or the University of Georgia (UGA) stratigraphy lab (strata.uga.edu) websites.

Many boundaries in sequence stratigraphy are identified by flooding surfaces. A flooding surface is a surface that separates younger from older strata across which there is evidence of an abrupt increase in water depth (Van Wagoner, 1995). Posamentier and Allen (1999) referred to the maximum flooding surface as the maximum landward position of shoreline deposition at the time of maximum transgression.

The cyclic nature of the rise and fall of eustatic sea level is also characteristic in variations of base level. Fluctuation in base level directly effects the space available for sediments to accumulate, a concept termed “accommodation” by Jervey (1988). Accommodation is eventually consumed by sedimentation, so base level and in turn accommodation must increase before deposition can continue. Catuneanu (2002) notes that analysis of these sedimentary responses to varying accommodation is a core component of sequence stratigraphy. The variation in water depth created by the balance between base level and sedimentation causes the shifts in facies more distally or proximally in relation to the shoreline.

Work by Plint (1988) and Posamentier et al. (1992) identifies three main facies shifts that are a result of sedimentation and base level relationships. The first of these occurs when accommodation, or base level rise, outpaces sedimentation and is referred to as a transgression. During a transgression the retrogradation or landward shift of the shoreline and facies occurs. A regression is characterized by the seaward shift of the shoreline and facies, or progradation. There are two types of regressions. A normal regression is determined by sediment supply and the ability for it to outpace base level rise. A forced regression occurs regardless of sediment supply or rate and is the result of base sea level fall. These processes occur directly with the cyclic nature of base level fluctuation and sedimentation rates and are outlined in Figure 1.6. Packages of these shifts and processes are described within system tracts, introduced by Brown and Fisher (1977) as a way to link sequences with depositional systems.

1.3.4. System Tracts

Brown and Fischer (1977) first introduced the term system tract to describe the relationship between sequences with depositional systems. Depositional systems are three dimensional assemblages of lithofacies that are linked by processes and environments and a system tract is the three-dimensional unit of deposition (Brown and Fischer, 1977). The specific stages of relative sea level and the associated stratigraphy of the system tracts were first described by Posamentier et al. (1988). The lowstand systems tract (LST) represents deposits that accumulate on the preceding sequence boundary after the onset of a relative sea-level rise. Following this, the transgressive systems tract (TST) records the onlapping deposits that accumulate from the onset of coastal transgression until the time of maximum flooding. Finally, the highstand systems tracts (HST) mark when sedimentation outpaces the increase in accommodation space, resulting in prograding deposits.

Further work has added and categorized additional systems tracts, including the identification of the regressive systems tract by Embry and Johannessen (1993). The regressive systems tract lies between two transgressive systems tracts and includes the sediments of the highstand system tract and/or the start of the lowstand systems tract, termed the early lowstand systems tract by Posamentier and Allen (1999). Additionally, Plint and Nummedal (2000) described the falling stage systems tract that includes all the regressive deposits that accumulated after the onset of a relative sea-level fall and before the start of the next relative sea-level rise.

1.3.5. Parasequences

Sequences that are part of a relatively conformable succession of genetically related beds or bedsets bound by a marine flooding surface are termed parasequences (Van Wagoner, 1995). Parasequence sets describe successions of these parasequences that form a distinctive stacking pattern (Van Wagoner et al., 1990). The cyclic sediment deposition creating these parasequences are commonly identified in core and well logs for correlation. Additionally, parasequence sets are used to define system tracts (Van Wagoner et al., 1988).

One to ten-meter thick shallowing upward cycles, representing a parasequence, are common in many stratigraphic sequences. In well data, parasequences are identified by their maximum flooding surface. Because sea level (bathymetry) is changing through their deposition and as a result current or wave energy level changes, typically in the cycle of sedimentation of a parasequence they either coarsen or fine upward. Geophysical gamma emission data picks up the abrupt change in grain size associated with the change in water depth, thus making the flooding surface an identifiable marker. However, depending on the range of facies and environments a parasequence represents, in particular mixed siliciclastic-carbonate facies and environments, this can become much more complicated.

Parasequences stacked on top of one another in stratigraphy occur in three patterns that describe the architecture, or vertical changes in facies within a parasequence: retrogradational, aggradational and progradational. These are

schematically illustrated in Figure 1.7. Retrogradational parasequence stacking represents the landward migration of successively younger parasequences, as deposition moves landward as rising sea level creates new accommodation space on the coastal plain. In progradational parasequences the vertical stacking of successively younger parasequences represents deposition further basinward as deposition outpaces the creation of accommodation space on the inner shelf. Aggradational parasequence stacking shows successively younger parasequences having no significant lateral shifts basinward or landward because deposition and accommodation space stay in balance.

Work by Posamentier and Vail (1988) applied trends in parasequence thickness to make interpretations that characterized the sedimentation and accommodation in a depositional sequence. In their work, they proposed that upward-thickening parasequences would characterize deposition in a lowstand prograding wedge and parasequences deposited in highstand prograding wedges would be upward-thinning. These patterns occur because of accelerating and decelerating relative sea level rise. However, these interpretations can become more complex when varying sedimentation rate is incorporated. For example, if there is ample accommodation space, but no sediment being deposited, then the upward-thickening may not be seen.

1.4. Vermont/New York Stratigraphic Relationships

A summary of the biostratigraphic relationships between the New York, Vermont Shelf and Vermont Basin units are summarized in (Figure 1.4). *Ptychoparia adamsi* and *Ollenellus* zone trilobites are present in the Monkton Formation, which places this unit's age as Lower Cambrian (Schuchert, 1933, 1937). The underlying Dunham Dolostone

contains *Salterella conulata*, a Lower Cambrian index fossil (Mehrtens and Gregory, 1984) correlative with the lower *Olenellus* trilobite zone. The basal horizons of the Parker Slate, a fine-grained unit deposited in the Franklin Basin, also contain Lower Cambrian age *Ollenellus* zone trilobites (Palmer, 1970; Shaw, 1958), indicating that the Monkton and part of the Parker are correlative. However, upper horizons of the Parker contain trilobites of the *Bolaspidella* zone of Middle Cambrian age (Palmer and James, 1980). These authors interpret the five missing trilobite zones between *Olenellus* and *Bolaspidella* to record an unconformity within the basin stratigraphy. Unconformities at this same time are also present in other Cambrian units along the Iapetus margin in the Appalachians. Palmer and James (1980) suggested that this basin-wide event be termed the Hawke Bay Event. It is therefore not clear whether the entire Monkton is Lower Cambrian in age or if it extends into the Middle Cambrian. The overlying Winooski Dolostone is dated as Middle Cambrian only based on interbedding with the younger trilobite-bearing Parker Slates.

In New York the biostratigraphic data constrains the basal unit of the Potsdam Group, the Altona Formation, as latest Lower Cambrian (*Olenellus* zone) to middle Middle Cambrian (*Bathyuriscus-Erathina* zone) in age. This is based on the identification of fragments of an *Olenellid* trilobite by Landing et al. (2009) which indicate a Lower Cambrian age. Landing also retrieved fragments of *Ehmaniella* from the upper half of the formation, indicating a Middle Cambrian age for the top of the Altona. Because the Altona and Monkton Formations both contain *Olenellid*-zone assemblages this makes them at least partially coeval. The presence of the *Crepicephalus* Zone trilobites in the

overlying lowest Keeseville Formation of the Potsdam Group bracket the upper age of the Ausable to Middle Cambrian (Landing, 2007).

Constraining the ages of this Vermont and New York stratigraphy to the Lower and Middle Cambrian allows us to identify that these sedimentary units were deposited during an overall transgressive period at the base of the Lower Paleozoic which Sloss (1949) called the Sauk Sequence. This sequence describes a high-order eustatic rise that resulted in the drowning of the Laurentian margin and craton that is traceable across North America. This sequence includes strata between an interregional late Pre-Cambrian conformity and an interregional unconformity at the base of the succeeding Tippecanoe Sequence, or ages from latest Precambrian to Early Ordovician (James et al., 1987; Sloss, 1963).

Few authors have made interpretations of sea level fluctuation within the Sauk transgression in the Northern Appalachians. As discussed above, Palmer and James (1980) identified late Lower Cambrian regressive sandstones based on trilobite fauna that they believed to be associated with a more localized regressive event unrelated to the late Sauk Sequence of Sloss (1963). Landing et al. (1992) suggested that the fluctuating sea levels influenced basin aerobic and anaerobic cycles on the continental slope, which are reflected in the varying coloration of shale units. They used these cycles in shale color to determine that two deepening cycles are recorded in the late Early Cambrian deep water deposits. Based on the presence of a shale and dolostone interval within the Altona Formation sandstones, Brink (2015) interpreted that this portion of the Altona

stratigraphy represented deposition during sea level highstand. He suggested that the portion of the Altona stratigraphy associated with highstand conditions may represents a condensed sequence that is correlative to the post-Monkton (Winooski Dolostone) strata in Vermont.

1.5. Monkton Sedimentology/Stratigraphy

The Monkton Formation is a greater than 300 m thick heterolithic unit comprised of sand, silt and dolostone (Cady, 1945). Rahmanian (1981) first helped to characterize this mixed siliciclastic-carbonate unit by identifying facies recording supratidal, intertidal and shallow subtidal deposition with repeating shallowing up cycles or parasequences. Both Rahmanian and Speyer (1983) interpreted the parasequences to represent tidal flat progradation.

The Monkton was included in Palmer and James (1980) identification of regressive sand units along the Appalachian margin following the Hawke Bay Event and is also confirmed in the work of Rahmanian (1981). Work by Goldberg and Mehrtens (1998) recognized a facies in the lower Monkton representing a non-marine fluvial environment. The presence of fluvial facies in the lower Monkton was attributed by these authors to localized tectonic uplift, an interpretation not seen in by Palmer and James (1980) in coeval stratigraphy elsewhere along the Iapetus Margin.

1.5.1 Cambrian Continental Shelves

The shallow-marine shelf setting was unique during the Cambrian for a variety of reasons. The lack of land-based plants at this time meant the craton was dominated by

subaerial dune fields and braided fluvial environments (Cant and Hein, 1986; Dalrymple et al., 1985; Simpson and Eriksson, 1990). The predominance of eolian processes ensured that much of the sediment deposited on the shelf from the interior of the continent was compositionally mature (Dalrymple et al., 1985). Sloss (1963) identified that sediment deposited on the Iapetus shelf margin, now the eastern half of North America, from latest Precambrian to Early Ordovician, was composed predominantly of quartz-rich sandstone, limestone, and dolostone. Dalrymple et al. (1985) attributed the limited presence of silt and clay in these strata to the preferential large- scale sediment distribution by paleo-trade winds to the southern and western United States and southwestern Canada. Lowe (2016) notes that fluvial units within the Potsdam Group also recorded unique sedimentation from the lack of stabilizing vegetation.

The global sea level rise that followed the breakup of Rodina in the late Precambrian created accommodation space on the newly formed thermally subsiding Iapetus continental margin. High sedimentation rates at this transgressive time are attributed to fluvial systems that transported large amounts of siliciclastic sediment from the craton to the shelf (Durbano et al., 2015). The Cambrian shelf on the Iapetus Ocean margin, characterized by a lack of fine grained material, high sedimentation rates and ample accommodation space, generated mixed siliciclastic-carbonate facies indicating tidal and storm processing (Desjardins et al., 2012).

1.5.2 Tide-Dominated Environments

Though there is evidence of storm and wave processes found in the Monkton, the dominant depositional processes are tidally influenced. This interpretation is based on the presence of mud cracks, suggesting that sedimentary structures were formed from tidally generated currents and waves. Also present in the Monkton are features that are characteristic of, but not limited to, tidally-influenced deposition such as combined flow ripples and bipolar flow directions (Reineck and Singh, 1975). The geometry of continental shelves can often amplify the processes that affect these tidal systems (Clarke and Battisti, 1981). A tidal system is any depositional setting that is affected by a periodic fluctuation in sea level generated by gravitational forces from the sun or moon (Dalrymple, 1992). A range of environments including tidal flats, deltas, estuaries and shelves are often characterized by these tidal processes. The tidal range and the tidal current strength are more influential than geomorphological setting in producing a range of sedimentary structures (Dalrymple, 1992; Hayes, 1975).

Dalrymple (1992) notes the two common environments in tidal systems are (1) tidal flats on the fringes of shorelines; (2) offshore tidal sand ridges and bars. The Monkton is an example of a sand and silt dominated tidal flat, however it does have facies present representing the tidal sand ridges and bars. Sedimentary structures include mud cracks, herringbone cross stratification and flaser bedding (Brink, 2015). Mud cracks found in finer-grained terrigenous material form during subaerial exposure in a supratidal setting (Reineck and Singh, 1975). Flaser bedding commonly forms in intertidal settings where the tides create a rhythmic interbedding from back and forth mud deposition and ripple

migration (Dalrymple et al., 1991). Subtidal sands in the Monkton contain decimeter scale cross stratification, medium to coarse sand grain size and moderate sorting. The presence of a cryptalgal laminated dolostone lithology is additional evidence of a peritidal setting as this lithology indicates episodic sedimentation within the photic zone. All these features suggest that the Monkton was deposited on a tidally-influenced shallow marine shelf. The abundance of dolostone and arenaceous dolostone in the Monkton warrants a review of both peritidal carbonate and mixed siliciclastic and carbonate environments, both of which can contain varying siliciclastic/carbonate composition.

1.5.3. Peritidal Carbonate Environments

While mudcracks are the best evidence for subaerial exposure they are not ubiquitous in the Monkton Formation and many features, such as bipolar flow directions, can be associated with tidal deposition but perhaps not attributed to a particular supra- inter- or sub-tidal setting. The term peritidal describes the range of nearshore and shoreline environments that are around or near tidal influence (Folk, 1973). Peritidal carbonate environments have many of the same characteristics created from the tidal process in siliciclastic environments as outlined by Dalrymple (1992). This includes the three bathymetric zones, (subtidal, intertidal and supratidal) and the equivalent set of sedimentary structures. However, in mixed environments containing both carbonate and siliciclastic sediment, the deposition and re-deposition of carbonate material in multiple bathymetric zone adds to the complexity.

James (1992) describes two common ways carbonate material can be generated in the subtidal zone in what is termed the “carbonate factory”. Schlager (2005) defines the carbonate factory as the sea floor lying within the photic zone, where carbonate sediment particles are generated. The first way carbonate sediment form is from the crystallization of skeletal remains (biomineralization and cementation) and the second way is through the precipitation of carbonates directly from seawater. Because of its impact on water clarity and sunlight penetration, one of the primary regulators of carbonate production in the carbonate factory is siliciclastic input. If turbidity is high, carbonate productivity is diminished. However, a unique biogenic sedimentary structure can be formed when some siliciclastic sediment is mechanically trapped and bound on organic films of cyanobacterial algal mats in the intertidal and supratidal environment (Rouchy and Monty, 1981). The back and forth of the deposition of thin layers of sediment to the formation of the algal mats on top helps creates a structure termed cryptalgal laminates (Pratt, 1976). The sensitive and specific generation of carbonate material interlayered with thin laminations of terrigenous sediment make cryptalgal laminates excellent paleobathymetric indicators in tidal environments (Pratt et al., 1992). Facies that are not completely carbonate or clastic and somehow to generate a compositional range of textures within the rocks.

1.5.3. Clastic Carbonate Mixing

Because conditions that lead to carbonate productivity are inhibited by siliciclastic input, it is difficult to explain how both lithologies occur together. This issue was addressed by Mount (1984) who described the genesis of facies comprised of sediments

with textural mixtures of carbonate and siliciclastic material in shallow shelf environments. Mount suggested that mixing could occur in 4 ways: 1) punctuated mixing; 2) facies mixing, 3) *in situ* mixing and 4) source mixing. Punctuated mixing represents the transfer of sediment between contrasting depositional environments during rare, high intensity sediment input such as a fluvial discharge event. Facies mixing occurs along diffuse borders between contrasting facies that contain siliciclastic and carbonate material respectively. *In situ* mixing describes the generation of carbonate material autochthonously within siliciclastic sediments. Finally, when carbonate terranes are eroded or uplifted, admixtures of detrital clastic carbonates and siliciclastics and are deposited in what Mount (1984) calls source mixing.

The Monkton contains examples of the punctuated facies and *in situ* mixing processes described by Mount (1984). Punctuated mixing is seen in the Monkton in event beds where terrigenous material is rapidly deposited on the tidal flat, producing interstratified and mixed terrigenous and carbonate lithologies. Facies mixing occurs in the Monkton along the interface between nearshore siliciclastic tidal flat facies and offshore carbonates. *In situ* mixing of the autochthonous generated carbonate within siliciclastic environments, representing mixing in place, is seen in the cryptalgal laminate dolostone.

1.5.4. Tidal Flat Progradation

Progradation of the tidal flat is recorded by the succession of shallowing-upward cycles or parasequences. A complete parasequence in a peritidal carbonate environment

would include a basal subtidal, intermediate intertidal and upper supratidal facies potentially with a terrestrial cap (James, 1984). Pratt et al. (1992) notes that finding a complete shallowing succession can be difficult because of erosion and non-deposition variability. Rahmanian (1981) recognized the shallowing upward cycles in the Monkton which he interpreted as recording tidal flat progradation. He identified cross-bedded sandstones overlain by rippled shale-draped sandstones capped by dolostones, as representing a succession of subtidal to peritidal environments produced by tidal flat progradation. Rahmanian (1981) noticed that the number of these cycles diminished down depositional dip as the tidal flat passed basinward into the subtidal environment.

For cyclic deposition to occur, accommodation space must be made for the successive parasequences to form. This can happen because of external processes, such as sea level change, in which case the driving mechanism is termed allocyclic, or internal processes related to lateral facies migration, termed autocyclic processes. An example of autocyclicity is the production of fining-upwards sequences from fluvial channel migration. Beerbower (1964) suggested that autocyclic processes must occur within the sedimentary system and their effects tend to be local and, in geologic terms, instantaneous. They are described as aperiodic because they generally occur randomly in time and space (Cecil, 2003). Einsele et al. (1991) also suggested that beds in autocyclic sequences often have limited lateral continuity. Allocyclic processes are driven by tectonic activity, climate change and eustasy and others factors external to the sedimentary systems. Cecil (2003) notes that allocyclic change often directly affects autocyclic processes.

Autocyclic and allocyclic processes must both be considered when interpreting the shallowing upward sequences of the Monkton. There are two primary models for autocyclic processes on tidal flats. Ginsburg's (1971) model describes, under continuous subsidence and stable sea level, the generation of material in the subtidal carbonate factory that is transported landward. The carbonate factory can produce and then deposit enough material such that the tidal flat progrades, however, at some point, carbonate production rates will decrease allowing for subsidence to create more accommodation space, allowing the next cycle to form. The second autocyclic model known as the "tidal flat island model" is described by Pratt and James (1986) and explains the lateral migration of subtidal areas and channels in peritidal environments to create aperiodic and random parasequences.

Both of the autocyclic models fall short in describing the repeating parasequences seen in the Monkton Formation. Ginsburg's (1971) model would be difficult to apply to the Monkton because of variable siliciclastic sedimentation input. The shutting off of the carbonate factory, in the model, is attributed to the progradation of the tidal flat that is comprised of the previously generated carbonate sediment. However, siliciclastic input would also disrupt the carbonate factory, making Ginsburg's model difficult to apply directly to the Monkton. Channel avulsion and sand bar migration, examples of lateral facies migration characteristic of the tidal flat model, are present in the Monkton stratigraphy, but these are not the lithofacies that comprise parasequences in this unit. The cycles representing tidal flat progradation in the Monkton are repeating and periodic over hundreds of meters of stratigraphy, which based on the work of Beerbower (1964)

and Einsele et al. (1991) would be less indicative of autocyclic processes. For this reason, the cycles identified by Rahmanian (1981) are attributed to allocyclic processes. Interpretations can be made about sea level change in the Monkton by identifying trends in parasequence architecture and thickness.

CHAPTER 2: ZIRCON

2.1. Introduction

This chapter addresses the geochronologic work done on the Monkton and Danby Formations of the Cambrian shelf stratigraphic sequence in Western Vermont (VT). Biostratigraphic relationships of the Monkton Formation to the Potsdam Group in New York (NY) by previous workers suggest these units would be at least partially correlative (Landing et al., 2009). Detrital zircon studies have been completed on the Potsdam Group by Chiarenzelli et al. (2010), Montario and Garver (2009) and Lowe (2016) to identify and help constrain the age and provenance of this stratigraphy. This study was the first detrital zircon study of Cambrian stratigraphy in the Champlain Valley of Vermont (VT) and helped constrain the provenance of this stratigraphy and helped to better correlate it with the Cambrian strata of NY.

2.2. Background

2.2.1 U-Pb Geochronology

The use of radiometric age determinations in geology can be traced back to Bertram Boltwood and Ernest Rutherford who, prior to suggesting its use in dating rocks, had been investigating the concept of radioactive series. Boltwood (1907) and Rutherford and Boltwood (1906) recognized that Pb was one of the final products of U decay. They looked at the ratio of Pb and U concentrations in rock samples taken from strata of known relative ages and the data showed an increase in this ratio in older rocks (Badash, 1968). Their continued work with lead/uranium ratios was used to estimate an age of ~ 2.2 Ga in samples, which, at the time, was five times greater than any previous estimate for the age

of the Earth itself. This age was a major overestimation— (the true age of this sample is now known to be ~500 Ma)—because Boltwood attributed lead in the sample to be due only to the uranium decay series, however this study was the inception of what would become one of the most significant analytical methods in geology (Badash, 1968).

In modern geochronology the U-Pb, or more precisely the U-Th-Pb, system has been identified as the independent radioactive decay system from parent to daughter isotopes of $^{238}U \rightarrow ^{206}Pb$, $^{235}U \rightarrow ^{207}Pb$, and $^{232}Th \rightarrow ^{204}Pb$ with half-lives 4.47 Ga, 0.70 Ga and 14.01 Ga, respectively (Gehrels, 2014). In these systems, the parent isotopes do not directly decay to the stable daughters, but a series alpha and beta decays create intermediate daughter isotopes before ending up at the stable Pb daughter isotope (Schoene, 2014). The $^{232}Th \rightarrow ^{204}Pb$ system is of less use in zircon studies because of lower Th concentration in zircons and the potential for decoupling between the Pb/Th and Pb/U systems. Work by Hiess et al. (2012) in identifying a constant $^{238}U/^{235}U$ value of 137.82 allows us to calculate radiometric age based on the $^{206}Pb/^{207}Pb$ measurements. $^{206}Pb/^{207}Pb$ radiometric determinations are primarily used when looking at ages > ~1.0 Ga because of the low, ~1-2% (at 2-sigma level), uncertainty in age (Gehrels et al., 2006).

The widespread existence of detrital zircons in sedimentary systems provides an ideal target for U-Pb analysis. Additionally, advancement in analytic methods, especially Laser-Ablation Multicollector Inductively Coupled Plasma Mass Spectrometry (LA-MC-ICPMS), allows for rapid determination of U-Th-Pb ages at relatively low cost compared to other methods (Gehrels et al., 2006). For these reasons there is an ever-greater capacity to generate statistically robust large (e.g., >100 analyses) geochronological

datasets (Pullen et al., 2014). These detrital datasets can be used for many interpretations including reconstructing provenance, characterizing a sedimentary unit, establishing stratigraphic correlation. and characterizing different aspects of source regions (Gehrels, 2014; Lowe et al., 2018).

In detrital zircon studies, several factors need to be accounted for to be able to make robust and accurate interpretations of provenance. An understanding of potentially where and how the initial crystallization of zircons occurred is essential. This will help in interpretations about sediment transport and deposition, and identification of zircons from terranes with distinct morphologies. Additionally, the likelihood of multiple episodes of zircon growth and recrystallization within a single grain of zircon from metamorphic or magmatic events must be taken into consideration. Therefore, looking at a regional tectonic history from the time of zircon inception to the time of deposition, and post deposition, is critical.

2.2.2 Tectonic History

Detrital zircon age distributions of the Lower-Middle Cambrian Potsdam Group stratigraphy from northern New York and southern Quebec and Ontario by Montario and Garver (2009), Chiarenzelli et al. (2010b), and Lowe (2016) have shown a majority of age determinations to fall between 1350 to 1000 Ma. These dates indicate a Grenville orogenic cycle-related source (McLelland et al., 1996). Grenville terranes (Figure 2.1) associated with this study stretch hundreds of kilometers from the Adirondack Highland in northern New York to the Central Gneiss belt in southern Ontario. The Adirondack Mountains are geologically divided into the Central Highlands and the Northwest

Lowlands. The Central Highlands consist mostly of metaplutonic rocks and the Northwest Lowlands mostly of metasedimentary and metavolcanic separated by the Carthage-Colton Mylonite Zone (Isachen et al., 1991). The Frontenac arch connects this southern extension of the Grenville Province (Adirondack Mountains) with the rest of the Grenville terranes (McLelland et al., 1996) (Figure 2.1).

Major regionally relevant tectonic and magmatic events occurring during the Grenville time period include the Elzevirian Orogeny (1245-1220 Ma), Shawinigan Orogeny (1190-1140 Ma), magmatic intrusion of the anorthosite-mangerite-charnockite-granite (AMCG) suite (1150-1140 Ma), the ca. 1106-1093 Hawkeye Granite Event and the Ottawan orogeny (1090-1030 Ma) (McLelland et al., 2010; McLennan et al., 2001). In the previously mentioned detrital studies, there are several minor U-Pb age peaks (<20% of grains) occurring at ~1.35 to 1.42 Ga, ~1.7 Ga and ~2.7 Ga. These minor age modes represent a province that had zircon growth associated with the Elzevirian Arc (pre-collision), the Yavapai and Mazatzal accretionary orogens, and mid-continent Superior terranes respectively (Karlstrom et al., 2001; Lowe, 2016; Montario and Garver, 2009).

The start of the Grenville orogenic cycle is marked by Elzevirian Arc colliding with Laurentia (McLelland et al., 1996). The Late Paleoproterozoic to Mesoproterzoic Elzevirian Arc terrane, that formed on southwestern Laurentia, is described by Rivers (1997) to have formed in calc-alkaline arc/back-arc tectonic environment. This back-arc formed from the divergence of the Adirondis Block (Gower, 1996) from Laurentia. Failed rifting within this back-arc setting created a basin in which sediments that

eventually make up the Central Metasedimentary Belt (CMB) were deposited (Dickin and McNutt, 2007). Convergence of the arc terranes with Laurentia marks the start of the Elzevirian orogeny (1245-1220 Ma). Thrusting to the northwest of the CMB along the Central Metasedimentary Belt Thrust Zone (CMBTZ) occurred at (1190-1140 Ma) and (1090-1030 Ma). These events record the Shawinigan and Ottawan orogenies, respectively (McLelland et al., 2010; Rivers et al., 2002). McLelland and colleagues (2010) and Platt and England (1994) suggest that the Shawinigan orogeny was driven by the contractional uplift caused by delamination of the lithosphere where the Ottawan was a result of collision between Amazonia and Laurentia.

Additional magmatic events are thought to have occured in the time between some of these major Grenvillian-aged orogenies. Radiometric age determinations by McLelland and Chiarenzelli (1990) and Silver (1968) identified peaks between 1150 to 1145 Ma, approximately 40 My after the Elzevirian Orogeny ended. These ages record the intrusion of the AMGC into the country rock (McLelland et al., 2004; Montario and Garver, 2009). Additionally, approximately 60 My after the AMGC intruded, the Hawkeye Granite Event (1106-1093 Ma) occurred, resulting in the Hawkeye granite suite that is found only within the Adirondacks (Figure 2.2) (McLelland et al., 2004).

In addition to understanding the tectonic context for zircon generation, the tectonothermal history during and after zircon crystallization needs to be understood when interpreting provenance from U-Pb age determination data. It is estimated that during the Grenville orogenic cycle (1350-1000 Ma) present day Adirondack rocks saw minimum peak temperatures of 790^{o}C and pressures between 7-9 kbar (Storm and Spear,

2005). Work by Heizler and Harrison (1998) on $^{40}Ar/^{39}Ar$ data from hornblende and $^{40}Ar/^{39}Ar$ diffusion data of potassium feldspar identifies cooling temperatures of Adirondack rocks of approximately 450-550ºC around 900-950 Ma. These data help constrain the post-Grenville cooling thermal history subsequent to peak pressure and temperature. High-resolution step-heating data of K-feldspars was used by Heizler and Harrison (1998) to identify that the western Adirondacks had cooled below 350 ºC by approximately 800-900 Ma while the eastern region did not cool until 100 to 200 million years later (~700 Ma). The samples from the eastern Adirondacks were collected on the unconformity, they identified as ~520 Ma (Lower Cambrian), between the Grenville basement rock and Potsdam Group sandstones, indicating that by this time these Grenville rocks were at or near surface temperature (Heizler and Harrison, 1998). Between the time of the Grenville Orogeny and the deposition of the Cambrian sediments, two widespread thermal events associated with the Iapetus margin rifting at ~approximately 750 Ma and ~588-544 Ma occurred (Aleinikoff et al., 1995). Major thermal events that occurred following deposition at ~450, ~360 and ~300 Ma are believed to be associated with the Taconic, Acadian and Alleghenian orogenies, respectively (Montario and Garver, 2009). Thermal events can cause re-recrystallization, metamorphism and growth in zircon grains that may be identified in geochronologic data. It should be noted that work by Roden-Tice et al. (2000) recognized a regionally variable unroofing history in samples of the Potsdam Group. Their work resulted in apatite fission track ages for two Potsdam samples from north of the Adirondack Mountains yielding ages of ~125 and ~143 Ma, whereas their sample from the southeast had a much younger

age of ~92 Ma. It was identified from the significantly younger age to the southeast that unroofing occurred later here. Fission-track dating by Montario and Garver (2009) in samples from the Potsdam Group did not produce any ages younger than Potsdam deposition, indicating that insufficient post-depositional heating occurred to reset zircon fission tracks.

2.3. Methods

2.3.1. Detrital Zircon Sampling and Processing

Thin sections from previous petrographic studies were used to determine the location for bulk sampling of zircon-bearing sandstone for U-Pb geochronology in the Monkton and Danby Formations. Samples of the Monkton Formation were collected at Redstone Quarry in Burlington, VT within sandstone horizons on the eastern and north wall, while sandstone in the Danby was sampled at Shelburne Falls in Shelburne, VT on a bedding plane just north of the bridge (Figure 2.3). An aggregate amount of approximately 15 kg was sampled from each unit. Samples were then disaggregated using a jaw crusher and plate grinder and then sieved to a sieve fraction of <250 μm. Hydraulic gravity separation was completed using a Gemini table. The final steps performed at the University of Vermont were to isolate the nonmagnetic zircon via magnetic separation using both a hand magnet and Frantz Isodynamic Magnetic Separator. The samples where then sent to the University of Arizona Laserchron Center to undergo heavy liquid separation with methylene iodide and to be mounted in epoxy.

U-Pb age determination of the detrital zircon grains was done by Dr. Jeffrey Chiarenzelli (St Lawrence University) by LA-ICPMS at University of Arizona

Laserchron Center. Backscattered Electron (BSE) imaging for both samples was done to identify zircons for analysis within the mounts. LA-ICPMS analysis of 279 spots were completed for the Monkton and 298 for the Danby. Gehrels and Pecha (2014), Gehrels et al. (2006), Gehrels et al. (2008) and Lowe et al. (2018) contain details of the Arizona lab methodology.

Following LA-ICPMS analysis, cathodoluminescence (CL) imaging of the mounted Danby and Monkton zircon populations was done on the SEM at Middlebury College in order to understand the context of sampling sites within zircons and to identify the different zircon morphologies present in the samples.

2.3.2 Geochronological Data Processing

Detrital zircon results were processed using a series of Excel routine programs for data reduction and age picking. As recommended by Gehrels (2012), in-house Excel routine (E2agecalc; Gehrels et al., 2008) was used to reduce, pick and filter ages with >10% discordance from the (LA-ICPMS). Gehrels (2010b) Normalized Age Probability Plot Excel add-on was used to plot relative age probability distributions with minimum and maximum uncertainty values set to 1% and 10%, respectively, and ages with >10% discordance excluded (Figure 2.4). In order to gain quantitative measure of clustering, major and minor modes for the detrital data were determined using the Gehrels (2010) AGE PICK Excel add-on, which calculates the weighted mean age, uncertainty, and mean square weighted deviation (MSWD) of the data (Table 1).

2.4. Results

Peak $^{206}Pb/^{207}Pb$ detrital zircon age results of detrital zircon geochronology are summarized in Table 1. The Monkton and Danby Formations yielded major peak ages (>20% grains) of approximately 1.05-1.09 Ga and approximately 1.15-1.17 Ga, respectively. Additionally, minor peak ages (5-20% grains) were identified in the Monkton at approximately 1.393 Ga and in the Danby at approximately 1.35 Ga and 1.42 Ga. These peaks can be seen on the normalized $^{206}Pb/^{207}Pb$ ages of detrital zircon age-relative probability distributions showing are seen in Figure 2.4.

Examination of Table 2 shows that zircon age probability distribution results for both Vermont units were almost identical, having an overlap similarity correlation coefficient of 0.936. Overlap similarity correlation coefficients were calculated of 0.874 and 0.868 when comparing the Monkton to the Altona and the Danby to the Ausable, respectively. These coefficients show that the Vermont and the New York provenance statistically are highly similar and that within the Vermont sequence they are close to the same.

U/Th plots (Figure 2.5) help us to identify the igneous petrogenesis. Lower U/Th values, less than 5, are usually associated with crystallization from a melt while values higher than 10 are generally associated with metamorphic zircons (Rubatto, 2002; Rubatto et al., 2001; Williams, 2001). It should be noted that these values are not absolute, but rather a general reference and values in between the two may indicate the presence of metamorphic fluids. It can be seen in Figure 2.5 that the Monkton and Danby formations both have samples that would fall into this range of metamorphic zircon U/Th

values. The Altona Formation yields two samples falling into this U/Th >10 metamorphic range and 1-1.15 Ma age. Most of these metamorphic zircon ages span the range of 1-1.15 Ma associated with the Ottawan and Shawinigan Orogenies.

Identification of zircon characteristics, which can tell us about the genesis and history of the grain, was done in reference to the zircon atlas by Corfu et al. (2003) and by comparison with more local zircons described by Lowe et al. (2018). Detrital grains ranged in size from ~30–400 μm and were primarily rounded to subrounded, but subhedral grains were present (Figure 2.6). It should be noted that grains greater than the sieve size can make it through a sieve mesh if it has an elongated shape. Many of the grains were fragmented, making detailed characterization difficult (Figure 2.6). However, most of the LA-ICPMS ablation pits were identified as being in grain cores. The core of the zircon would best preserve the chemical characteristics of the rock in which it was originally crystallized. The detrital zircon population that Lowe and colleagues (2018) studied from the Altona and Ausable Formations were found to have a higher number of euhedral and subhedral grains than seen in the Vermont population. The significance of this is unclear but might be related to the influence of depositional processes on the textural maturity of the sand.

2.5. Discussion

The Monkton and Danby Formations yielded peak ages approximately 1.05-1.09 Ga and 1.15-1.17 Ga, respectively, (Figure 2.4) indicating a Grenville-age provenance. Zircon age probability distribution results for both Vermont units were highly related, having an overlap similarity correlation coefficient of 0.936 (Table 2.2). There are two

possible explanations for similar geochronological ages for two units whose biostratigraphy suggests that one (Monkton) is significantly older (Late Lower Cambrian) than the other (Danby, Upper Cambrian). The Monkton sandstones could have been recycled and redeposited into the Danby. It is equally plausible that the Danby was sourced from the same Grenville rocks as the Monkton. Both possibilities suggest no major changes in provenance through the Cambrian. In addition to the major age peaks seen in the samples from Vermont a number greater than Grenville age minor age peaks are identifiable in Figure 2.4. Though not the dominant provenance for the Vermont stratigraphy, these minor peaks represent and older provenance from further within the craton that's sediment was deposited out onto the shelf.

In their studies of the zircon ages of the Potsdam Group in northern New York and adjacent Quebec and Ontario, Lowe (2016) and Chiarenzelli et al. (2010) produced detrital data that shows significant variation in age modes and more variation than seen in the Vermont population (Figures 2.4 and 2.8). This variation can be primarily attributed to basin constraints and position within the Ottawa-Bonnechere Graben depositional age. The samples most comparable in age to the Vermont stratigraphy are those analyzed by Chiarenzelli et al. (2010) from Altona and Ausable Formation sampled near West Chazy, N.Y. (Just north of Plattsburgh, N.Y.) in the most easterly portion of the outcrop belt (Figure 1.3). These Altona and Ausable zircons have a unimodally distributed single peak age of approximately 1.16 Ga. Though these samples are statistically very similar to the Vermont samples (Table 2.2), they do not contain any of the minor age modes seen in the Monkton and Danby. Additionally, other samples of the Potsdam Group from locations

further north and west in the Ottawa-Bonnechere Graben contained more complex age distributions. The lack of complexity in the ages was attributed by Lowe, et al. (2018) to the opening of fault-bounded sub-basins during the early to middle Cambrian that derived sediment primarily from adjacent terranes (Figure 2.7) which, considering the proximity and geometry of the shelf, would suggest that the Grenville-age sediment was sourced from the ancestral Adirondacks and Frontenac terranes were the primary sources.

Not all of the Potsdam Group zircon ages are similar to those of Chiarenzelli et al. (2010) West Chazy, NY samples. Potsdam Group samples from more northern and westerly portions of the Ottawa Embayment and northern locations in Quebec Basin, most of which are also stratigraphically younger than Chiarenzelli's (2010) West Chazy samples, show additional major age modes of 1.01-1.1 Ga, 1342 Ma. and 1442 Ma, ages also seen in Vermont units. Variation in the zircon populations from younger strata in the Potsdam Group may indicate that other source areas were introduced, perhaps associated with a tectonic uplift event, occurring after deposition of the West Chazy, Altona samples. This variation could also be attributed to restrictions in provenance from sub-basin architecture within the Ottawa Embayment and Quebec Basin. This interpretation would explain the complete lack of certain age modes in the most easterly portions of the outcrop belt as described by Lowe et al. (2018).

The biostratigraphic relationship of the Monkton Formation to the Altona Formation of the lower Potsdam Group suggest they would be at least partially correlative and we would expect to see a similar pattern in the zircon populations that we see in Table 2, between the Monkton and the younger Danby Formation and the Potsdam

Group. The zircon population results by Chiarenzelli et al. (2010) of the lower members of the Potsdam Group (the Altona and Ausable Formations) show strong similarities with the distributions seen in Vermont (Figure 2.4). Analysis of peak ages found in these samples as well as those by Lowe (2016) would suggest that all of these formations, at least regionally, were also sourced primarily from the Adirondacks and Frontenac terranes. However, it should be noted that a large amount of rock potentially covered the modern-day Adirondacks, meaning the original source rock may have eroded away. The provenance interpretations are based on the present day potential provenance sources.

Summary

Comparing the provenance relationships of the Cambrian sedimentary sequences within Vermont and to New York proves difficult because of the regionally complex tectonic history. There are, however, some interpretations that constrain aspects of these sedimentary sequences' deposition and sources. The nearly identical age modes between the Monkton and Danby Formations leads to two possible interpretations about the Danby's source. It was either comprised of reworked sands from the Monkton or that the provenance of sand remained the same. When comparing the Vermont stratigraphy to the most easterly New York stratigraphy, there are some similarities. The Danby and the Monkton Formations both have minor peaks of pre-Grenville age, however most of their grain's ages are similar to the Altona and Ausable Formation's 1300-1000 Ma Grenville-aged source. Because of this relationship, the interpretations of the Altona and Ausable Formations by Brink (2015) and Lowe et al. (2018) as being primarily sourced from the

Grenville-aged Adirondack Mountains and Frontenac Terrane can also be applied to the Monkton and the Danby Formations.

CHAPTER 1: FIGURES

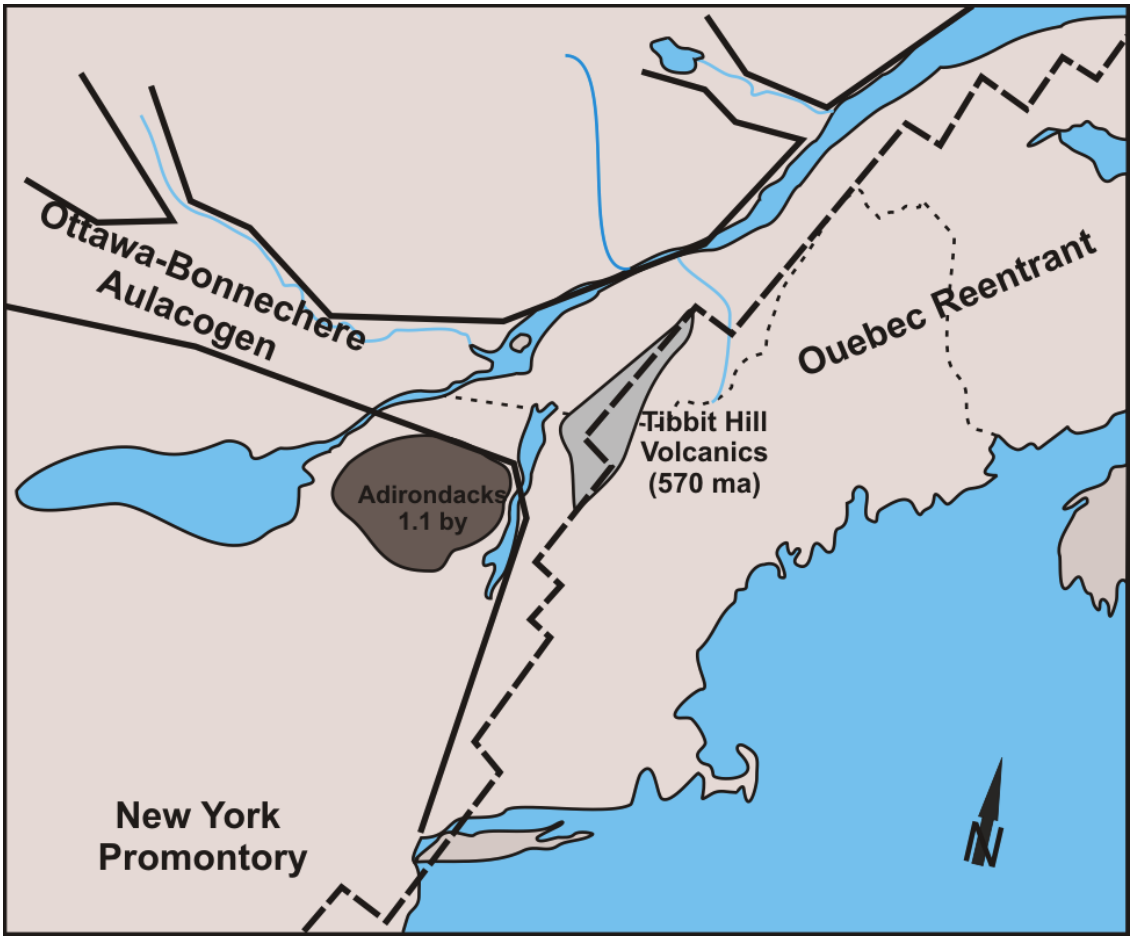

Figure 1.1. Geologic overview map from Brink (2015) of the present day northeastern United States showing major tectonic structures from the rifting of the Iapetus Ocean and the location of the rift related basalts of the Tibbit Hill Formation.

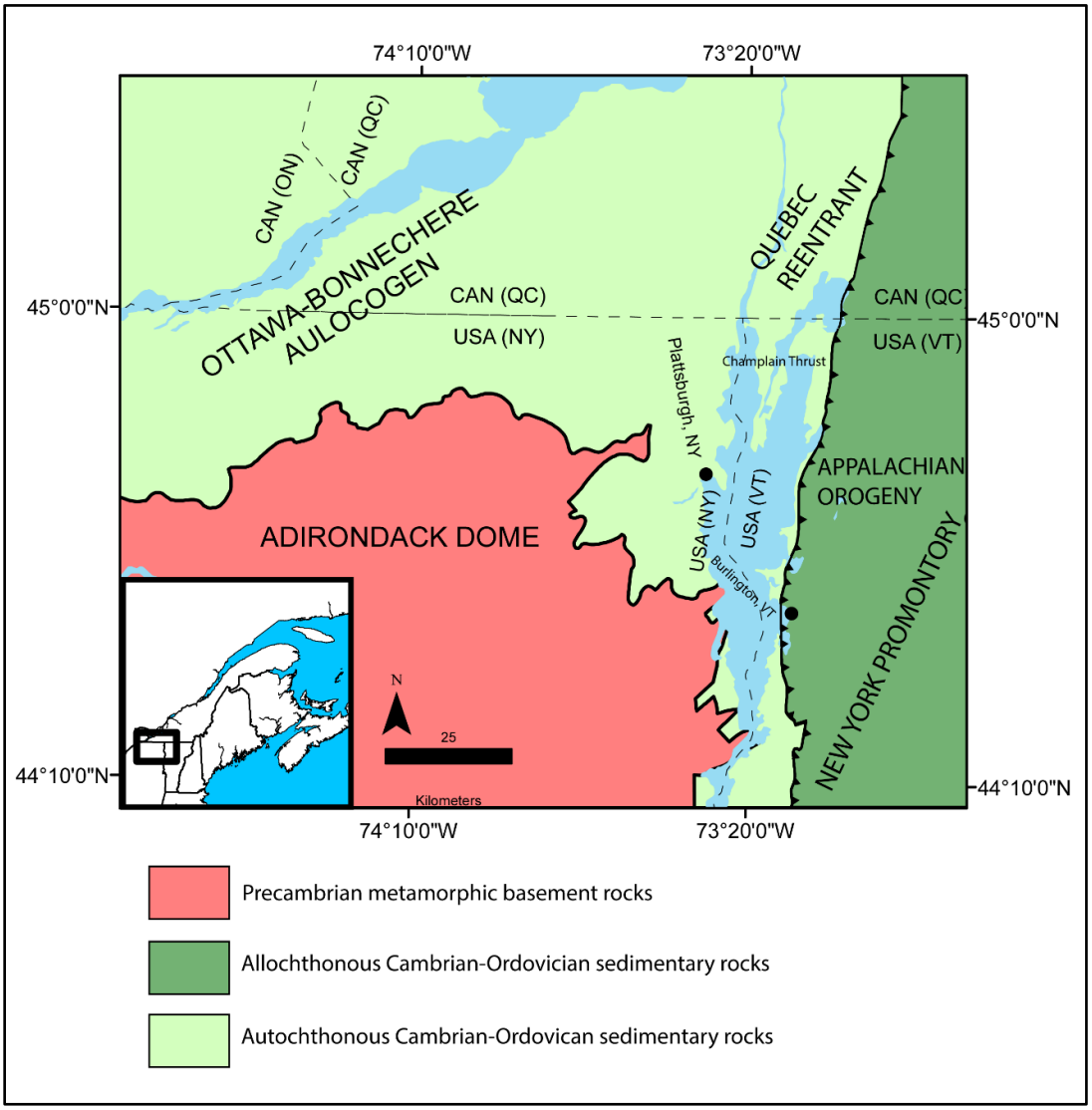

Figure 1.2. Physiographic map showing major Cambrian geographic features and locations of outcrops. Major geographic regions post-Rodina rifting include the Ottawa-Bonnechere Aulacogen, Quebec Reentrant and New York Promontory. Stratigraphy in the aulacogen, including the Potsdam Group, has been relatively undeformed during the Taconic Orogeny. The allochthonous stratigraphy on the upper plate of the Champlain thrust has been displaced westward nearly 80km. This displaced stratigraphy, of the Quebec Reentrant and New York Promontory, includes the Monkton and the rest of the Vermont Cambrian sedimentary sequence located in the Champlain Valley.

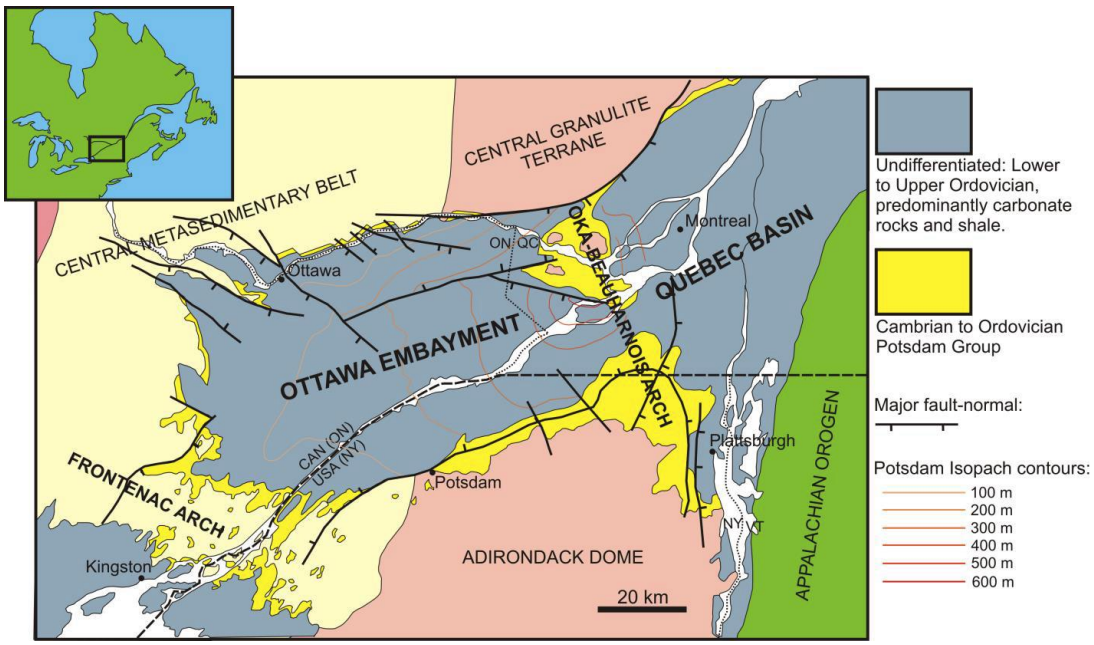

Figure 1.3. Generalized geological, structural and isopach map of the Ottawa Embayment, Quebec Basin and surrounding area, highlighting the distribution of the Cambrian Potsdam Group. Cambrian Potsdam strata most relatable to the Vermont sedimentary sequence are located on the southern portion of the Ottawa Embayment along the northern border of the Adirondack dome. The ispoach map shows that the Potsdam is thicker towards the center of the embayment, however the exposed Cambrian Potsdam stratigraphy is on the fringe of the embayment. From Lowe et al. (2018) modified from Sanford and Arnott (2010).

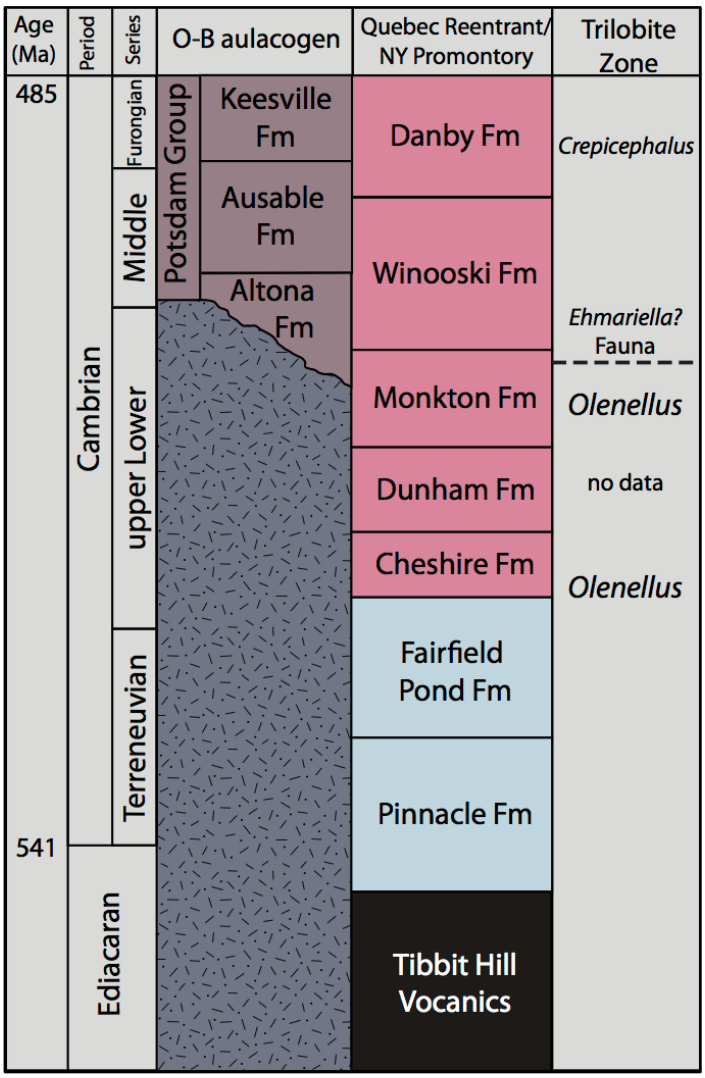

Figure 1.4. Stratigraphic relationships between the Potsdam Group (Ottawa-Bonnechere (OB) Aulacogen) of Quebec and Northwestern NY and the allochthonous stratigraphy in the New York Promontory and Quebec Reentrant that are the Vermont shelf units from Brink (2015). Trilobite zones are shown highlighting that Monkton and Altona are at least partially coeval based on biostratigraphy (Landing et al., 2009).

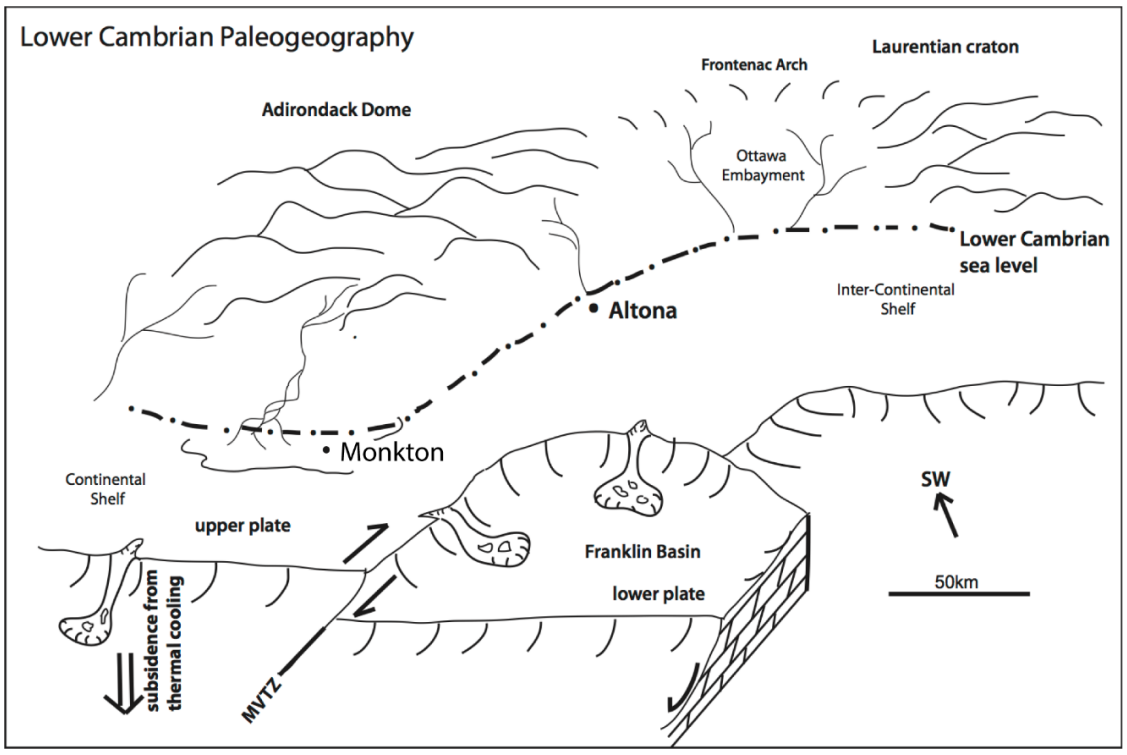

Figure 1.5. Paleogeographic reconstruction of the Laurentian Iapetus margin during the Lower Cambrian during Monkton (Vermont) and Altona (New York) deposition. The northwestern Vermont stratigraphy associated with the shelf and basin are seen on the map represented by the continental shelf and the Franklin Basin, respectively. These two areas are separated by the late Precambrian and early Cambrian rift related Missisquoi Valley Transfer Zone (MVTZ) identified by Cherichetti et al. (1998) to mark the transition from lower plate (basin) to upper plate (shelf). Roughly 100 km west along the trend of the MVTZ, within the Ottawa Embayment on the intercontinental shelf, the shallow water Altona Formation was deposited. Figure adapted from Brink (2015).

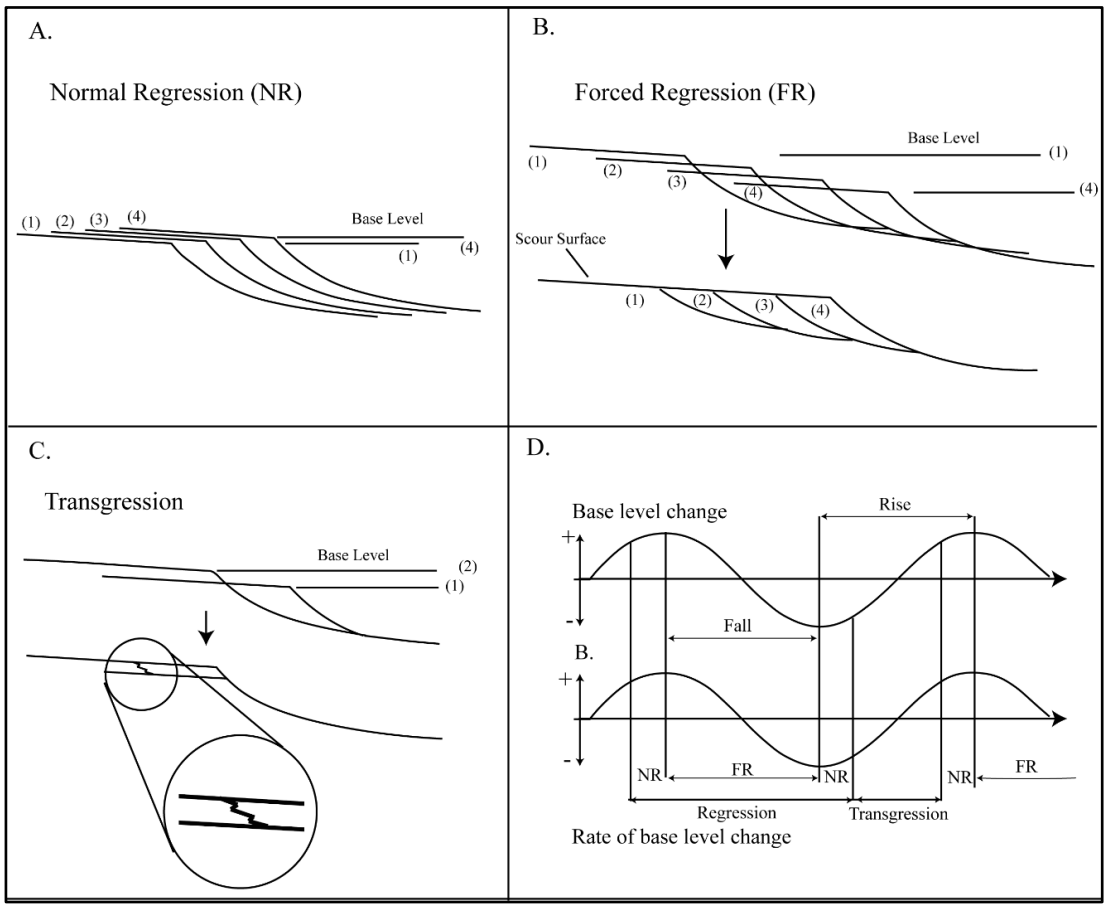

Figure 1.6. Visual representation of shoreline depositional sequences that occur during varying stages of base level change. (A.) In the normal regression sedimentation is outpacing the ability of sea level to create accommodation space, thus there is facies aggradation and progradation seaward. (B.) During the forced regression there is a rapid base level change and the shoreline moves seaward, prograding, while also incising the now aerially exposed land. (C.) During the transgression base level rise is outpacing sedimentation so there is a shift of facies landward (as seen in the zoomed-in circle). (D.) Graph showing cyclic base level change and rate of change and where these shoreline sequences would occur in the cycle. Modified after Catuneanu (2002).

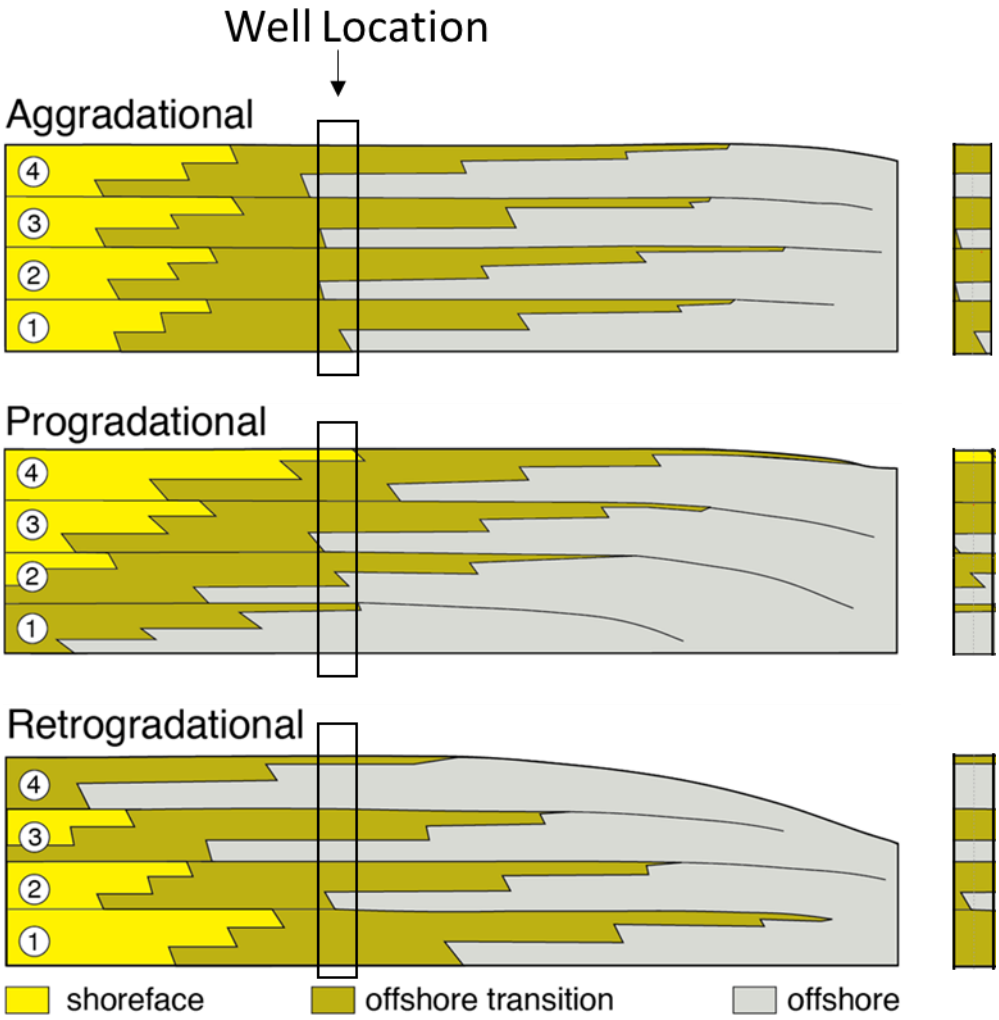

Figure 1.7. Summary of the three major parasequence stacking patterns (adapted from Van Wagoner et al. (1990)). The aggregational stacking pattern illustrates what happens when deposition rates and the ability to create accommodation space are in relative equilibrium. There is no migration of the shoreline seaward or landward. The progradational stacking pattern visuals what happens when deposition rates outpace the ability to create accommodation space. Under these conditions there is a seaward migration of the shoreline. The retrogradational stacking pattern visuals what happens when deposition rates cannot keep up with accommodation space being generated. As a result, there is a landward migration of the shoreline. To the right of each are the sequences as they might appear in a well.

CHAPTER 2: FIGURES

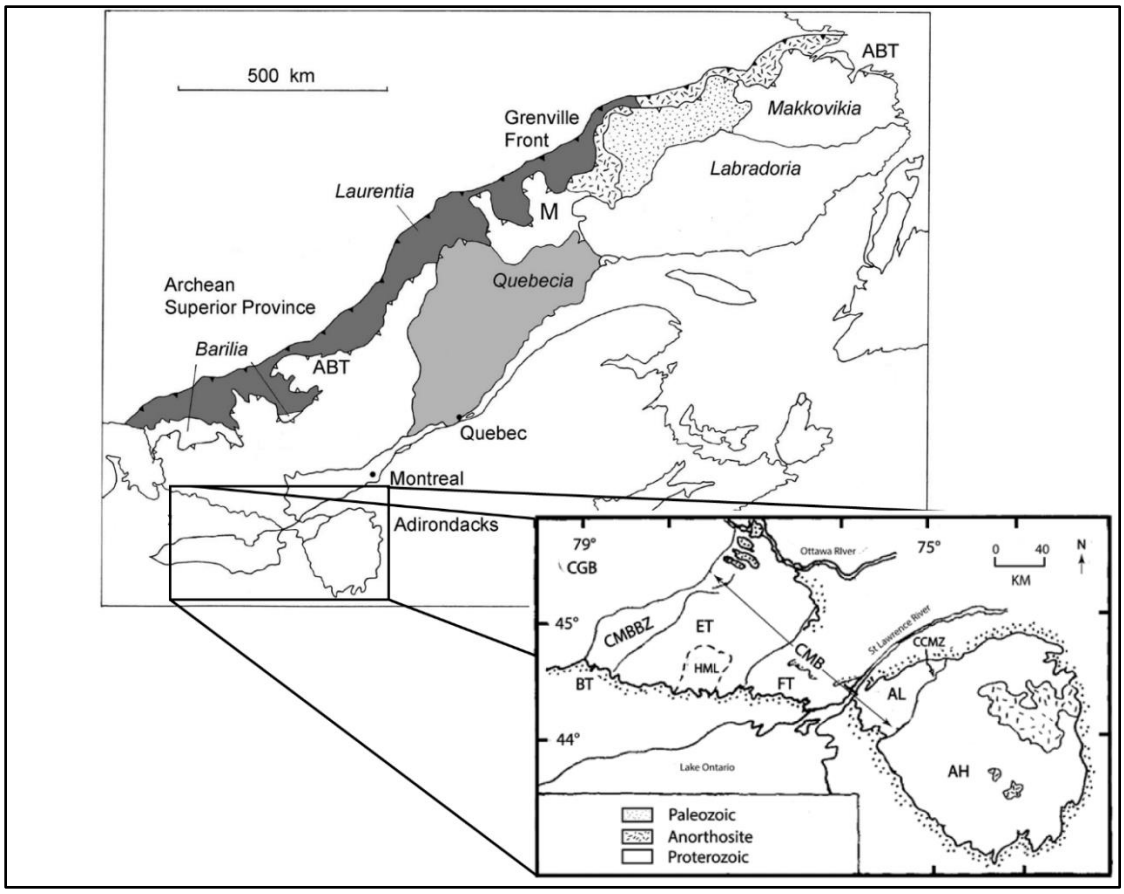

Figure 2.1. Map of Grenville Province with major terranes and inset of a generalized geologic map showing Grenville terranes regional to the Adirondacks. Starting with terranes closest to the Vermont stratigraphy are the Adirondack Highlands (AH), Adirondack Lowlands (AL), Central Metasedimentary Belt (CMB), Carthage-Colton mylonite zone (CCMZ), Frontenac Terrane (FT), Hastings metamorphic low (HML), Elzevirian Terrane (ET), (CMBBZ), Bancroft terrane (BT), Central Gneiss belt (CGB). and Allochthon boundary thrust (ABT). Figure adapted from Daly and McLelland (1991) and Zelek and Dickin (2013).

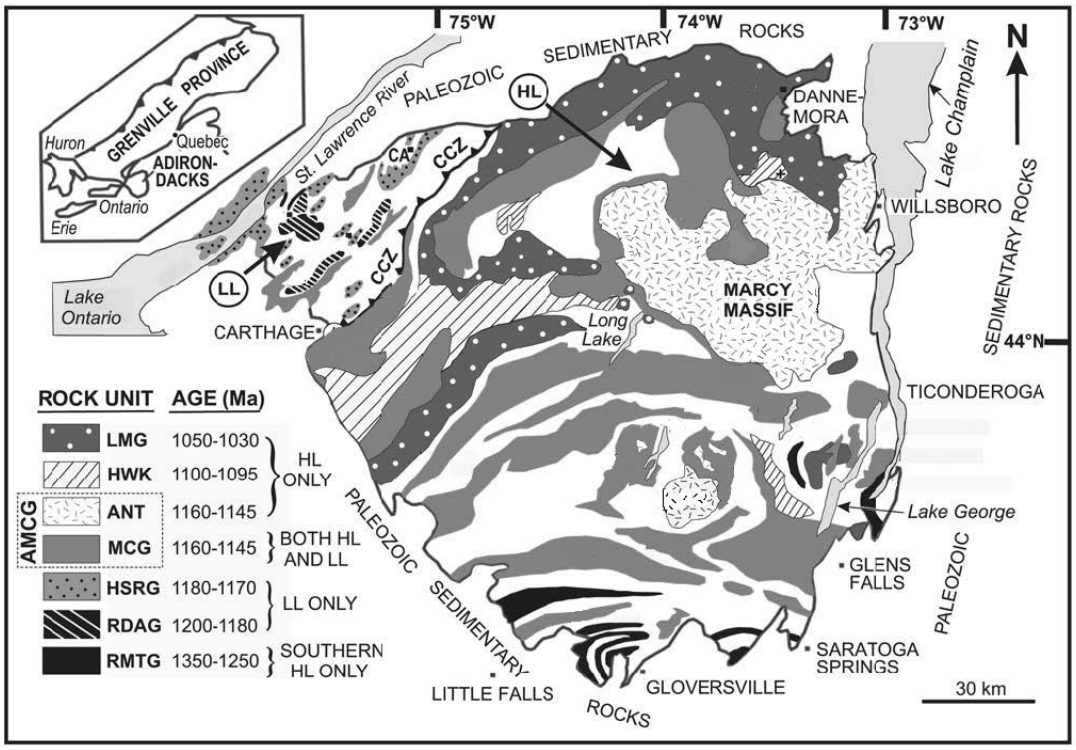

Figure 2.2. Generalized geologic map of the Adirondacks units showing metaplutonic rocks dated by through U-Pb zircon geochronology. Within the Adirondack Highlands (HL) are the RMTG—Royal Mountain tonalite and granodiorite (southern HL only), HWK—Hawkeye granite, LMG—Lyon Mountain Granite, and ANT—anorthosite. Units only contained in the Adirondack Lowlands (LL) include HSRG—Hyde School and Rockport granites RDAG—Rossie diorite and Antwerp granodiorites. The Granitoid members of the anorthosite-mangerite-charnockitegranite suite (AMCG) are found in both the HL and LL. Figure adapted from McLelland et al. (2004).

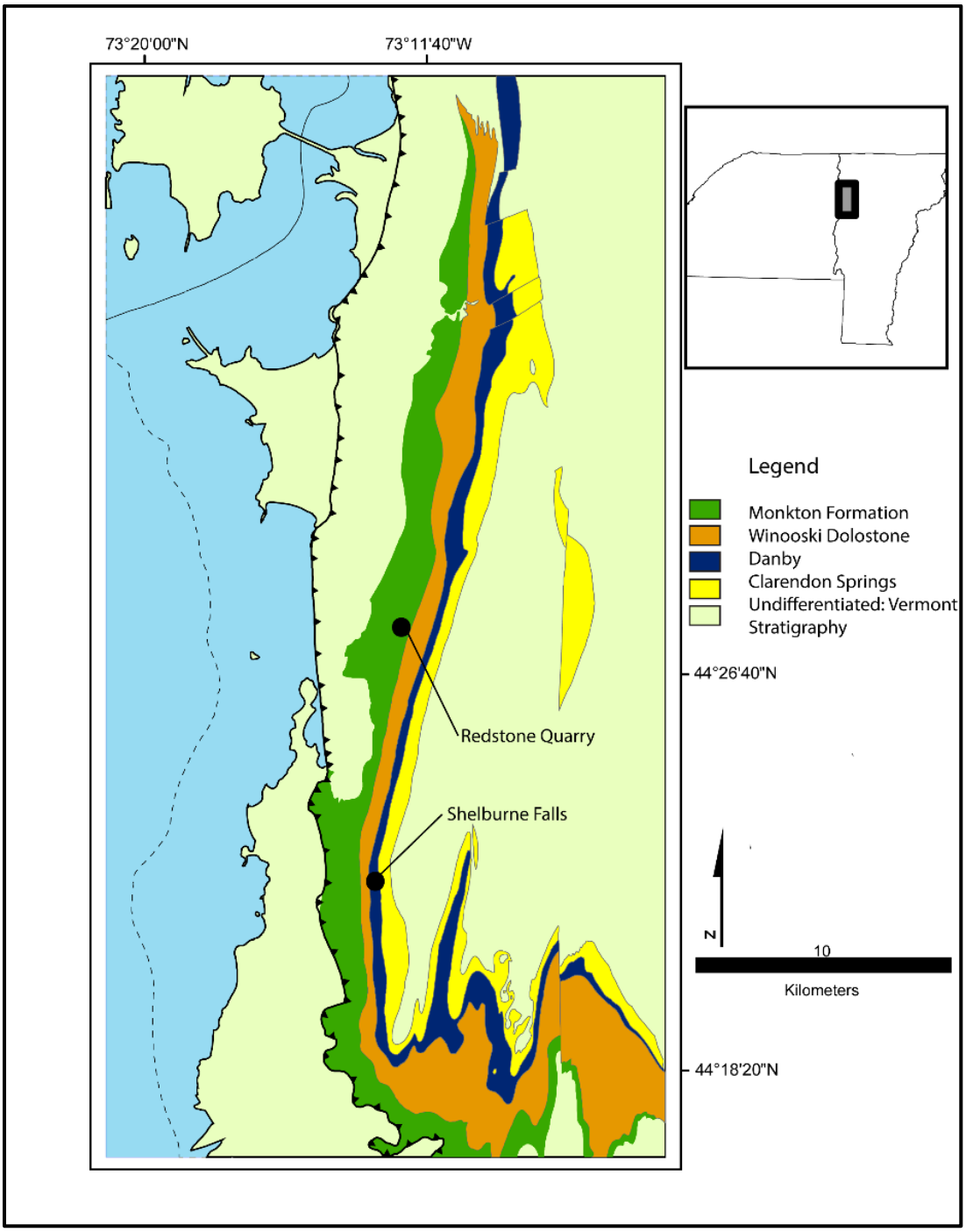

Figure 2.3. Simplified bedrock geologic map of Vermont showing localities for sampling and outcrop studies. Redstone Quarry and Shelburne Falls, locations for detrital zircon sampling, are labeled on map. UTM coordinates for Redstone Quarry are 18T 0642749.91 E 4924714.39 N and Salmon Hole is 18T 0643963.35 E 4927567.01 N. Base map is the bedrock geologic map of Vermont Ratcliffe et al. (2011)

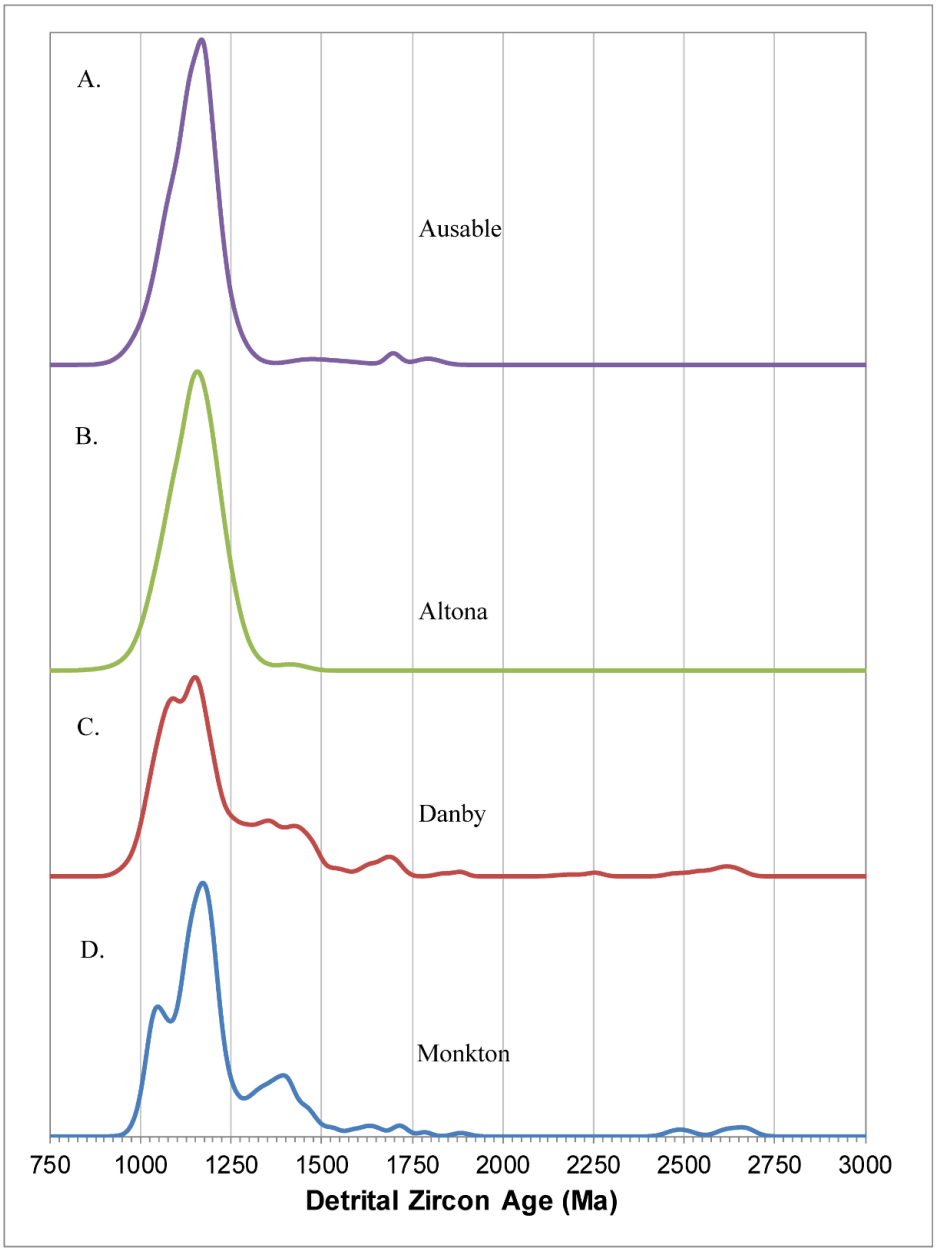

Figure 2.4. Normalized $^{206}Pb/^{207}Pb$ ages of detrital zircon age-relative probability distributions of the Monkton (D.) and Danby (C.) from this study and Ausable (A.) and Altona (B.) from Chiarenzelli et al. (2010). Zircon population distribution shows dominate age peaks of ~1.05-1.09 Ga and ~1.15-1.72 Ga for the Monkton and Danby suggesting either a continuity of provenance source or the cycling of the Monkton's sandstones. This dominate age peak is similar to the ~1.16 Ga age peak seen in the Altona and Ausable Formations of the lower Potsdam Group of NY. Graph created using (Gehrels, 2010b)

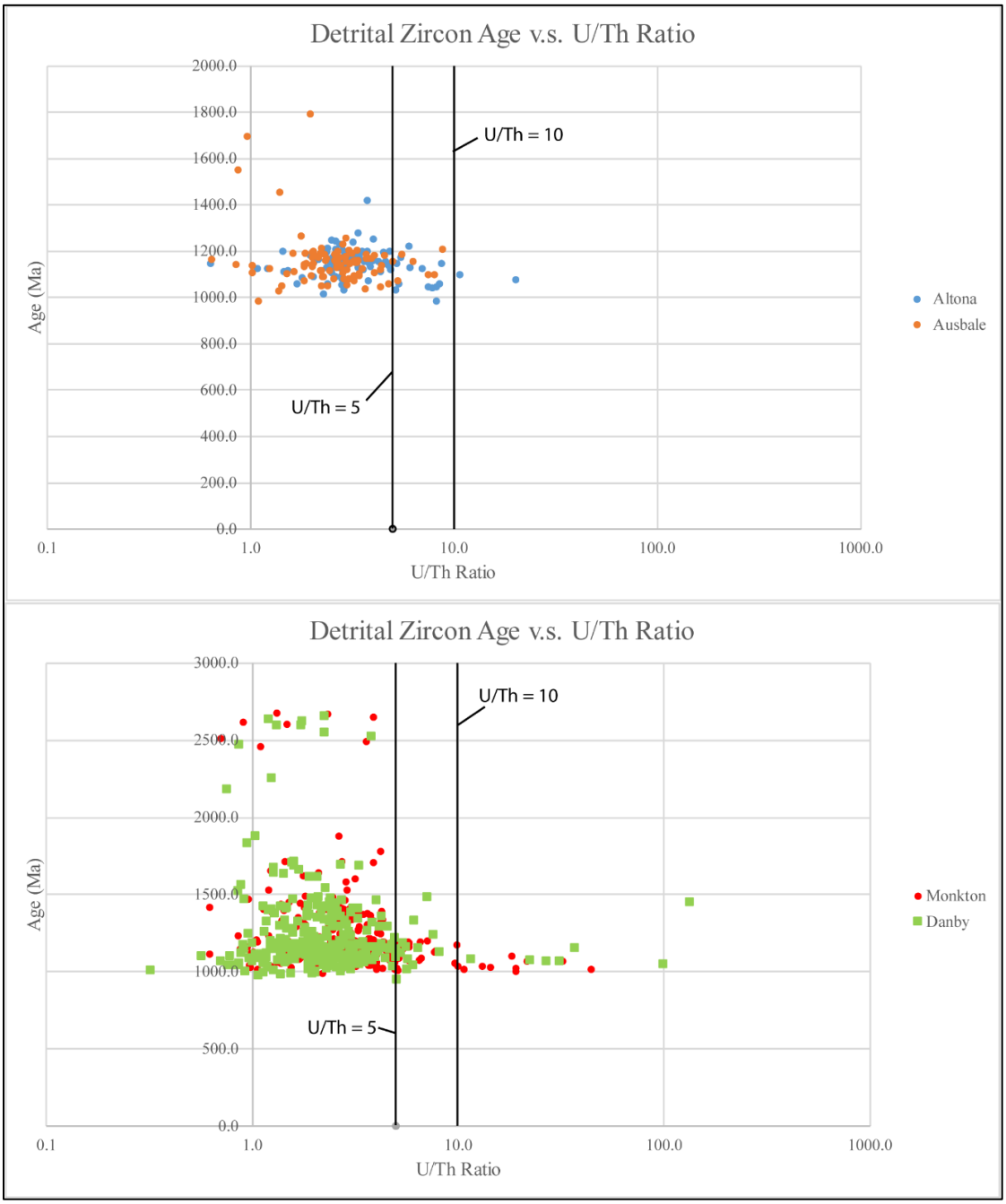

Figure 2.5. U–Pb isotopic data from zircon collected using laser-ablation ICPMS, plots of U/Th versus age. The y axis represents the age of the detrital zircon in millions of years and the x axis shows the U/Th ratio. U/Th cutoffs are labelled for values of 5 and 10 on each graph.

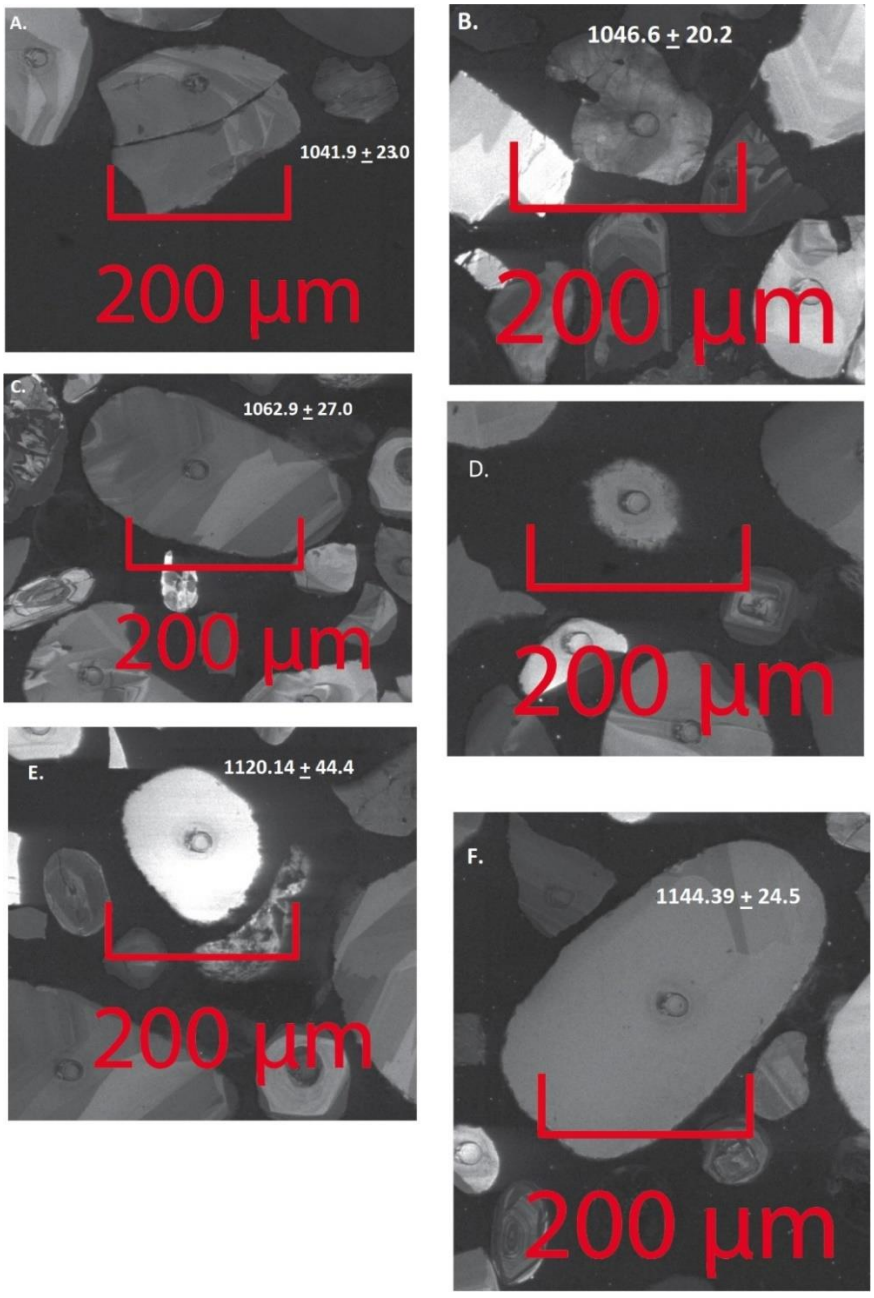

Figure 2.6. Post-ablation CL images of detrital zircons from the Monkton sample with their $^{206}Pb/^{207}Pb$ ages indicated with 2σ uncertainties. (A) Fragmented subhedral detrital zircon. (B) Fragmented detrital zircon. (C) Subrounded detrital zircon with multi-stage zoning. (D) Well-rounded weakly zoned detrital zircon. (E) Well-rounded detrital unzoned zircon. (F) Subrounded unzoned detrital zircon.

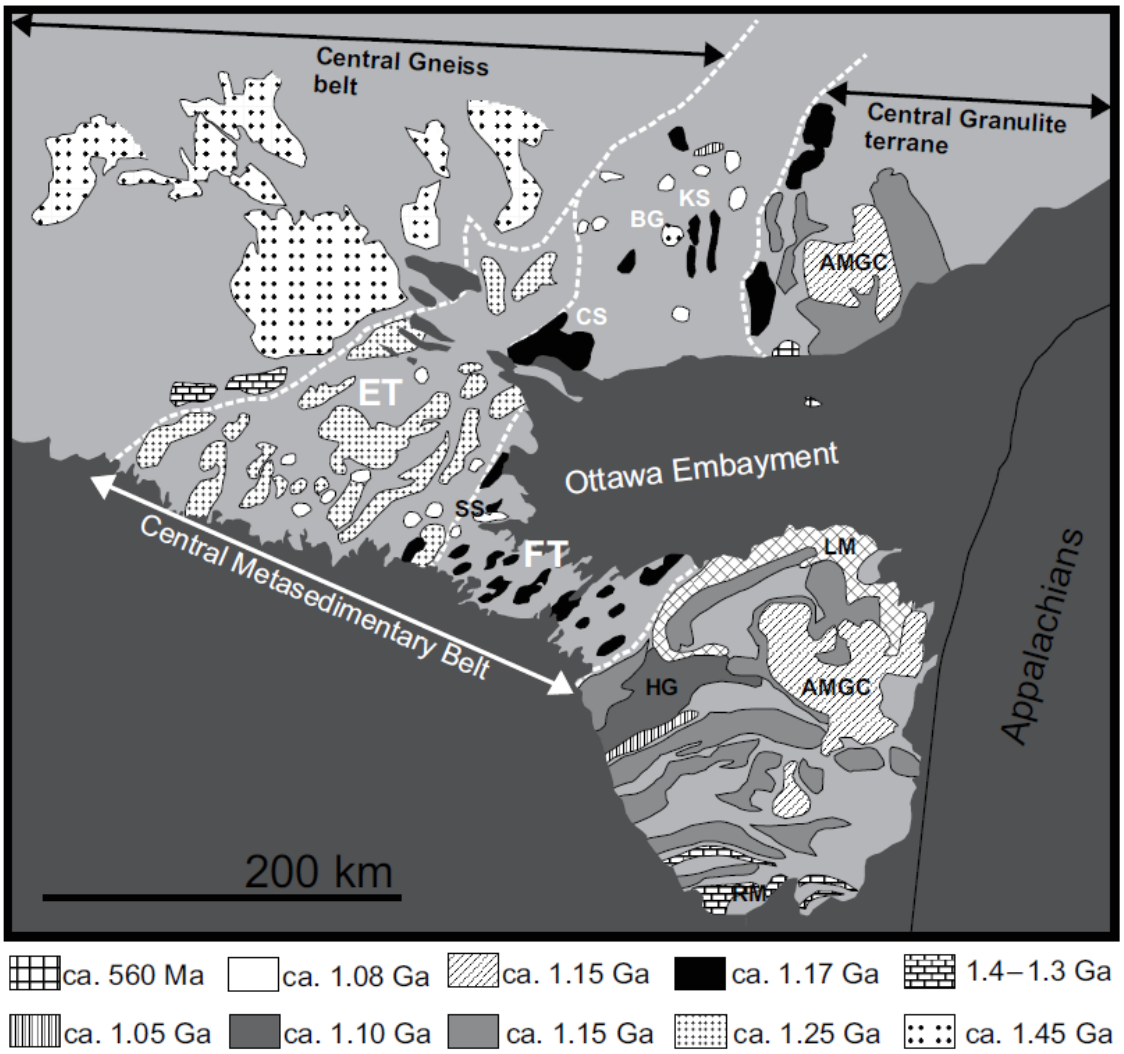

Figure 2.7. Potential source rocks of Grenville age in Northern NY, Ontario and Quebec from Lowe et al. (2018). Paleocurrent data from the Vermont stratigraphy preclude Grenville aged rocks in Vermont as a source for the Monkton and Danby Formation sand. Accessory mineral assemblages in the Monkton (Goldberg and Mehrtens, 1998) suggest that the sediment was predominantly sourced from the Adirondack Dome. Potential sources include the Elsevier terrane (ET), Frontenac terrane (FT), Skootamata Suite (SS), Chevreuil Suite (CS), Bondy Gneiss complex (BG), Kensington Suite (KS), Hawkeye Granite (HG), Royal Mountain Suite (RM), Lyon Mountain Granite (LM), Adirondack anorthosite-mangerite-granite-charnockite suites (AMGC). Though this map shows of potential provenance sources of various ages, it is not representative of geology at the time of deposition of the Cambrian. Minor peaks in detrital zircon age populations could contain grains from bedrock that has been eroded away or is no longer exposed.

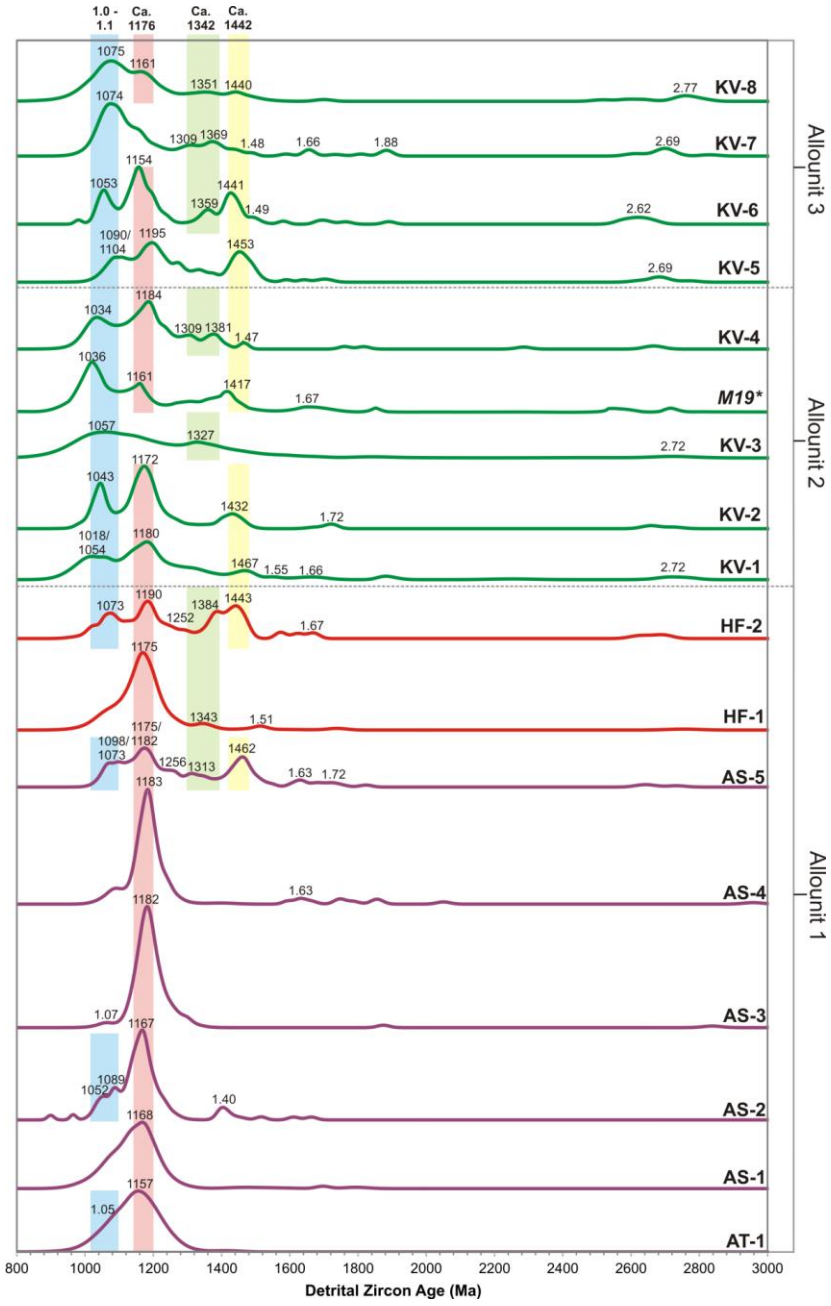

Figure 2.8. Detrital zircon population age group distributions of the Potsdam Group graph from Lowe (2016). Data in this figure is arranged stratigraphically with the Altona (AT) at the bottom, followed in ascending order by the Ausable (AS), Hannawa Falls (HF) and Keeseville (KV). The younger members of the Potsdam (above the Ausable) contain more complex population age distribution with multiple major and minor modes.

CHAPTER 1: TABLES

Order	Nomenclature	Thickness (ft)	Duration (Ma)	Associated Processes
1st	Megasequence	1000+	50 to 100+	The formation and breakup of supercontinents (tectonic)
2nd	Supersequence	500-5000+	5 to 50	Magmatic production in mid-ocean ridges
3rd	Sequence	500-1500	.5 to 5	Glacio-eustatic processes
4th	Parasequence Set	20-800	.1 to .5	Glacio- and hydro-eustatic processes
5th	Parasequence	10-200	.01 to .1	Global climate changes driven by orbital parameters (Milankovitch Cycles)

Table 1.1: Summary of sea level cycles hierarchal ordering from Mitchum and Van Wagoner (1990). This includes the names of the various sea level cycles and the potential thicknesses and time frame for the deposited rock intervals. The last column lists common processes that affect sea level change with their associated order (Hallam, 1963; Rovere et al., 2016; Vail et al., 1977; Williams, 1993).

CHAPTER 2: TABLES

	Altona DZ AGES				
MIN AGE	MAX AGE	# GRAINS	PEAK AGE	# GRAINS	%
910	1394	95	1157	79.00658	83.16482
	Ausable DZ AGES				
MIN AGE	MAX AGE	# GRAINS	PEAK AGE	# GRAINS	%
914	1331	92	1168	77.00177	83.69757
	Montkon DZ AGES				
MIN AGE	MAX AGE	# GRAINS	PEAK AGE	# GRAINS	%
952	1759	269	1048	59.00498	21.93494
2477	2495	1	1172	122.0019	45.35388
2623	2679	3	1393	29.00065	10.78091
			1632	4.008954	1.490318
			1714	3.017966	1.12192
			2489	3.006659	1.117717
			2658	4.003096	1.48814
	Danby DZ AGES				
MIN AGE	MAX AGE	# GRAINS	PEAK AGE	# GRAINS	%
927	1738	286	1090	102.0032	35.66544
2522	2526	0	1151	103.003	36.01505
2557	2582	0	1351	31.00193	10.83984
2592	2656	4	1424	23.00174	8.042567
			1686	8.004145	2.798652
			2622	5.009132	1.751445

Table 2.1: Results from Gehrels (2010a) AGE PICK Excel add-on calculating peak ages for the detrital zircon populations. Zircon population for the Monkton and Danby shows peak ages of 1.05-1.09 Ga. The Altona and Ausable have a single peak age ~1.16 Ga.

	Similarity			
Altona	**Altona**			
Ausable	0.936	**Ausable**		
Monkton	0.874	0.885	**Monkton**	
Danby	0.857	0.868	0.936	**Danby**

Table 2.2: Similarity results from Arizona Laserchron Center's OVERLAP-SIMILARITY PROGRAM 2010 from using detrital zircon age data of the Monkton, Danby, Altona and Ausable Formations. The degree of similarity is calculated by summing, over the time period of interest, the square root of the product of each pair of probabilities. Like an R value, the closer the value is to 1 the more similar the populations are. All populations show a high similarity value with the other member of their respective stratigraphy; however, it should be noted that similarity values were also high when comparing the Vermont and New York stratigraphy.

CHAPTER 3: ARTICLE FOR JOURNAL SUBMISSION

3.1. Abstract

The Monkton Formation is described as a Lower Cambrian regressive sandstone unit containing shallowing-up cycles, called parasequences, which record tidal flat progradation. Spatial variation and limited outcrops of continuous stratigraphy have made it difficult to characterize how cycles change in architecture and thickness through the entirety of the Monkton Formation. This study seeks to identify stratigraphic trends in the parasequence architecture and thickness from the successful recognition of facies in the subsurface, information that will clarify how the sea level changed and impacted accommodation space.

New geophysical data allows this research project to explore the stratigraphy of the Monkton at higher levels of resolution than previously achieved. Initial statistical study of gamma ray data from a well through the Monkton suggests that meter-scale parasequences are identifiable in geophysical logs. Using continuous gamma log data, this work identified clastic carbonate ratios from a 1034' deep geothermal well drilled at Champlain College in Burlington, VT. Although cycles were identified in the gamma log, the spatial variation, complexity and variety of parasequence types within the Monkton made it difficult to correlate the sequences with specific environments or changes in sea level.

To see if specific architectural elements of parasequences and lithologies could be characterized by gamma values, outcrops of the Monkton were surveyed containing both parasequences and lithologies that are useful paleobathymetric indicators. The survey determined gamma ray patterns and relative values of a common Monkton parasequence representing tidal flat progradation and a carbonate lithology indicating an abrupt sea level rise. Gamma data from a second well on the University of Vermont campus, along with accompanying borehole camera video, confirmed that the outcrop survey results could be useful in subsurface interpretations of the Monkton. Intervals representing the parasequences and carbonate lithologies were identified in the Champlain College Well and were combined with the UVM Fleming Well findings to create a composite stratigraphic section of the Monkton. The parasequences and lithologic trends identified in the composite section indicate that, over the entirety of the Monkton, accommodation space decreased. The decrease in accommodation space is interpreted to represent a change in the rate of sea level rise. The Monkton Formation deposition occurred in a transgressive systems tract with varying rates of sea level rise, which implies that the overlying Winooski Formation would represent highstand systems tract deposition.

3.2. Introduction

The characterization of parasequences is a key component for interpreting depositional systems and systems tracts in the field of sequence stratigraphy. Parasequences represent the cyclic deposition of a conformable succession of genetically related beds or bedsets bound by a marine flooding surface (Van Wagoner, 1995) and the identification of stratigraphic trends in parasequence architecture and thickness is used to clarify how sea level changed and impacted accommodation space (Posamentier and Vail, 1988). Understanding how sea level fluctuated within a depositional sequence, allows for that stratigraphy to be put into the context of systems tracts and sequence stratigraphy.

The Monkton Formation of northwestern Vermont is described as a Lower Cambrian regressive sandstone unit containing shallowing-up cycles (SUCs) recording tidal flat progradation (Palmer and James, 1980; Rahmanian, 1981). This heterolithic unit is greater than 300 meters in thickness and is comprised of sand, silt and dolostone (Cady, 1945). Rahmanian (1981) studied this mixed siliciclastic-carbonate unit, identifying facies recording supratidal, intertidal and shallow subtidal deposition which were interpreted to represent prograding tidal flat sedimentation. Rahmanian (1981), and later Speyer (1983), described the unit as being characterized by repeating shallowing-up cycles or parasequences, representing this tidal flat progradation.

Repeating meter-scale shallowing-upward parasequences of mixed siliciclastic-carbonate rocks in the Monkton are identifiable at a variety of outcrops in the Champlain

Valley of Vermont. However, spatial variation and limited outcrops of continuous stratigraphy make it difficult to characterize how cycles change in architecture and thickness through the entirety of the unit. Kim *et al.* (2013) collected gamma log data through a significant portion of Monkton stratigraphy in a 1034' deep geothermal well drilled at Champlain College in Burlington, Vermont and identified cyclic patterns, interpreted as parasequences, in the gamma log data. However, the nature of the mixed siliciclastic-carbonate facies and the depositional complexities in the subtidal, intertidal and supratidal environments of the Monkton made it difficult for the authors to confidently interpret the parasequences in the well log data. Building on their preliminary work, this study has several objectives, including outcrop analysis of gamma emission patterns, analysis of gamma emission and borehole camera data from a second well, and syntheses of these data to identify parasequence architecture trends through the Monkton and use this information to interpret how sea level and accommodation space changed.

3.3. Geologic Setting

The Monkton Formation, along with the entirety of the Cambrian stratigraphic sequence in Western Vermont, was deposited on a thermally subsiding tectonically stable shelf along the Laurentian-Iapetus Ocean margin that formed following the breakup of Rodina (Bond, 1997). Recent work by Li et al. (2013) using paleomagnetic, lithologic and geochronologic data suggests that the breakup of Rodina was complete by 580 Ma. The formation of the Laurentian-Iapetus Ocean margin has been constrained between 615 and 580 Ma based on radiometric age determinations of rift-related, Tibbit Hill

Formation, basalts that formed in modern Vermont and Southern Quebec at a triple junction associated with the breakup of Rodina (Kumarapeli et al., 1989).

The triple junction, created during rifting, formed three major features that controlled large scale sediment distribution along the Iapetus margin. On the two successfully rifted arms, northwest-striking transform faults offset northeast-striking rift segments including the (convex ocean-ward) New York Promontory and (convex land-ward) Quebec Reentrant features (Thomas, 1977). The failed third arm of the triple juncture forms the 55km wide and 700km long topographic low known as the Ottawa-Bonnechere aulacogen (Kay, 1942). The Cambrian sequence in Vermont was deposited on the New York Promontory portion of the shelf. The shallow water Monkton, Cheshire, Dunham, Winooski and Danby Formations make up the Vermont Iapetus shelf units whereas the Parker, Skeels Corners, Rugg Brook and Rockledge Formations represent the basinal environments (Dorsey and Stanley, 1983). These deeper water formations were deposited in a depocenter known as the Franklin Basin located north of Colchester, Vermont (Shaw, 1958).

The allochthonous Cambrian stratigraphy found in the Champlain Valley was transported ~80 km to the west emplaced over Ordovician limestone and shales, on the upper-plate of the Champlain Thrust (Stanley, 1999). Even with this Middle Ordovician displacement of the Champlain Thrust the Cambro-Ordovician stratigraphy in the Champlain Valley has remained relatively undeformed. The outcrop belt of the Vermont Iapetus Shelf units extends from the Franklin Basin to the north, southward the length of

Vermont. As can be seen on the bedrock geologic map of Vermont (Ratcliff et al., 2011), this stratigraphy is located on the western limb of broad synclines, to the north the St. Albans Synclinorium and to the south, the Middlebury Synclinorium.

The age of the Monkton is based on biostratigraphic data. *Ptychoparia adamsi* and *Ollenellus* zone trilobites present in the Monkton, place the formation's age as Lower Cambrian (Schuchert, 1933, 1937). The underlying Dunham Dolostone contains *Salterella conulata*, a Lower Cambrian index fossil (Mehrtens and Gregory, 1984) correlative with the lower *Olenellus* trilobite zone. The basal horizons of the Parker Slate, a fine-grained unit deposited in the Franklin Basin, also contain Lower Cambrian age *Ollenellus* zone trilobites (Palmer and Holland, 1971 & Shaw, 1958), indicating that the Monkton and part of the Parker are correlative. However, upper horizons of the Parker contain trilobites of the *Bolaspidella* zone of Middle Cambrian age (Palmer and James, 1980). These authors identify the five missing trilobite zones between *Olenellus* and *Bolaspidella*, a gap that occurs in stratigraphy along the Iapetus margin elsewhere in the Appalachians, and which represents a basin-wide unconformity they termed the Hawke Bay Event. Because of this unconformity, it is not clear whether the entire Monkton is Lower Cambrian in age or if it extends into the Middle Cambrian. The overlying Winooski Dolostone is dated as Middle Cambrian on the basis of interbedding with the younger trilobite-bearing Parker Slate.

During the time interval of Monkton deposition, the North American craton was in the early stages of a sea level rise termed the Sauk megasequence by Sloss (1963). The

Sauk megasequence includes strata from latest Precambrian to Early Ordovician in age, an interval based on its position between an interregional pre-Cambrian conformity and an interregional unconformity at the base of the succeeding Tippecanoe sequence (James et al., 1987; Sloss, 1963). Palmer and Taylor (1981) subdivided the Sauk megasequence into transgressive-regressive cycles termed supersequences and even these are further subdivided into depositional cycles referred to as sequences. Mitchum and Van Wagoner (1990) recast the terms megasequences, supersequences and sequences in terms of sequence stratigraphy as first, second, and third order cycles, respectively, and estimated their time durations as 50-100 My, 5-50 My and 0.5-5 My, respectively.

Several authors made interpretations of sea level fluctuation within the Sauk transgression in the Northern Appalachians. The Hawke Bay unconformity described by Palmer and James (1980) marks the boundary between the Sauk I and II super sequences (Raine and Smith, 2012), which in the Vermont Cambrian sedimentary sequence is marked by the unconformity separating the Dunham Dolostone and the overlying Monkton Formation. In addition to Palmer and James' (1980) previously cited study, Landing et al. (1992) suggested that the fluctuating sea levels influenced basin aerobic and disaerobic cycles on the Iapetan continental slope, producing varying coloration of shale units which they interpreted as recording two deepening in these late Early Cambrian deep water deposits.

3.3. Monkton Formation

The greater than 300 meter thick mixed siliciclastic-carbonate Monkton Formation was studied by Rahmanian (1981) and Speyer (1983), both of whom identified facies recording supratidal, intertidal and shallow subtidal deposition. More recent work by Goldberg and Mehrtens (1998) identified a fluvial facies of the Monkton in erosional contact with the Dunham Dolostone; the contact between these two units is commonly in a covered interval.

Although the first detailed description and thickness estimate of the Monkton was done by Cady (1945), it was Rahmanian (1981) who characterized the cyclic nature of deposition in the Monkton Formation. He identified two repeating types of sedimentary cycles within Monkton Formation (Figure 3.1). The first of these is a mixed siliciclastic-carbonate cycle that is more carbonate-rich towards the top of the cycle. The cycle is interpreted to record the transition from subtidal and channel system facies to a carbonate dominated intertidal-supratidal facies. This mixed siliciclastic-carbonate carbonate cycle identified by Rahmanian (1981) is useful in making sea level interpretations because the carbonate facies characteristic of the peritidal setting makes an excellent paleobathymetric indicator. The second cycle is siliciclastic-dominated and is interpreted to have formed in a subtidal bar and tidal channel environment moving stratigraphically upwards into a mixed sand and mud intertidal flat. Rahmanian (1981) interpreted the down slope pinch out of the tidal flat to represent overall regressive sedimentation recording tidal flat progradation.

Using the terminology of sequence stratigraphy, shallowing-up cycles are also called parasequences. Parasequences can be considered a fourth or fifth order sea level cycles which represents durations of between 0.01-0.5 Ma (Mitchum and Van Wagoner, 1990). The cyclic sediment deposition creating these parasequences are commonly identified in core and well logs and are often used by stratigraphers for correlation between wells. Parasequence sets describe successions of parasequences that form a distinctive stacking pattern (Van Wagoner et al., 1990) and they are used to define systems tracts (Van Wagoner et al., 1988).

Cyclic deposition of parasequences can develop if accommodation space is sequentially created. This can happen as a result of external processes, such as sea level change, in which case the driving mechanism is termed allocyclic, or internal processes related to lateral facies migration, termed autocyclic processes. Beerbower (1964) suggested that autocyclic processes occur within a particular depositional setting, such as a fluvial system, and their effects tend to be local and, in geologic terms, instantaneous. They are described as aperiodic because they generally occur randomly in time and space (Cecil, 2003).

Rahmanian's (1981) Type 1 cycle recording the progradation of tidal flat sediments is interpreted to record allocyclic deposition because the space needed to produce the vertical accretion of such shallow water sediment implies that space was created through repeated sea level changes (Figure 3.1). Rahmanian's Type 2 subtidal sandstone cycles, associated with the lateral migration of tidal channels and sand bars,

would be the product of autocyclic processes, however these may also occur during sea level fluctuation (Figure 3.1). For this study we are most interested in the cycles produced by the prograding tidal flat deposits (Rahmanian's Type 1), because the depositional environments represented by these cycles are accurate bathymetric (sea level) indicators.

Table 3.1 summarizes the five lithofacies of the Monkton that define bathymetric and sea level conditions. Lithofacies 1-3 represent the range of environments (subtidal, intertidal and supratidal) found within Type 1 and 2 cycles, while lithofacies 4 and 5 indicate deposition under specific environmental conditions; lithofacies 4 describes a clear water platform carbonate that would only form when there is little siliciclastic input and this lithology is interpreted to have been deposited during a rapid base level rise. These flooding events trap clastic sediment in more proximal alluvial systems, allowing for the return to clear water carbonate deposition on the shelf. Lithofacies 5 is a poorly sorted arkosic sandstone containing abundant accessory minerals and displaying features such as dewatering and load structures (Figure 3.2). This lithofacies is interpreted as an event bed related to rapid deposition from storm-generated sediment discharge onto the tidal flat. Though lithofacies 5 is not necessarily a bathymetric indicator, the ample accessory minerals were found to have a unique gamma signature.

Because of the association with different gamma emissions from different lithologies, characterizing the gamma signatures of the facies representing these environments and of the parasequences they create would lead to successful recognition of facies in the subsurface. Wells drilled through the Monkton provide the thickest

continuous section of Monkton stratigraphy and allowed us to identify stratigraphic trends in parasequence architecture. Such trends in architecture and thickness can clarify how the sea level changed and impacted accommodation space through Monkton deposition. However, in order to confirm that the lithofacies within a parasequence can be accurately recognized in a well log, outcrop examples of parasequences were logged using a methodology described below.

3.4. Survey Methods

3.4.1 Outcrop Survey

Outcrops were chosen where parasequences and distinct lithologies within the Monkton were well exposed and easily identified and where the relative position of the exposure relative to the base of the overlying Winooski Formation is known. Gamma emission data collection was completed through stratigraphic intervals at three localities: Redstone Quarry, Salmon Hole, and at Pease Mountain (Figure 3.3). Gamma ray data was collected in counts per second (cps) using a Radiation Solutions hand held gamma-ray spectrometer (RS-230 BGO *Super-SPEC).*

In order to mimic the continuous curve data collection in gamma well log data, surveys were completed by hand-held logging in 5 and 10 cm increments, collecting data through the thickness of the stratigraphy. Readings were taken for one minute at each position and then averaged to get a single gamma (cps) value at that point. With this data, a continuous curve of gamma emission through the interval of stratigraphy was produced by connecting these points.

While of the focus of data collection was from the parasequences in the Monkton, the unit also contains lithologies (ex, lithofacies 5) that are not part of a cycle. Like the continuous survey through a cycle, readings were taken for one minute and then averaged to get a gamma value in (cps) for these lithologies. The gamma-ray spectrometer was positioned as much in the middle of the bed of interest as possible. These values were not used to produce any sort of curve, just to identify relative gamma values for certain lithofacies.

3.4.2 Well Survey

Both the Fleming and the previously logged Champlain College wells are located within the city limits of Burlington, Vermont. The Fleming well is a former teaching well located on the University of Vermont campus (Figure 3.3) that was drilled in 1996. The total depth of the well is ~ 91 meters with the first 41 meters in casing. Gamma data was collected using a Mount Sopris Instruments 2PGA-1000 POLY- GAMMA PROBE taking readings in 5 cm increments. The well was logged twice with the gamma tool. A caliper tool was also used to log the diameter of the entire well to be used in open-hole well water corrections. Water is located within the well at ~68 meters in depth. Additionally, a downhole camera was used to get imagery of the stratigraphy through the uncased portion of the well. The previously logged Champlain College data was acquired from Jon Kim of the Vermont Geologic Survey. This well was logged by Jon Kim and Edwin Romanowicz (S.U.N.Y Plattsburgh) in 2012 using the same Mount Sopris Instruments 2PGA-1000 POLY- GAMMA PROBE taking reading in 3 cm increments.

The raw and filtered data for both the Fleming well and Champlain College wells can be found in Maguire, et al. (2018).

Both the wells and outcrops in the Burlington area could be correlated using strike and dip data for bedding and DEM elevation data. Using strike, dip and distance data, the stratigraphic sections of Fleming and Champlain College wells and the outcrops at Redstone Quarry and the Salmon Hole were hung from the contact of the overlying Winooski Formation (Figure 3.4). From this it was determined that ~12 m of uncased stratigraphy overlapped between the two wells and that the Salmon Hole and Redstone Quarry outcrops lay within the casing of the Fleming well.

In order to test the physical correlation between the two wells a statistical method was also used. The goal of this statistical method was to compare the gamma curve from the portions of the Fleming and Champlain wells that overlap, according to physical stratigraphy. A statistical test would confirm if our original physical correlation was statistically viable or if there are other correlations that are more likely. A correlation coefficient, or linear dependence of two variables or sets of data, was used to see how strong the correlation is of an interval of the Fleming well gamma data to an interval of the Champlain College well gamma data. To do this, the portion of the Fleming well that overlaps (according to our physical correlation) was broken into thirds of approximately 4 meters in thickness to create manageable intervals of comparison. The correlation coefficient was calculated sequentially descending through the Champlain College well. This process was repeated for each of the three segmented intervals through the entire

Champlain College well. Results indicate the physical correlation between wells has a high (~0.7) statistically significant correlation for each of the three segments, suggesting that the physical correlation is correct. However, there were other levels within the Champlain College well that also had a high statistical correlation coefficient to the Fleming well. If these alternative correlations are accepted it would require a more complicated scenario. The closest and least complicated alternative position was located between 50-55 m depth in the Champlain College well. For this to be possible the two wells could be offset by a high angle fault with a displacement of 23.5 m. Additionally, a bedding attitude change of 3 degrees between the two wells could also explain the alternative correlation. A broad fold that changes dip magnitude a few degrees over .61 miles is plausible, however there is no evidence of this. Neither is there evidence of faulting. Finally, because of the repetitive occurrence of cycles with a similar architecture and gamma values the statistically significant correlation coefficients may occur simply because of in a segment of a stratigraphic sequence it wouldn't be possible to distinguish one cycle from another; a thicker record would be needed. For these reasons we believe that the physical correlation shown in Figure 3.4 is correct. However, the alternative interpretations cannot be completely ruled out. Based on the original correlation as a whole, nearly 350 meters of Monkton stratigraphy was represented in our well and outcrop data.

3.5. Data Processing Methods

3.5.1 Well Log Filtering

The intensity of gamma emissions is controlled by the abundance of radioactivity-emitting minerals present in different lithologies, however gamma log data is subject to random *noise* due to the counting statistics other sources of error and because radioactive processes are inherently subject to statistical variation (Czubek, 1986). Additionally, variation in gamma log data can vary between logs due to logging speed and tool calibration (Doveton, 1994).

A series of data filtering steps were taken to remove unusable data, adjust for water within the wells and to reduce noise. The same filtering procedures were done on both wells. All data from in well casings was deemed unusable and omitted from discussions. Though attenuation from well casing can be adjusted for, data in both well casing was omitted from this study because of the limited amounts of bedrock stratigraphy within them. Both the Champlain College and Fleming wells contained water below ~56 and ~68 meters, respectively. An industry standard correction factor for all points, within open water filled holes, based on hole diameter was applied to these portions of the wells. (Mont Sopris Instruments, 2008).

Smoothing of the raw gamma emission data was completed to suppress statistical noise and account for variation in vertical resolution inherent to gamma logging tools. Two assumptions about borehole gamma logging were used in setting the parameters for filtering. First, the vertical resolution of a gamma probe is between 30-60 cm which means that any gamma data point could be measuring emissions over this interval of well

stratigraphy. Second, across this vertical resolution readings are being picked up in a symmetrical probability distribution relative to the center of the sensor (Cannon, 2015; Gadeken et al., 1997; Theys, 1999). To account for these two factors a moving average was taken vertically over ~40 cm of data points in the well log and weighted over a symmetrical distribution. The symmetrical distribution curve used was a Hann Curve, such that values in the center of the data points being averaged were weighted more in the moving average than those at the top and bottom or, in other words, the gamma probe, over the vertical resolution, was less influenced by rocks further away from it than by the rocks directly adjacent to it.

3.5.2. Outcrop Survey

From outcrop data, four endmember Monkton lithofacies were identified to be most useful in subsurface interpretations (1) clear water subtidal platform carbonates; (2) a variety of subtidal sandstones and sandy dolostones; (3) the intertidal sand, silts and dolostones representative of the tidal flat; (4) supratidal/high intertidal cryptalgal laminate dolostone. The relative gamma values measured from these lithologies are shown in Figure 3.5.

The results of the survey from Redstone Quarry can be seen in Figure 3.6 which illustrates the observed gamma ray curve from two mixed siliciclastic-carbonate parasequences. Both cycles represent the transition from the clastic dominated intertidal sandstones and siltstones vertically into the carbonate dominated supratidal dolostones. The abrupt lithologic change at the base of a cycle, transitioning from carbonate to

siliciclastic lithologies, is interpreted as the marine flooding surface (MFS) and can be identified from the abrupt gamma value increase. The higher gamma value holds steady in the heterolithic intertidal lithology until it gradually decreases in value moving up in the stratigraphy. This gradual decrease represents the gradational transition into the supratidal cryptalgal laminate dolostone. Comparing the two cycles illustrated in Figure 3.6 illustrates that the thicker cycles show more internal variation in gamma emission data; the serrated shape of the lower curve represents the interbedding of sandstone and siltstone lithologies that is not developed in the thinner parasequence.

3.5.3. Fleming Well

The relative gamma values for the lithologies and the gamma curve shapes predicted for cycles, based on outcrop results, were used to identify the parasequences and platform carbonate intervals within the Fleming Well gamma log. The gamma curve interpretations in the Fleming well were confirmed using the borehole camera imagery within the well log, details of which can be found in Maguire, et al. (2018). Results confirm what was observed from the outcrop logging: the platform dolostones have the lowest gamma values while the interbedded sands, silts, and dolostones recording tidal flat environments are characterized by the highest relative gamma values. The cryptalgal laminate dolostone lithology is characterized by a lower-middle gamma value.

3.5.4 Champlain College Well

The Fleming and Champlain College Wells were both logged at different speeds and sampling intervals which lead to overall variation in absolute gamma emission

values. Correlations, in the ~11 m of uncased overlapping stratigraphy between the peaks in the gamma logs identified that the Champlain College Well gamma peak values were ~25 (cps) higher on average than the Fleming Well peak values. This slightly higher gamma value was factored into interpretations within the Champlain College Well.

Unlike the Fleming Well, the Champlain College Well did not have borehole camera data to help identify subsurface characteristics. The ability to recognize parasequences and certain lithologies was developed from the analysis of the Fleming well. The Champlain College Well was analyzed using the same approach as the Fleming well. The intertidal to supratidal parasequence illustrated in Figure 3.6 and described from the Fleming Well was the easiest cycles to recognize in the Champlain Well. The characteristically low gamma values of significant dolostone horizons, interpreted as subtidal platform carbonates, are also clearly identifiable.

3.6. Results

Using the gamma curves and bedding attitudes the Fleming and Champlain College wells were correlated and their positions with respect to the Monkton/Winooski contact determined. Parasequences that record inter-to supratidal shallowing up cycles and thicker subtidal platform dolostone horizons were identified and compiled and plotted relative to their position below the Monkton and Winooski contact (Figure 3.7). The composite data from the two wells will be used to identify the stratigraphic distribution and thicknesses of parsequences to make interpretations regarding stratigraphic trends.

In Figure 3.7 Parasequence sets have been-identified and separated by the thin red horizontal lines. The red arrows within the sets indicate decreasing or increasing thickness trends of the cycles of that parasequence set. After examining the data the stratigraphy has been broken into three distinguishable segments identified on Figure 3.7 as “Intervals”. An “Interval” is identified based on the frequency and thickness of parasequence sets and the frequency of the platform carbonate lithology.

The portion of the well identified as “Interval 2” in Figure 3.7 contains stratigraphy with the most well-developed Type 1 parasequence sets. Interval 2 contains both the thickest single parasequences and thickest parasequence sets seen in the entire composite section. The parasequence sets in Interval 2 are deposited one after another without interruption. Additionally, in Interval 2 there is only one occurrence in the stratigraphy of the platform carbonate. Since the parasequences representing tidal flat progradation are well developed and uninterrupted and because of the low frequency of occurrence of the platform carbonate lithology, Interval 2 is interpreted to represent deposition on a well-developed tidal flat and the generation of accommodation space that was able to keep up with deposition.

Interval 3 contains Type 1 parasequence sets like Interval 2, however they are not in succession and the parasequences within them are not as thick. These changes are interpreted to represent decreasing accommodation space because with less space for sediment being created in the nearshore, sediment would be moved further out onto the shelf instead of accumulating on the tidal flat. Interval 3 also contains the highest

frequency of the platform carbonate lithology, often found separating the parasequence sets. We interpret these carbonates as recording clear water deposition following periodic flooding events that trap siliciclastic sediment on the coastal plain, allowing for a return to clear water carbonate deposition.

Interval 1 contains few repeating parasequence sets and only one instance of the platform carbonate lithology. A large portion of Interval 1, between ~265-295 meters below the Monkton/Winooski contact, is characterized as poorly cyclic, based on the lack of identifiable parasequences. The gamma values seen in this interval of poor cyclicity are consistent with subtidal sand values. We interpret the lack of cyclicity to the complex depositional processes in the subtidal and the likelihood that the tidal flat is never established, thus the identifiable Type 1 cycles are not being generated.

Figure 3.7 also shows a generalized sea level curve representing the Sauk II transgression (blue line) and an interpreted accommodation space curve (black line) based on our data. The accommodation space curve was generated by interpreting the bathymetry associated with the parasequences identified in the well log. The cryptalgalaminite lithology (Lithofacies 3) represents sediment which accreted up to/at sea level and thus represents minimum space for additional sediment, in other words, minimal accommodation space, and the sea level rise which followed deposition of this lithofacies created new accommodation space. This sea level rise can also result in deposition of the platform carbonate lithology as a result of clastic sediment trapping on the coastal plain, so the platform carbonate lithofacies represent flooding events. A

thinning parasequence set corresponds to a decrease in accommodation space while a thickening set indicates an increase in available accommodation space.

3.7. Discussion

The successful identification of parasequence sets and lithologies that signify variation in accommodation space through the composite section allows us to describe and interpret changes that occurred throughout the Monkton Formation. The interpretations of Intervals I-III on Figure 3.7 indicate that there is an overall decrease in accommodation space being generated through the Monkton stratigraphy. Though the Monkton was being deposited during the overall transgression at the start of Sauk II, on this portion of the Iapetus shelf the ability to generate accommodation space decreased over time. Since in the case of the Monkton Formation changes in sea level were the primary control on accommodation space generation, these results would conclude that the *rate* of sea level rise changed through deposition. The combination of relative sea level rise during Sauk II and decreasing accommodation space can only be generated by a decrease in the *rate* of sea level rise during Monkton Deposition.

As discussed in Posamentier and Allen (1999), trends in accommodation space through a unit are a useful tool for interpreting the systems tract it formed in, and by extrapolation, how overall sea level was changing. Posamentier and Allen (1999) described a highstand system tract as commonly containing progradational deposits that form when sediment accumulation exceeds the rate of increase in accommodation space. However, progradational deposits can also form during a transgressive systems tract

when the rate of sediment accumulation exceeds the rate of increase in accommodation space. Because our data indicates a loss in accommodation space over time, progradation of the tidal flat deposits that characterize the Monkton Formation and the decreasing trend in accommodation space suggests that transgressive system tract deposition was coming to an end as highstand conditions are approached (Figure 3.8 A). If this were the case, we would also expect to see the onset of clear water carbonate deposition marking the transition to a highstand systems tract. No such interval is present within the Monkton, however, the contact between the Monkton and Winooski Formations, with the shoreline at its maximum landward position, could be interpreted to represent this transition. If the Monkton was deposited, as we think, entirely in the transgressive systems tract, then the decreasing accommodation space generation documented in this unit would represent a decreasing rate in sea level rise within the transgression (Figure 3.8). Following this decreasing sea level rise, Monkton deposition ceases, possibly due to a rapid increase in sea level at the end of the transgression system tract, marking the beginning of the Winooski Dolostone deposition. This transition marks the start of the highstand systems tract, represented by the onset of clear water carbonate deposition and of the Winooski Dolostone.

CHAPTER 3: FIGURES

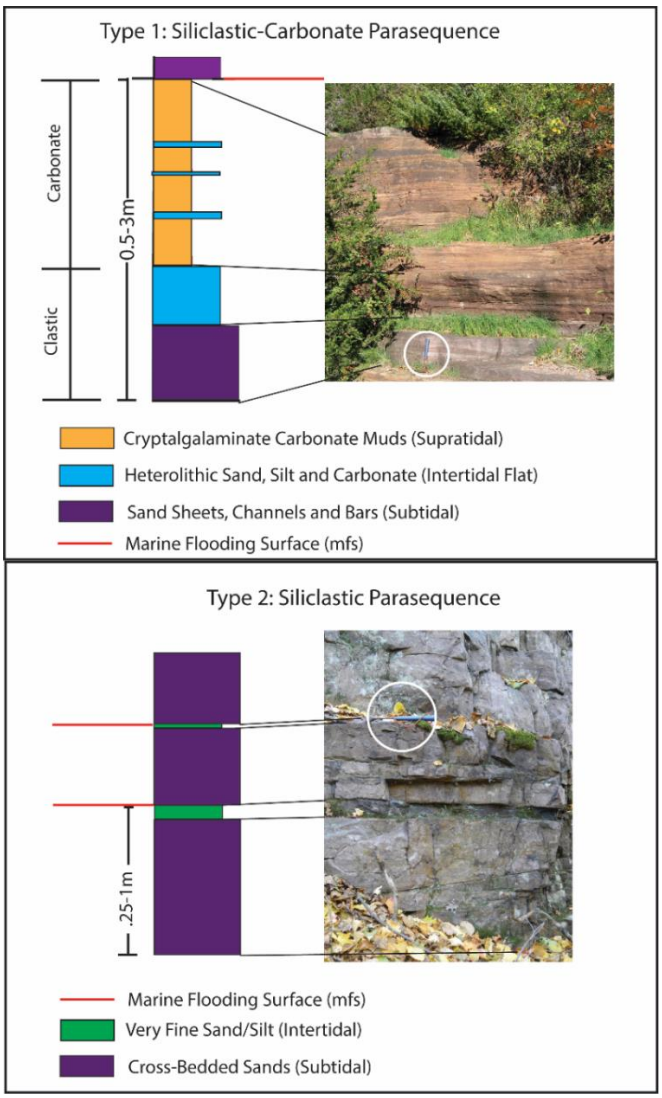

Figure 3.1. Stratigraphic columns and corresponding outcrop examples of Rahmanian's Type 1 and Type 2 parasequences (Rahmanian, 1981). The Type 1 cycle architecture example is from Redstone Quarry and represents the transition from subtidal and tidal channel deposits at the base into intertidal heterolotihic deposits and eventually towards a carbonate dominated intertidal-supratidal deposit at the top. The Type 2 cycle architecture illustrated is from Pease Mountain and represents the transition from a subtidal bar and tidal channel deposit moving up into a mixedsand and mud intertidal flat deposit. The red lines on the columns mark the maximum flooding services at the top of the parasequences. Circled in white are rock hammers for scale.

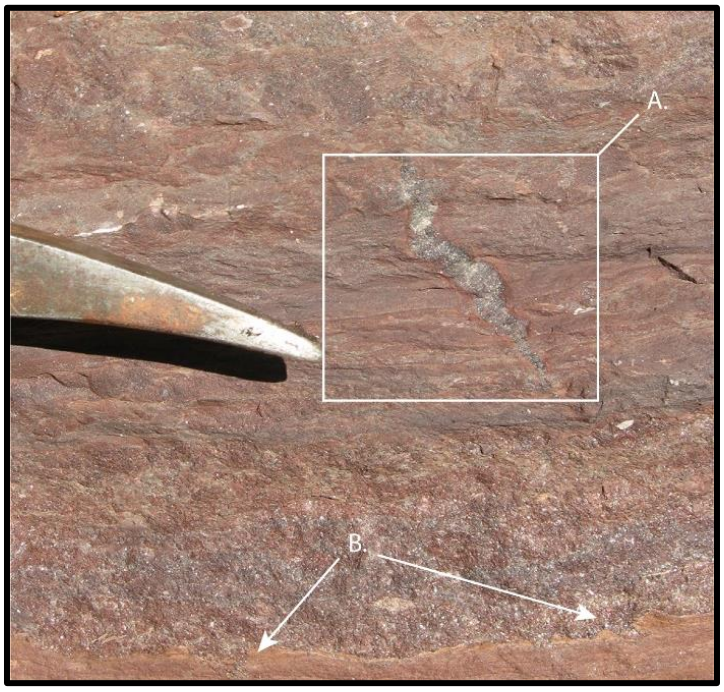

Figure 3.2. Outcrop photograph of lithofacies 5 from Redstone Quarry. This lithofacies is a poorly sorted arkosic sandstone with abundant accessory minerals. Dewatering (A) and load cast structures (B) are labeled. Both are interpreted to record rapid sedimentation in a shallow subtidal envrionemnt. The hammer head is for scale and its length is approximately 8 cm.

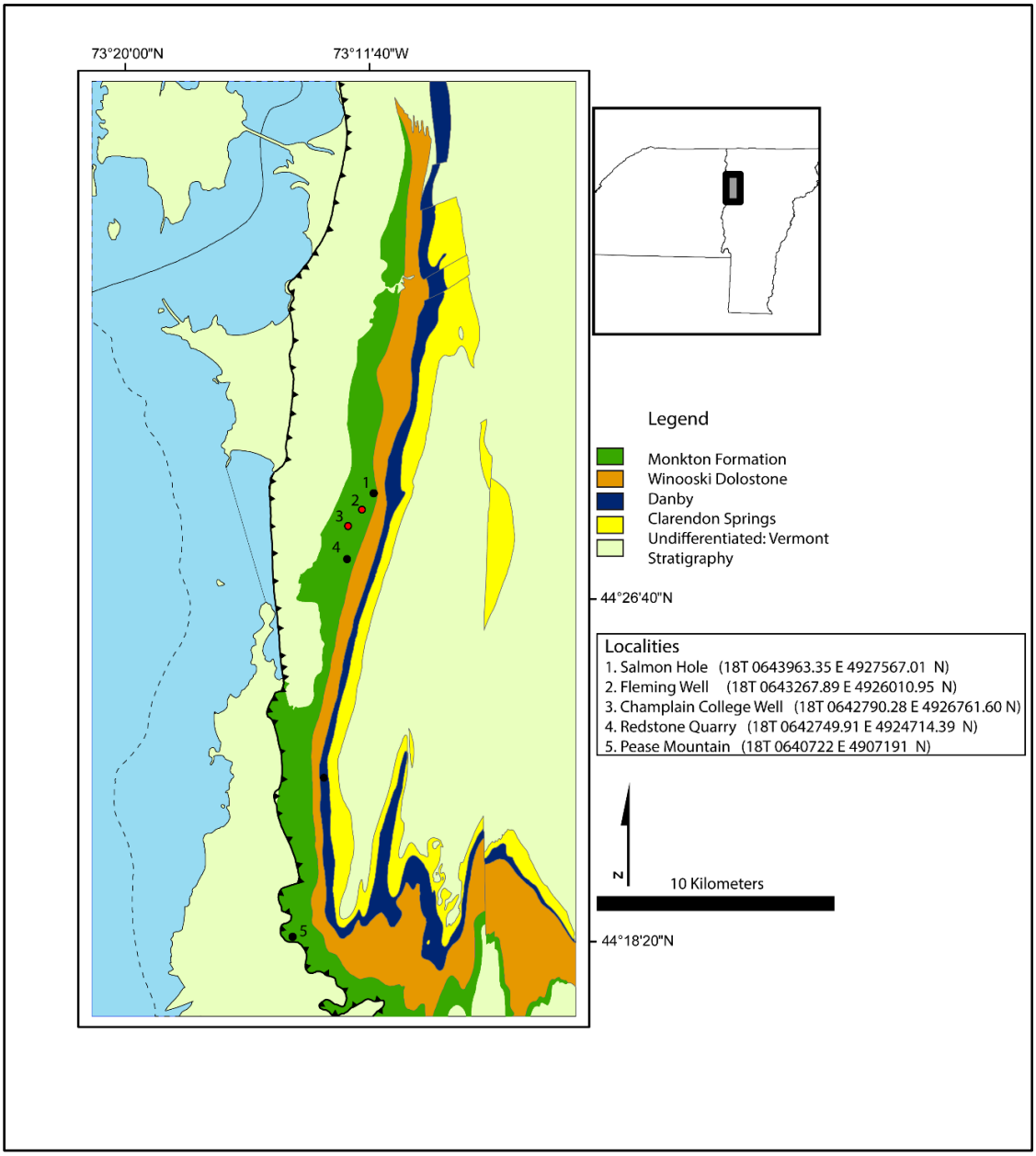

Figure 3.3. Simplified bedrock geologic map of Vermont showing localities for wells and outcrop studies within the Monkton Formation. Base map is the bedrock geologic map of Vermont Ratcliffe et al. (2011).

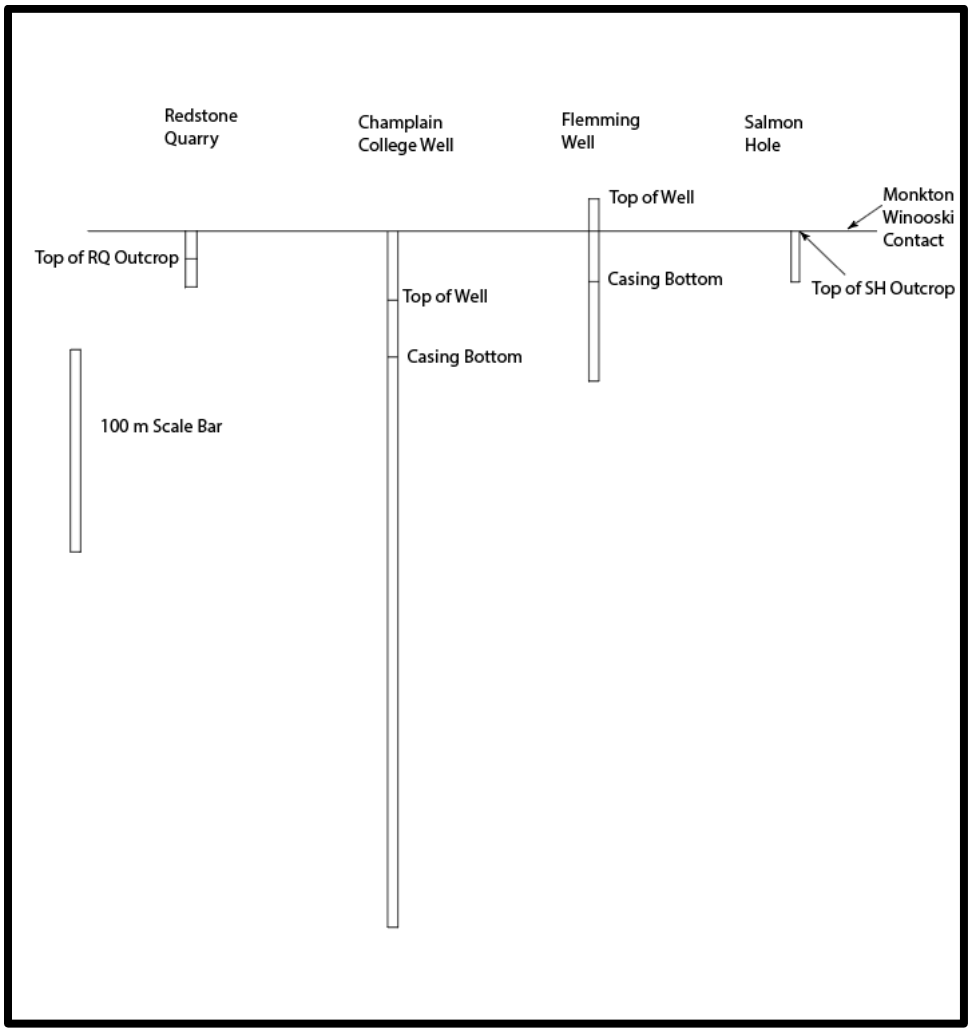

Figure 3.4. Relationships between Monkton stratigraphic intervals from wells and outcrops. The stratigraphic intervals were hung with their relationship to the contact between the Winooski and Monkton Formations. These relationships were identified using elevation and distance data from DEM maps and dip data from two outcrops to the north and south of the wells. The attitude measured from the two outcrops was of bedding planes and a mean strike and dip of 015^{o} 07^{o}, respectively. The intervals of stratigraphy could then be projected with respect to their relationship with the Winooski Monkton contact.

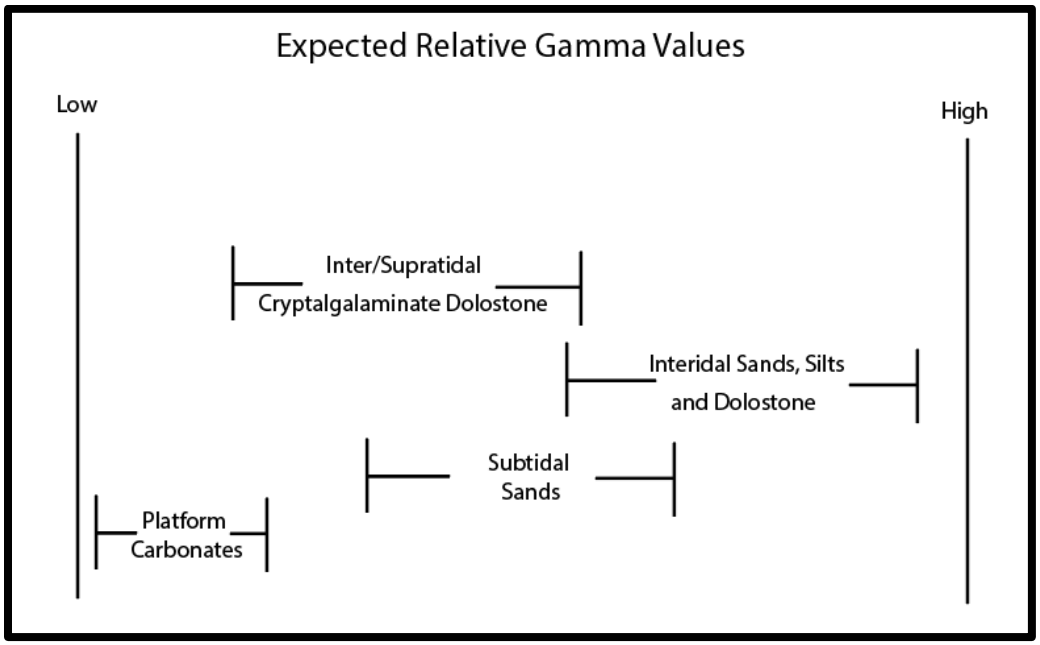

Figure 3.5. Expected relative gamma values for lithologies used in subsurface interpretations. These are not assigned exact gamma values but show the relative overlap and relationship between them. Because of the overlap it is also essential that the gamma ray curve shape must also be incorporated into interpretations of gamma emission patterns.

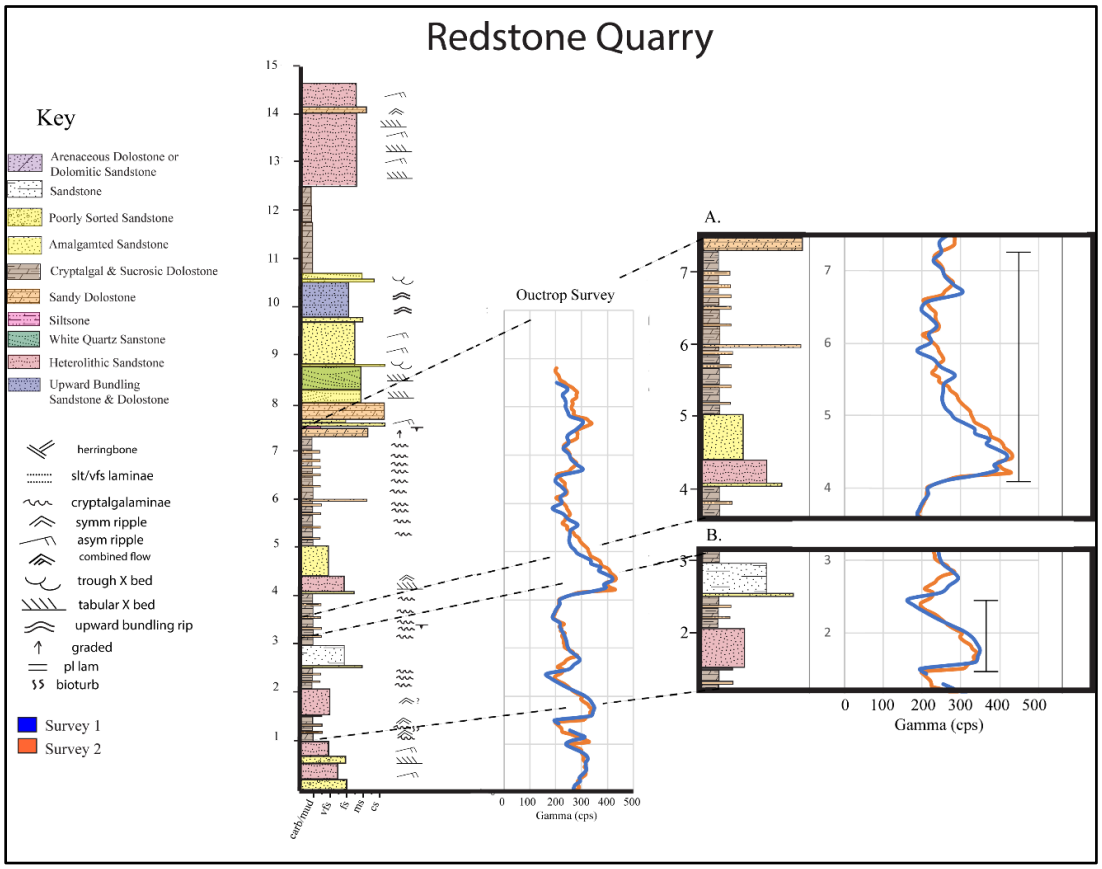

Figure 3.6. Redstone Quarry stratigraphic column with outcrop survey gamma results. Survey 1 was completed in 10 cm increments and survey 2 in 5 cm. Outcrop survey results of intervals representing two of the Rahmanian's Type 1 parasequences are highlighted (Rahmanian, 1981). Both cycles have an abrupt boundary on the bottom of the gamma curve and then gradually grades upward through the cycle. Example A is a thicker parasequence and as a result the interbedding of lithologies can be seen in the jagged gamma emission curve. The detailed jagged curve representing interbedded silt and cryptalgal dolostone is not seen in example B, the nature of the survey would not necessarily pick up the interbedding in thin interval. It should be noted that neither of the examples illustrated here contain a subtidal basal unit that is seen elsewhere.

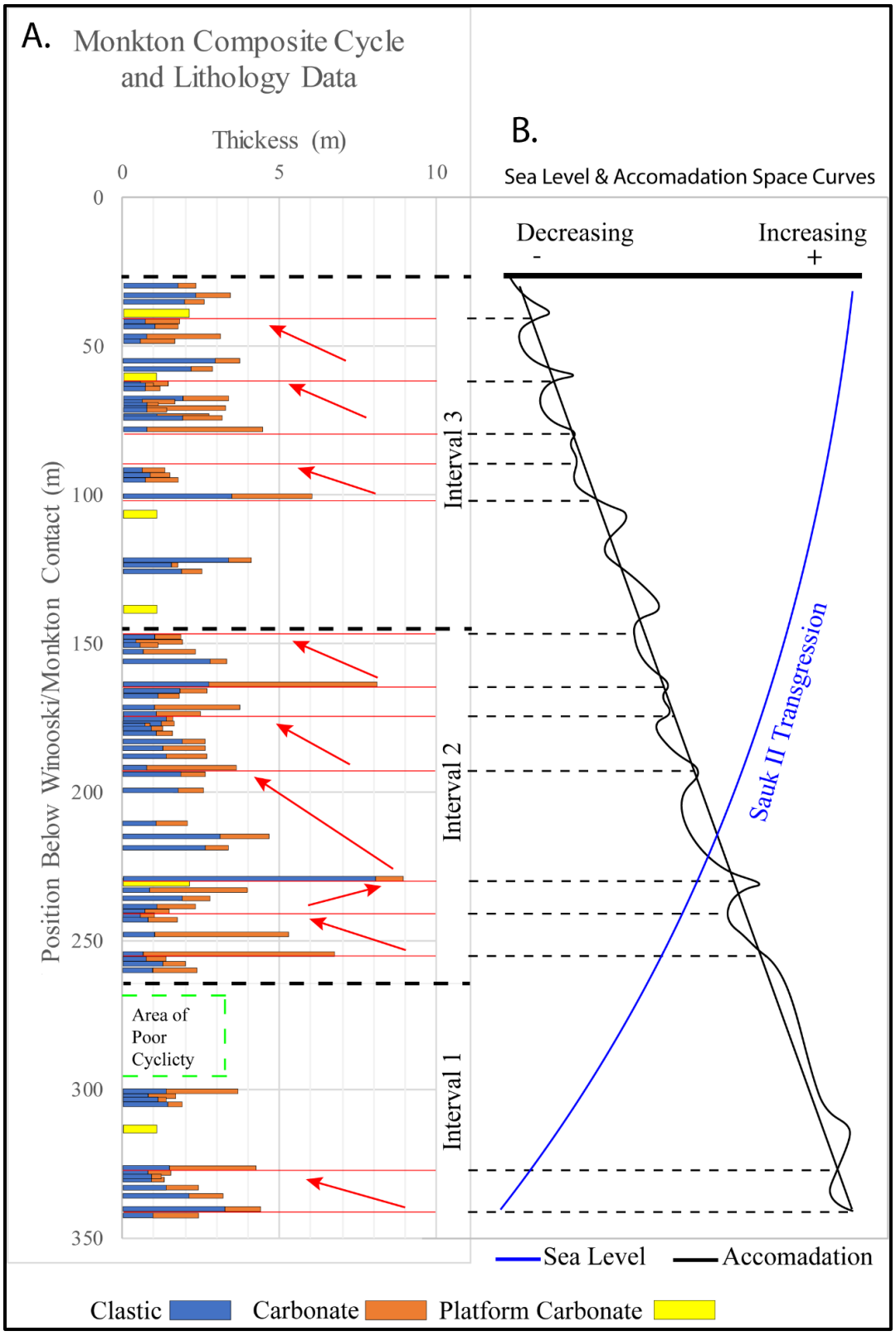
A.
Monkton Composite Cycle and Lithology Data
Thickess (m)
0
5
10
0
50
100
150
200
250
300
350
Position Below Winooski/Monkton Contact (m)
Interval 3
Interval 2
Interval 1
Area of Poor Cyclicty
B.
Sea Level & Accomadation Space Curves
Decreasing
-
Increasing
+
Sauk II Transgression
Sea Level
Accomadation
Clastic
Carbonate
Platform Carbonate

Figure 3.7. Interpretation of parasequence architecture through the composite Champlain and Fleming wells (A) are plotted (B) versus the Sauk II transgression (blue line) and the interpreted changes in accommodation space (black line). A. Parasequence thickness and stratigraphic position relative to the Monkton/Winooski contact. Colors represent the thickness of clastic and carbonate components of Rahmanian's Type 1 parasequences and of the platform carbonate lithology. The red horizontal lines represent the boundaries between parasequence sets, while the red arrows identify the trends in parasequence thickness within a set. B. Interpreted accommodation space curve (black line) is related to the thinning or thickening of parasequence sets and the presence of the platform carbonate lithology. See text for further discussion.

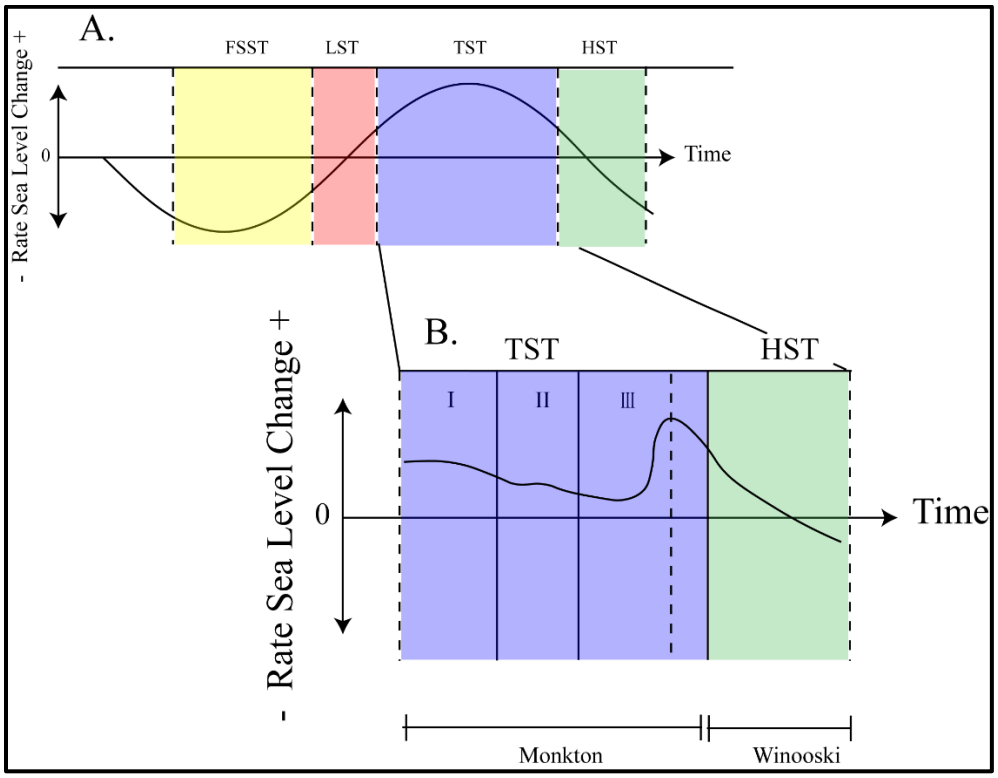

Figure 3.8. Rate in sea level change curves for systems tracts model (A) and interpretation of sea level changes through Monkton deposition (B). For both curves the x axis represents time while the y the rate in sea level change. Any values above 0 on the Y axis would represent sea level rise, just at varying rates. (A.) modified from Catuneanu (2002) shows the predicted rate in sea level change during falling stand systems tract (FSST), lowstand systems tract (LST), transgressive systems tract (TST) and highstand systems tract (HST). The sea level curve in (B.) shows the how rates have changed over Monkton and Winooski deposition. The area shaded purple shows where the TST is and the green shaded areas is where HST is believed to have occurred. Looking at (B.) the curve through Intervals I-III it is overall decreasing. This decreasing rate would indicate a decreasing generation of accommodation space. There is a dashed line at the end of Interval III because according to our projections of the Winooski Monkton contact there is a portion of Monkton stratigraphy above it not represented by well log data. The interval between Winooski deposition and Interval III is believed to contain a rapid rate in sea level rise, marking the maximum flooding surface and the transition to HST.

CHAPTER 3: TABLES

Lithofacies	Lithologies	Sedimentary Structures	Depositional Environment	Expected Well Log Gamma Values
1	moderately to well sorted sandstone, variably dolomitic	trough and tabular, herringbone cross stratification, horizontal laminations	subtidal sand bars	~100-200 (cps)
2	sandstone, siltstone, dolostone	ripples, mudcracks, bioturbation, flaser bedding	intertidal sand flat	~150-250 (cps)
3	dolostone, siltstone	crypyalgalaminations, rip up clasts	tidal ponds	~60-150 (cps)
4	sucrosic dolostone, arenaceous dolostone	uncommonly rippled or cross stratified	subtidal shelf	<~60 (cps)
5	Poorly sorted arkosic sandstone, abundant accesssory minerals	dewatering structures, load casts and burrows	"event beds", rapidly deposited unsorted sediment on the tidal flat	>~250 (cps)

Table 3.1: Summary of lithologies identified in outcrop and subsurface studies. The depositional environments of these lithologies are identified by their sedimentary structures. These identified depositional environments make these lithologies ideal bathymetric indicators. The expected gamma values of these lithologies within the well log are a general guide and not absolute in interpretations, depending on the thickness of the bed and the adjacent lithologies this can vary.

CHAPTER 3: BIBLIOGRAPHY

Beerbower, J. R., 1964, Cyclothems and cyclic depositional mechanisms in alluvial plain sedimentation: Kansas Geological Survey Bulletin, v. 169, no. 1, p. 31-32.

Bond, G. C., 1997, New constraints on Rodinia breakup ages from revised tectonic subsidence curves. In Geological Society of America Abstracts with Programs, v. 29, no. 5, p. 280.

Cady, W. M., 1945, Stratigraphy and structure of west-central Vermont: Geological Society of America Bulletin, v. 56, no. 5, p. 515-588.

Cannon, S., 2015, Petrophysics: a practical guide, John Wiley & Sons, New York, NY.

Catuneanu, O., 2002, Sequence stratigraphy of clastic systems: concepts, merits, and pitfalls: Journal of African Earth Sciences, v. 35, no. 1, p. 1-43.

Cecil, C. B., 2003, The concept of autocyclic and allocyclic controls on sedimentation and stratigraphy, emphasizing the climatic variable: SEPM Special Publication, No. 77.

Czubek, J.A., 1986, January. Quantitative interpretation of gamma-ray logs in presence of random noise, In: SPWLA 27th Annual Logging Symposium. Society of Petrophysicists and Well-Log Analysts.

Doveton, J.H., 1994. Geological log interpretation, SEPM (Society for Sedimentary Geology) Short Course, No 29.

Gadeken, L.L., Jacobson, L.A. and Merchant, G.A., Halliburton Logging Services Inc, 1997. Method for filtering gamma ray well logging tool response to enhance vertical detail while suppressing statistical noise. U.S. Patent 5,672,867.

Goldberg, J., and Mehrtens, C., 1998, Depositional environment and sequence stratigraphy interpretation of the lower Middle Cambrian Monkton Quartzite, Vermont: Northeastern Geology and Environmental Sciences, v. 20, p. 11-27.

James, N. P., Botsford, J. W., and Williams, S. H., 1987, Allochthonous slope sequence at Lobster Cove Head: evidence for a complex Middle Ordovician platform margin in western Newfoundland: Canadian Journal of Earth Sciences, v. 24, no. 6, p. 1199-1211.

Kay, G. M., 1942, Ottawa-Bonnechere graben and Lake Ontario homocline: Bulletin of the Geological Society of America, v. 53, no. 4, p. 585-646.

Kim, J., Romanowicz, E., and Mehrtens, C., 2013, Using Deep Bedrock Well Logs to Constrain Stratigraphic and Structural Problems in Vermont, *in* Proceedings, NGWA Conference on Groundwater in Fractured Rock and Sediments: Middlebury, VT, NGWA.

Kumarapeli, Pintson, H., Dunning, G. R., & Stearn, C. W., 1989, Age of the Tibbit Hill Formation and its implications on the timing of Iapetan rifting. Program with Abstracts - Geological Association of Canada; Mineralogical Association of Canada: Joint Annual Meeting, v. *14*, p. 125-125.

Landing, E., Benus, A. P., and Whitney, P. R., 1992, Early and early middle Ordovician continental slope deposition: shale cycles and sandstones in the New York promontory and Quebec reentrant reentrant region, New York State Museum Bulletin, No. 474.

Li, Z.-X., Evans, D. A., and Halverson, G. P., 2013, Neoproterozoic glaciations in a revised global palaeogeography from the breakup of Rodinia to the assembly of Gondwanaland: Sedimentary Geology, v. 294, p. 219-232.

Maguire, H.C., Mehrtens, C. J., Kim and J., Romanowicz, E., 2018, Data Processing for Two Well Logs in Burlington, VT:Vermont Geological Survey, Open-File Report 2018. Manuscript in Preperation.

Mehrtens, C. J., and Gregory, G., 1984, An occurrence of Salterella conulata Clark in the Dunham Dolomite (Lower Cambrian) of northwestern Vermont and its stratigraphic significance: Journal of Paleontology, p. 1143-1150.

Mitchum, R., and Van Wagoner, J. C., 1990, High-frequency sequences and eustatic cycles in the Gulf of Mexico basin, *in* Proceedings Sequence stratigraphy as an exploration tool: concepts and practices in the Gulf Coast: Gulf Coast Section SEPM, 11th Annual Research Conference Proceedings 1990, SEPM, p. 257-267.

Mount Sopris Instruments., 2008, 2PGA-1000 POLY- GAMMA PROBE Manual, p. 12.

Palmer, A., and Taylor, M., 1981, Subdivision of the Sauk sequence, *in* Proceedings Short Papers for the Second International Symposium on the Cambrian System: US Geological Survey, Open-File Report, p. 81-743.

Palmer, A. R., 1971, The Cambrian of the Appalachian and eastern New England regions, eastern United States: Wiley-Interscience., London-New York.

Palmer, A. R., and James, N. P., 1980, The Hawke Bay event: a circum-Iapetus regression near the Lower–Middle Cambrian boundary. Memoir - Virginia Polytechnic Institute, Department of Geological Sciences, v. 2, p. 15-18.

Posamentier, H.W., Vail, P.R., 1988. Eustatic controls on clastic deposition. II. Sequence and systems tract models. In: (Eds Wilgus, C.K., Hastings, B.S., Kendall, C.G.St.C., Posamentier, H.W., Ross, C.A., Van Wagoner, J.C.), Sea Level Changes—An Integrated Approach, SEPM Special Publication, v. 42, p. 125-154.

Posamentier, H. W., and Allen, G. P., 1999, Siliciclastic sequence stratigraphy: concepts and applications, SEPM Concepts in Sedimentology and Paleontology, no. 7, p. 210.

Rahmanian, V., 1981, Transition from carbonate to siliciclastic tidal flat sedimentation in the Lower Cambrian Monkton Formation, West central Vermont: The Green Mountain Geologist, v. 7, no. 4, p. 20-21.

Raine, R. J., and Smith, M. P., 2012, Sequence stratigraphy of the Scottish Laurentian margin and recognition of the Sauk Megasequence, In: Derby, J.T., Fritz, R.D., Longacre, S.A., Morgan, W.A., and Sternbach, C.A., eds., The Great American Carbonate Bank: The Geology and Economic Resources of the Cambrian-Ordovician Sauk Megasequence of Laurentia; AAPG Memoir., 98, p. 575-596.

Ratcliffe, N. M., Stanley, R. S., Gale, M. H., and Thompson, P. J., 2011, Bedrock geologic map of Vermont: U.S. Geological Survey Scientific Investigations Map 3184, scale 1:100,000, 3 sheets.

Schuchert, C., 1933, Cambrian and Ordovician stratigraphy of northwestern Vermont: American Journal of Science, no. 149, p. 353-381.

Schuchert, C., 1937, Cambrian and Ordovician of northwestern Vermont: Bulletin of the Geological Society of America, v. 48, no. 7, p. 1001-1078.

Shaw, A. B. 1958. Stratigraphy and structure of the Saint Albans area, northwestern Vermont. Geological Society of America Bulletin, v. 69, no. 5, p. 519-567.

Sloss, L., 1963, Sequences in the cratonic interior of North America: Geological Society of America Bulletin, v. 74, no. 2, p. 91-114.

Speyer, S., 1983, Subtidal and intertidal clastic sedimentation in a Lower Cambrian sequence; Monkton Quartzite, northwestern Vermont: Northeastern Geology, v. 5, no. 1, p. 29-39.

Stanley, R. F., 1999, The Champlain thrust fault at Lone Rock Point, *in* Proceedings, Annual Meeting New England Intercollegiate Geological Conference, 91st Annual Meeting, 1999, Burlington, VT, p. 359-364.

Theys, P., 1999, Log data acquisition and quality control: Editions Technip. Paris, France, 330p.

Thomas, W. A., 1977, Evolution of Appalachian-Ouachita salients and recesses from reentrants and promontories in the continental margin: American Journal of Science, v. 277, no. 10, p. 1233-1278.

Van Wagoner, J., Posamentier, H., Mitchum, R., Vail, P., Sarg, J., Loutit, T., and Hardenbol, J., 1988, An overview of the fundamentals of sequence stratigraphy and key definitions. In: *Sea Level Changes – An Integrated Approach* (Eds C.K. Wilgus, B.S. Hastings, C.G.St.C. Kendall, H.W. Posamentier, C.A. Ross and J.C. Van Wagoner), SEPM Special Publication, 42, 39-45.

Van Wagoner, J. C., 1995, Overview of sequence stratigraphy of foreland basin deposits: terminology, summary of papers, and glossary of sequence stratigraphy. In: *Sequence Straigraphy of Forland Basin Deposits: Ouctrop and Subsurface Examples from the Cretaceous of North America* (Eds J.C. Van Wagoner and G.T. Bertram), AAPG Memoir., 64, ix-xxi

Van Wagoner, J. C, Mitchum, R. M, Campion, K. M, & Rahmanian, V. D., 1990, Siliciclastic sequence stratigraphy in well logs, cores, and outcrops : *concepts for high-resolution correlation of time and facies.* Tulsa (Okla.): American association of petroleum geologists

COMPREHENSIVE BIBLIOGRAPHY

Aleinikoff, J. N., Zartman, R. E., Walter, M., Rankin, D. W., Lyttle, P. T., and Burton, W. C., 1995, U-Pb ages of metarhyolites of the Catoctin and Mount Rogers Formations, central and southern Appalachians: Evidence for two pulses of Iapetan rifting: American Journal of Science, v. 295, no. 4, p. 428-454.

Badash, L., 1968, Rutherford, Boltwood, and the age of the earth: the origin of radioactive dating techniques: Proceedings of the American Philosophical Society, v. 112, no. 3, p. 157-169.

Beerbower, J. R., 1964, Cyclothems and Cyclic Depositional mechanisms in alluvial plain sedimentation: Kansas Geological Survey Bulletin, v. 169, no. 1, p. 31-32.

Boltwood, B. B., 1907, ART. VII.--On the Ultimate Disintegration Products of the Radio-active Elements. Part II. The Disintegration Products of Uranium: American Journal of Science (1880-1910), v. 23, no. 134, p. 77.

Bond, G. C., 1997, New constraints on Rodinia breakup ages from revised tectonic subsidence curves. In Geological Society of America Abstracts with Programs, v. 29, no. 5, p. 280.

Brink, R. A., 2015, Depostional Environments and Provenance of the Late Lower-Earyl Middle Cambrian Altona Formation (Potsdam Group) [M.S. Thesis]: University of Vermont.

Brown Jr, L.F. and Fisher, W.L., 1977. Seismic-Stratigraphic Interpretation of Depositional Systems: Examples from Brazilian Rift and Pull-Apart Basins: Section 2. Application of Seismic Reflection Configuration to Stratigraphic Interpretation: AAPG Memoir, m. 26, p. 2-13-248.

Cady, W. M., 1945, Stratigraphy and structure of west-central Vermont: Geological Society of America Bulletin, v. 56, no. 5, p. 515-588.

Cannon, S., 2015, Petrophysics: a practical guide, John Wiley & Sons, New York, NY.

Cant, D. J., and Hein, F. J., 1986, Depositional sequences in ancient shelf sediments: some contrasts in style: Canadian Society of Petroleum Geologists Special Publications.

Catuneanu, O., 2002, Sequence stratigraphy of clastic systems: concepts, merits, and pitfalls: Journal of African Earth Sciences, v. 35, no. 1, p. 1-43.

Cecil, C. B., 2003, The concept of autocyclic and allocyclic controls on sedimentation and stratigraphy, emphasizing the climatic variable: SEPM Special Publication, No. 77.

Cherichetti, L., Doolan, B., and Mehrtens, C., 1998, The Pinnacle Formation: A late Precambrian rift valley fill with implications for Iapetus rift basin evolution: Northeastern Geology and Environmental Sciences, v. 20, p. 175-185.

Chiarenzelli, J., Aspler, L. B., Donaldson, J. A., Rainbird, R., Mosher, D., Regam, S. P., Ibanez-Mejia, M., and D.A, F., 2010, Detrital zircons of Cambro-Ordovician sandstone units in eastern Ontario and northern New York: Abstracts with Programs - Geological Society of America, v. 42, p. 118.

Clarke, A. J., and Battisti, D. S., 1981, The effect of continental shelves on tides: Deep Sea Research Part A. Oceanographic Research Papers, v. 28, no. 7, p. 665-682.

Conrad, C. P., 2013, The solid Earth's influence on sea level: Geological Society of America Bulletin, v. 125, no. 7-8, p. 1027-1052.

Corfu, F., Hanchar, J. M., Hoskin, P. W., and Kinny, P., 2003, Atlas of zircon textures: Reviews in mineralogy and geochemistry, v. 53, no. 1, p. 469-500.

Cross, T., 1994, High-resolution stratigraphic correlation from the perspective of base-level cycles and sediment accommodation, *in* Proceedings Proceedings of northwestern European sequence stratigraphy congress, Volume 123.

Czubek, J.A., 1986, January. Quantitative interpretation of gamma-ray logs in presence of random noise, In: SPWLA 27th Annual Logging Symposium. Society of Petrophysicists and Well-Log Analysts.

Dalrymple, R., Narbonne, G., and Smith, L., 1985, Eolian action and the distribution of Cambrian shales in North America: Geology, v. 13, no. 9, p. 607-610.

Dalrymple, R.W. (1992) Tidal Depositional Systems. In: Walker, R.G. and James, N.P., Eds., Facies Models: Response to Sea Level Change, Geological Association of Canada, Newfoundland, 195-218.

Dalrymple, R. W., Makino, Y., and Zaitlin, B. A., 1991, Temporal and spatial patterns of rhythmite deposition on mud flats in the macrotidal Cobequid Bay-Salmon River estuary, Bay of Fundy, Canada: CSPG Special Publication, m. 16, p. 137-160.

Daly, J., and McLelland, J., 1991, Juvenile middle Proterozoic crust in the Adirondack highlands, Grenville province, northeastern North America: Geology, v. 19, no. 2, p. 119-122.

Desjardins, P.R., Buatois, L.A., Pratt, B.R. and Mángano, M.G., 2012. Sedimentological–ichnological model for tide-dominated shelf sandbodies: Lower Cambrian Gog Group of western Canada: Sedimentology, v.59, no. 5, pp.1452-1477.

Dickin, A., and McNutt, R., 2007, The Central Metasedimentary Belt (Grenville Province) as a failed back-arc rift zone: Nd isotope evidence: Earth and Planetary Science Letters, v. 259, no. 1, p. 97-106.

Dorsey, R. J., and Stanley, R. S., 1983, Bedrock geology of the Milton quadrangle, northwestern Vermont: Vermont Geological Survey.

Doveton, J.H., 1994. Geological log interpretation, SEPM (Society for Sedimentary Geology) Short Course, No 29.

Dura, T., Engelhart, S. E., Vacchi, M., Horton, B. P., Kopp, R. E., Peltier, W. R., and Bradley, S., 2016, The role of Holocene relative sea-level change in preserving records of subduction zone earthquakes: Current Climate Change Reports, v. 2, no. 3, p. 86-100.

Durbano, A. M., Pratt, B. R., Hadlari, T., and Dewing, K., 2015, Sedimentology of an early Cambrian tide-dominated embayment: Quyuk formation, Victoria Island, Arctic Canada: Sedimentary Geology, v. 320, p. 1-18.

Einsele, G., Ricken, W., and Seilacher, A., 1991, Cycles and events in stratigraphy, Springer-Verlag, Berlin.

Embry, A., and Johannessen, E., 1993, T–R sequence stratigraphy, facies analysis and reservoir distribution in the uppermost Triassic–Lower Jurassic succession, Western Sverdrup Basin, Arctic Canada: Norwegian Petroleum Society Special Publications, Volume 2, Elsevier, p. 121-146.

Farrell, W., and Clark, J. A., 1976, On postglacial sea level: Geophysical Journal International, v. 46, no. 3, p. 647-667.

Fisher, W. L., and McGowen, J., 1967, Depositional Systems in the Wilcox Group of Texas and Their Relationship to Occurrence of Oil and Gas (1): Gulf Coast Association of Geological Societies Transactions, v. 17, p. 105-125.

Folk, R. L., 1973, Evidence for peritidal deposition of Devonian Caballos Novaculite, Marathon Basin, Texas: AAPG Bulletin, v. 57, no. 4, p. 702-725.

Gadeken, L.L., Jacobson, L.A. and Merchant, G.A., Halliburton Logging Services Inc, 1997. Method for filtering gamma ray well logging tool response to enhance vertical detail while suppressing statistical noise. U.S. Patent 5,672,867.

Gehrels, G., 2010a, Age Pick program: University of Arizona Laserchron Center, Tucson, AZ.

Gehrels, G., 2010b, Nomarlized Age Probability Plot: University of Arizona Laserchron Center, Tucson, AZ.

Gehrels, G., 2012, Detrital zircon U-Pb geochronology: Current methods and new opportunities: Tectonics of sedimentary basins: recent advances, p. 45-62.

Gehrels, G.,, 2014, Detrital zircon U-Pb geochronology applied to tectonics: Annual Review of Earth and Planetary Sciences, v. 42, p. 127-149.

Gehrels, G., Valencia, V., and Pullen, A., 2006, Detrital zircon geochronology by laser-ablation multicollector ICPMS at the Arizona LaserChron Center: The Paleontological Society Papers, v. 12, p. 67-76.

Gehrels, G. E., Valencia, V. A., and Ruiz, J., 2008, Enhanced precision, accuracy, efficiency, and spatial resolution of U-Pb ages by laser ablation–multicollector–inductively coupled plasma–mass spectrometry: Geochemistry, Geophysics, Geosystems, v. 9, no. 3.

Ginsburg, R. N., 1971, Landward movement of carbonate mud: new model for regressive cycles in carbonates: AAPG Bulletin, v. 55, no. 2, p. 340-340.

Goldberg, J., and Mehrtens, C., 1998, Depositional environment and sequence stratigraphy interpretation of the lower Middle Cambrian Monkton Quartzite, Vermont: Northeastern Geology and Environmental Sciences, v. 20, p. 11-27.

Gower, C. F., 1996, The evolution of the Grenville Province in eastern Labrador, Canada: Geological Society, London, Special Publications, v. 112, no. 1, p. 197-218.

Hallam, A., 1963, Major epeirogenic and eustatic changes since the Cretaceous, and their possible relationship to crustal structure: American Journal of Science, v. 261, no. 5, p. 397-423.

Hayes, M. O., 1975, Morphology of sand accumulation in estuaries: an introduction to the symposium: Geology and Engineering, p. 3-22.

Hays, J. D., and Pitman III, W. C., 1973, Lithospheric plate motion, sea level changes and climatic and ecological consequences: Nature, v. 246, no. 5427, p. 18.

Heizler, M. T., and Harrison, T. M., 1998, The thermal history of the New York basement determined from 40Ar/39Ar K-feldspar studies: Journal of Geophysical Research: Solid Earth, v. 103, no. B12, p. 29795-29814.

Hiess, J., Condon, D. J., McLean, N., and Noble, S. R., 2012, 238U/235U systematics in terrestrial uranium-bearing minerals: Science, v. 335, no. 6076, p. 1610-1614.

Isachen, Y., LANDING, E., LAUBER, J., RICKARD, L., and ROGERS, W., 1991, Geology of New York: A Simplified Account, Educational Leaflet No. 28: Albany, New York: The State Education Department, New York State Museum, Geological Survey, 284p.

James, N., 1992, Introduction to carbonate and evaporite facies models: Facies models-response to sea level change., p. 265-275.

James, N. P., 1984, Shallowing-upward sequences in carbon-ates: Facies and models (2nd edition), v. 1, p. 213-228.

James, N. P., Botsford, J. W., and Williams, S. H., 1987, Allochthonous slope sequence at Lobster Cove Head: evidence for a complex Middle Ordovician platform margin in western Newfoundland: Canadian Journal of Earth Sciences, v. 24, no. 6, p. 1199-1211.

Jervey, M., 1988, Quantitative geological modeling of siliciclastic rock sequences and their seismic expression: SEPM Special Publiction, no. 43.

Karlstrom, K. E., Åhäll, K.-I., Harlan, S. S., Williams, M. L., McLelland, J., and Geissman, J. W., 2001, Long-lived (1.8–1.0 Ga) convergent orogen in southern Laurentia, its extensions to Australia and Baltica, and implications for refining Rodinia: Precambrian Research, v. 111, no. 1, p. 5-30.

Kay, G. M., 1942, Ottawa-Bonnechere graben and Lake Ontario homocline: Bulletin of the Geological Society of America, v. 53, no. 4, p. 585-646.

Kemp, A. C., Dutton, A., and Raymo, M. E., 2015, Paleo constraints on future sea-level rise: Current Climate Change Reports, v. 1, no. 3, p. 205-215.

Kim, J., Romanowicz, E., and Mehrtens, C., 2013, Using Deep Bedrock Well Logs to Constrain Stratigraphic and Structural Problems in Vermont, *in* Proceedings, NGWA Conference on Groundwater in Fractured Rock and Sediments: Middlebury, VT, NGWA.

Kominz, M., 2009, Sea Level Variations Over Geological Time: Elements of Physical Oceanography: A derivative of the Encyclopedia of Ocean Sciences, p. 115.

Kumarapeli, P., 1985, Vestiges of lapetan rifting in the craton west of the northern Appalachians: Geoscience Canada, v. 12, no. 2.

Kumarapeli, S., 1981., Origin and development of the Ottawa graben, *in* Proceedings Processes of Planetary Rifting, Volume 457, p. 114.

Kumarapeli, S., Pintson, H., and Dunning, G., 1989, Age of Tibbit Hill Formation and its implications for the timing of Iapetan rifting, *in* Proceedings Geological Association of Canada, Annual Meeting, Program with Abstracts, Volume 14, p. A125.

Landing, E., 2007, Ediacaran-Ordovician of East Laurentia: SW Ford Memorial Volume, New York State Museum, v. 510.

Landing, E., Amati, L., and Franzi, D. A., 2009, Epeirogenic transgression near a triple junction: the oldest (latest early–middle Cambrian) marine onlap of cratonic New York and Quebec: Geological Magazine, v. 146, no. 4, p. 552-566.

Landing, E., Benus, A. P., and Whitney, P. R., 1992, Early and early middle Ordovician continental slope deposition: shale cycles and sandstones in the New York promontory and Quebec reentrant reentrant region, New York State Museum Bulletin, No. 474.

Larsen, C. F., Echelmeyer, K. A., Freymueller, J. T., and Motyka, R. J., 2003, Tide gauge records of uplift along the northern Pacific-North American plate boundary, 1937 to 2001: Journal of Geophysical Research: Solid Earth, v. 108, no. B4.

Li, Z.-X., Evans, D. A., and Halverson, G. P., 2013, Neoproterozoic glaciations in a revised global palaeogeography from the breakup of Rodinia to the assembly of Gondwanaland: Sedimentary Geology, v. 294, p. 219-232.

Llovel, W., Meyssignac, B., and Cazenave, A., 2011, Steric sea level variations over 2004–2010 as a function of region and depth: Inference on the mass component variability in the North Atlantic Ocean: Geophysical Research Letters, v. 38, no. 15.

Lowe, D., 2016, Sedimentology, Stratigraphic Evolution and Provenance of the Cambrian–Lower Ordovician Potsdam Group in the Ottawa Embayment and Quebec Basin [PhD Dissertation]: University of Ottawa-Carleton, 435 p.

Lowe, D. G., Arnott, R., Chiarenzelli, J. R., and Rainbird, R. H., 2018, Early Paleozoic rifting and reactivation of a passive-margin rift: Insights from detrital zircon provenance signatures of the Potsdam Group, Ottawa graben: Geological Society of America Bulletin.

Maguire, H.C., Mehrtens, C. J., Kim and J., Romanowicz, E., 2018, Data Processing for Two Well Logs in Burlington, VT:Vermont Geological Survey, Open-File Report 2018. Manuscript in Preperation.

McLelland, J., Daly, J. S., and McLelland, J. M., 1996, The Grenville orogenic cycle (ca. 1350-1000 Ma): an Adirondack perspective: Tectonophysics, v. 265, no. 1-2, p. 1-28.

McLelland, J. M., Bickford, M. E., Hill, B. M., Clechenko, C. C., Valley, J. W., and Hamilton, M. A., 2004, Direct dating of Adirondack massif anorthosite by U-Pb SHRIMP analysis of igneous zircon: Implications for AMCG complexes: Geological Society of America Bulletin, v. 116, no. 11-12, p. 1299-1317.

McLelland, J. M., and Chiarenzelli, J., 1990, Isotopic constraints on emplacement age of anorthositic rocks of the Marcy masiff, Adirondack Mts., New York: The Journal of Geology, v. 98, no. 1, p. 19-41.

McLelland, J. M., Selleck, B. W., and Bickford, M., 2010, Review of the Proterozoic evolution of the Grenville Province, its Adirondack outlier, and the Mesoproterozoic inliers of the Appalachians: Geological Society of America Memoirs, v. 206, p. 21-49.

McLennan, S. M., Bock, B., Compston, W., Hemming, S. R., and McDaniel, D. K., 2001, Detrital Zircon Geochronology of Taconian and Acadian Foreland Sedimentary Rocks in New England: Journal of Sedimentary Research, v. 71, no. 2, p. 305.

Mehrtens, C., Dorsey, R. J., Ratté, C. A., and Cushman, R., 1987, Stratigraphy and bedrock geology of the Northwestern portion of the St. Albans quadrangle and the adjacent Highgate Center quadrangle, Vermont: Vermont Geological Survey.

Mehrtens, C., and Hadley, A., 1995, Stratigraphy and bedrock geology of parts of the St. Albans and Georgia Quadrangles, Northwestern Vermont: Vermont Geological Survey Special Bulletin, no. 14.

Mehrtens, C., and Hillman, D., 1988, The Rockledge formation: A Cambrian slope apron deposit in northwestern Vermont: Northeastern Geology, v. 10.

Mehrtens, C. J., and Gregory, G., 1984, An occurrence of Salterella conulata Clark in the Dunham Dolomite (Lower Cambrian) of northwestern Vermont and its stratigraphic significance: Journal of Paleontology, p. 1143-1150.

Miller, K. G., Kominz, M. A., Browning, J. V., Wright, J. D., Mountain, G. S., Katz, M. E., Sugarman, P. J., Cramer, B. S., Christie-Blick, N., and Pekar, S. F., 2005, The Phanerozoic record of global sea-level change: Science, v. 310, no. 5752, p. 1293-1298.

Mitchum, R., and Van Wagoner, J. C., High-frequency sequences and eustatic cycles in the Gulf of Mexico basin, *in* Proceedings Sequence stratigraphy as an exploration tool: concepts and practices in the Gulf Coast: Gulf Coast Section SEPM, 11th Annual Research Conference Proceedings1990, SEPM, p. 257-267.

Montario, M., and Garver, J., 2009, The thermal evolution of the Grenville Terrane revealed through U-Pb and fission-track analysis of detrital zircon from Cambro-Ordovician quartz arenites of the Potsdam and Galway Formations: The Journal of Geology, v. 117, no. 6, p. 595-614.

Mount Sopris Instruments., 2008, 2PGA-1000 POLY- GAMMA PROBE Manual, p. 12.

Moore, J. G., 1987, Subsidence of the Hawaiian ridge: US Geol. Surv. Prof. Pap, v. 1350, no. 1, p. 85-100.

Mount, J. F., 1984, Mixing of siliciclastic and carbonate sediments in shallow shelf environments: Geology, v. 12, no. 7, p. 432-435.

Palmer, A. R., 1971, The Cambrian of the Appalachian and eastern New England regions, eastern United States: Wiley-Interscience., London-New York.

Palmer, A. R., and James, N. P., 1980, The Hawke Bay event: a circum-Iapetus regression near the Lower–Middle Cambrian boundary. Memoir - Virginia Polytechnic Institute, Department of Geological Sciences, v. 2, p. 15-18.

Palmer, A., and Taylor, M., 1981, Subdivision of the Sauk sequence, *in* Proceedings Short Papers for the Second International Symposium on the Cambrian System: US Geological Survey, Open-File Report, p. 81-743.

Platt, J., and England, P., 1994, Convective removal of lithosphere beneath mountain belts-Thermal and mechanical consequences: American Journal of Science, v. 294, no. 3.

Plint, A., 1988, Sharp-based shoreface sequences and "Offshore Bars" In the Cardium Formation of Alberta: Their Relationship to Relative Changes in Sea Level, In: (Eds Wilgus, C.K., Hastings, B.S., Kendall, C.G.St.C., Posamentier, H.W., Ross, C.A., Van Wagoner, J.C.), Sea Level Changes—An Integrated Approach, SEPM Special Publication, v. 42.

Plint, A. G., and Nummedal, D., 2000, The falling stage systems tract: recognition and importance in sequence stratigraphic analysis: Geological Society, London, Special Publications, v. 172, no. 1, p. 1-17.

Posamentier, H., Jervey, M., and Vail, P., 1988, Eustatic controls on clastic deposition I—conceptual framework. In: (Eds Wilgus, C.K., Hastings, B.S., Kendall, C.G.St.C., Posamentier, H.W., Ross, C.A., Van Wagoner, J.C.), Sea Level Changes—An Integrated Approach, SEPM Special Publication, v. 42.

Posamentier, H.W., Vail, P.R., 1988. Eustatic controls on clastic deposition. II. Sequence and systems tract models. In: (Eds Wilgus, C.K., Hastings, B.S., Kendall, C.G.St.C., Posamentier, H.W., Ross, C.A., Van Wagoner, J.C.), Sea Level Changes—An Integrated Approach, SEPM Special Publication, v. 42, p. 125-154.

Posamentier, H. W., and Allen, G. P., 1999, Siliciclastic sequence stratigraphy: concepts and applications, SEPM Concepts in Sedimentology and Paleontology, no. 7, p. 210.

Posamentier, H. W., Allen, G. P., James, D. P., and Tesson, M., 1992, Forced regressions in a sequence stratigraphic framework: concepts, examples, and exploration significance (1): AAPG bulletin, v. 76, no. 11, p. 1687-1709.

Pratt, B., and James, N., 1986, The tidal flat island model for peritidal shallow-upward sequences; St. George Group, western Newfoundland: Sedimentology, v. 33, p. 313-344.

Pratt, B. R., 1976, Algal Mats and Cryptalgal Structures, Boca Jewfish, Lac, Bonaire, Netherlands Antilles [PhD Dissertation]: McMaster University.

Pratt, B. R., James, N., and Cowan, C., 1992, Peritidal carbonates, Facies models: response to sea level change, Volume 1, Geological Association of Canada St. John's, p. 303-322.

Pullen, A., Ibáñez-Mejía, M., Gehrels, G. E., Ibáñez-Mejía, J. C., and Pecha, M., 2014, What happens when n= 1000? Creating large-n geochronological datasets with LA-ICP-MS for geologic investigations: Journal of Analytical Atomic Spectrometry, v. 29, no. 6, p. 971-980.

Rahmanian, V., 1981, Transition from carbonate to siliciclastic tidal flat sedimentation in the Lower Cambrian Monkton Formation, West central Vermont: The Green Mountain Geologist, v. 7, no. 4, p. 20-21.

Raine, R. J., and Smith, M. P., 2012, Sequence stratigraphy of the Scottish Laurentian margin and recognition of the Sauk Megasequence, In: Derby, J.T., Fritz, R.D.,

Longacre, S.A., Morgan, W.A., and Sternbach, C.A., eds., The Great American Carbonate Bank: The Geology and Economic Resources of the Cambrian-Ordovician Sauk Megasequence of Laurentia; AAPG Memoir., 98, p. 575-596.

Ratcliffe, N. M., Stanley, R. S., Gale, M. H., and Thompson, P. J., 2011, Bedrock geologic map of Vermont: U.S. Geological Survey Scientific Investigations Map 3184, scale 1:100,000, 3 sheets.

Reineck, H.-E., and Singh, I. B., 1975, Depositional sedimentary environments: with reference to terrigenous clastics, Springer-Verlag, New York, NY

Rivers, T., 1997, Lithotectonic elements of the Grenville Province: review and tectonic implications: Precambrian Research, v. 86, no. 3-4, p. 117-154.

Rivers, T., Ketchum, J., Indares, A., and Hynes, A., 2002, The high pressure belt in the Grenville Province: architecture, timing, and exhumation: Canadian Journal of Earth Sciences, v. 39, no. 5, p. 867-893.

Roden-Tice, M. K., Tice, S. J., and Schofield, I. S., 2000, Evidence for differential unroofing in the Adirondack Mountains, New York State, determined by apatite fission-track thermochronology: The Journal of Geology, v. 108, no. 2, p. 155-169.

Rouchy, J., and Monty, C., 1981, Stromatolites and cryptalgal laminites associated with Messinian gypsum of Cyprus, Phanerozoic Stromatolites: Springer, New York, NY, p. 155-180.

Rovere, A., Stocchi, P., and Vacchi, M., 2016, Eustatic and relative sea level changes: Current Climate Change Reports, v. 2, no. 4, p. 221-231.

Rubatto, D., 2002, Zircon trace element geochemistry: partitioning with garnet and the link between U–Pb ages and metamorphism: Chemical geology, v. 184, no. 1-2, p. 123-138.

Rubatto, D., Williams, I. S., and Buick, I. S., 2001, Zircon and monazite response to prograde metamorphism in the Reynolds Range, central Australia: Contributions to Mineralogy and Petrology, v. 140, no. 4, p. 458-468.

Rutherford, E., and Boltwood, B., 1906, ART. I.--The Relative Proportion of Radium and Uranium in Radio-Active Minerals: American Journal of Science (1880-1910), v. 22, no. 127, p. 1.

Sanford, B. V., 2007, Stratigraphic and structural framework of the Potsdam Group in eastern Ontario, western Quebec and northern New York State [PhD Dissertation]: Department of Earth Sciences, University of Ottawa, Ontario.

Sanford, B. V., and Arnott, R. W., 2010, Stratigraphic and Structural Framework of the Potsdam Group in Eastern Ontario, Western Quebec, and Northern New York State: Geological Survey of Canada Bulletin 5907, Geological Survey of Canada, Ottawa, Ontario.

Schlager, W., 2005, Carbonate sedimentology and sequence stratigraphy, SEPM Concepts in Sedimentology and Paleontology, v. 8.

Schoene B, 2013, U-Th-Pb Geochronology, In Holland, H.D. and Turekian, K.K., Treatise on Geochemistry 2nd edition, vol. 4, p 341-378. Oxford: Elsevier

Schuchert, C., 1933, Cambrian and Ordovician stratigraphy of northwestern Vermont: American Journal of Science, no. 149, p. 353-381.

Schuchert, C., 1937, Cambrian and Ordovician of northwestern Vermont: Bulletin of the Geological Society of America, v. 48, no. 7, p. 1001-1078.

Shaw, A. B., 1958, Stratigraphy and structure of the St. Albans area, northwestern Vermont: Geological Society of America Bulletin, v. 69, no. 5, p. 519-567.

Silver, L. T., 1968, A geochronologic investigation of the anorthosite complex, Adirondack Mountains, New York: Memoir-New York State Museum and Science Service, p. 233-251.

Simpson, E. L., and Eriksson, K. A., 1990, Early Cambrian progradational and transgressive sedimentation patterns in Virginia: an example of the early history of a passive margin: Journal of Sedimentary Research, v. 60, no. 1.

Sloss, L., 1948, Integrated Facies Analysis, *in* Proceedings Sedimentary facies in geologic history: conference at meeting of the Geological Society of America held in New York, NY, Geological Society of America, v. 39, p. 91.

Sloss, L., 1963, Sequences in the cratonic interior of North America: Geological Society of America Bulletin, v. 74, no. 2, p. 93-114.

Speyer, S., 1983, Subtidal and intertidal clastic sedimentation in a Lower Cambrian sequence; Monkton Quartzite, northwestern Vermont: Northeastern Geology, v. 5, no. 1, p. 29-39.

Stanley, R. S., and Roy, D., 1987, The Champlain thrust fault, lone rock point, Burlington, Vermont: Northeastern Section of the Geological Society of America: Geological Society of America Centennial Field Guide, v. 5, p. 225-228.

Stanley, R. S., 1999, The Champlain thrust fault at Lone Rock Point, *in* Proceedings, Annual Meeting New England Intercollegiate Geological Conference, 91st Annual Meeting, 1999, Burlington, VT, p. 359-364.

Storm, L., and Spear, F., 2005, Pressure, temperature and cooling rates of granulite facies migmatitic pelites from the southern Adirondack Highlands, New York: Journal of Metamorphic Geology, v. 23, no. 2, p. 107-130.

Theys, P., 1999, Log data acquisition and quality control: Editions Technip. Paris, France, 330p.

Thomas, W. A., 1977, Evolution of Appalachian-Ouachita salients and recesses from reentrants and promontories in the continental margin: American Journal of Science, v. 277, no. 10, p. 1233-1278.

Twenhofel, W. H., 1939, Principles of sedimentation: New York and London McGraw-Hill Book Co., p. 610.

Vail, P., and Mitchum, R., 1979, Global cycles of relative changes of sea level from seismic stratigraphy: resources, comparative structure, and eustatic changes in sea level, In:Geological and Geophysical Investigations of Continental Margins, AAPG Memoir, pg. 69-72.

Vail, P. R., Mitchum Jr, R., and Thompson III, S., 1977, Seismic stratigraphy and global changes of sea level: Part 3. Relative changes of sea level from Coastal Onlap: section 2. Application of seismic reflection Configuration to Stratigrapic Interpretation.

Van Wagoner, J., Posamentier, H., Mitchum, R., Vail, P., Sarg, J., Loutit, T., and Hardenbol, J., 1988, An overview of the fundamentals of sequence stratigraphy and key definitions. In: *Sea Level Changes – An Integrated Approach* (Eds C.K. Wilgus, B.S. Hastings, C.G.St.C. Kendall, H.W. Posamentier, C.A. Ross and J.C. Van Wagoner), SEPM Special Publication, 42, 39-45.

Van Wagoner, J. C., 1995, Overview of sequence stratigraphy of foreland basin deposits: terminology, summary of papers, and glossary of sequence stratigraphy. In: *Sequence Straigraphy of Forland Basin Deposits: Ouctrop and Subsurface Examples from the Cretaceous of North America* (Eds J.C. Van Wagoner and G.T. Bertram), AAPG Memoir., 64, ix-xxi

Van Wagoner, J. C, Mitchum, R. M, Campion, K. M, & Rahmanian, V. D., 1990, Siliciclastic sequence stratigraphy in well logs, cores, and outcrops : *concepts for high-resolution correlation of time and facies.* Tulsa (Okla.): American association of petroleum geologists

Williams, G. D., 1993, Tectonics and seismic sequence stratigraphy: an introduction: Geological Society, London, Special Publications, v. 71, no. 1, p. 1-13.

Williams, I., 2001, Response of detrital zircon and monazite, and their U–Pb isotopic systems, to regional metamorphism and host-rock partial melting, Cooma Complex, southeastern Australia: Australian Journal of Earth Sciences, v. 48, no. 4, p. 557-580.

Wilson, J. T., 1968, Static or mobile earth: the current scientific revolution: Proceedings of the American Philosophical Society, v. 112, no. 5, p. 309-320.

Zelek, M., and Dickin, A., 2013, Nd isotope mapping of crustal terranes in the Parent-Clova Area, Quebec: implications for the evolution of the Laurentian margin in the Central Grenville Province: Geosciences, v. 3, no. 3, p. 448-465.

APPENDIX A: MONKTON U-Pb ANALYTICAL RESULTS

Table 1. Monkton U-Pb analytical results of sample from Redstone Quarry: 18T 0642761E 4924710N

						Isotope ratios					Apparent ages (Ma)								
Analysis	U (ppm)	206Pb 204Pb	U/Th	206Pb* 207Pb*	± (%)	207Pb* 235U*	± (%)	206Pb* 238U	± (%)	error corr.	206Pb* 238U*	± (Ma)	207Pb* 235U	± (Ma)	206Pb* 207Pb*	± (Ma)	Best age (Ma)	± (Ma)	Conc (%)
Spot 24	105	13792	2.2	13.8501	1.0	1.6800	3.3	0.1688	3.2	0.95	1005.6	29.6	1001.0	21.3	991.6	21.1	991.6	21.1	101.4
Spot 7	92	19104	19.0	13.7321	1.3	1.6956	2.8	0.1689	2.5	0.89	1006.3	23.1	1006.9	17.8	1009.0	26.2	1009.0	26.2	99.7
Spot 81	104	15218	5.1	13.6908	1.1	1.7812	3.3	0.1769	3.1	0.94	1050.3	29.7	1038.6	21.2	1015.1	21.9	1015.1	21.9	103.5
Spot 106	304	35824	43.9	13.6767	1.1	1.7731	3.8	0.1760	3.6	0.96	1044.9	35.1	1035.7	24.7	1017.2	22.6	1017.2	22.6	102.7
Spot 127	16	7194	1.1	13.6722	1.9	1.7945	3.5	0.1780	2.9	0.83	1056.1	28.2	1043.4	22.7	1017.8	39.0	1017.8	39.0	103.8
Spot 116	45	29998	4.9	13.6672	1.5	1.8109	3.3	0.1796	3.0	0.89	1064.7	29.4	1049.4	21.9	1018.6	30.2	1018.6	30.2	104.5
Spot 206	52	6227	1.9	13.6644	1.3	1.7445	3.2	0.1730	2.9	0.91	1028.4	27.8	1025.1	20.8	1019.0	27.2	1019.0	27.2	100.9
Spot 34	131	19989	2.0	13.6575	1.1	1.7784	2.5	0.1762	2.2	0.89	1046.4	21.5	1037.6	16.2	1020.0	22.7	1020.0	22.7	102.6
Spot 291	192	17950	10.6	13.6565	1.3	1.7104	3.1	0.1695	2.8	0.91	1009.2	26.6	1012.4	20.0	1020.2	25.8	1020.2	25.8	98.9
Spot 215	35	7505	4.0	13.6485	1.5	1.7082	3.2	0.1692	2.8	0.89	1007.5	26.1	1011.6	20.2	1021.4	29.5	1021.4	29.5	98.6
Spot 105	196	51299	4.3	13.6315	1.0	1.7200	2.8	0.1701	2.6	0.93	1012.8	24.1	1016.0	17.8	1023.9	21.1	1023.9	21.1	98.9
Spot 174	264	91367	2.7	13.6274	1.1	1.7906	2.9	0.1770	2.7	0.92	1050.8	25.8	1042.0	18.8	1024.5	22.5	1024.5	22.5	102.6
Spot 148	427	204774	19.1	13.6159	0.8	1.7499	3.0	0.1729	2.9	0.96	1028.0	27.3	1027.1	19.3	1026.2	17.0	1026.2	17.0	100.2
Spot 57	243	30122	5.0	13.5969	1.2	1.8102	3.3	0.1786	3.1	0.93	1059.2	30.0	1049.1	21.6	1029.0	24.5	1029.0	24.5	102.9

Spot 263	24	3044	1.0	13.5884	1.3	1.8105	3.9	0.1785	3.7	0.94	1058.8	36.1	1049.3	25.7	1030.3	26.6	1030.3	26.6	102.8
Spot 123	116	44454	1.5	13.5754	0.8	1.7675	2.7	0.1741	2.6	0.96	1034.7	24.9	1033.6	17.6	1032.2	15.4	1032.2	15.4	100.2
Spot 196	177	351155	4.0	13.5702	1.0	1.7594	2.8	0.1732	2.6	0.93	1029.9	25.1	1030.6	18.4	1033.0	21.2	1033.0	21.2	99.7
Spot 240	109	24233	14.3	13.5585	1.0	1.7649	3.3	0.1736	3.1	0.96	1032.1	29.9	1032.7	21.2	1034.7	19.2	1034.7	19.2	99.7
Spot 271	118	18312	13.1	13.5473	0.9	1.7771	2.9	0.1747	2.8	0.95	1037.9	26.5	1037.1	18.9	1036.4	18.4	1036.4	18.4	100.1
Spot 224	126	18073	3.9	13.5470	1.2	1.7997	3.2	0.1769	3.0	0.93	1050.0	29.2	1045.4	21.1	1036.5	23.4	1036.5	23.4	101.3
Spot 79	210	35863	3.2	13.5362	1.0	1.7188	2.8	0.1688	2.6	0.93	1005.6	24.3	1015.6	18.0	1038.1	20.9	1038.1	20.9	96.9
Spot 233	97	26733	9.9	13.5226	1.2	1.7772	2.6	0.1744	2.3	0.89	1036.2	21.9	1037.2	16.7	1040.1	23.6	1040.1	23.6	99.6
Spot 229	67	15502	1.2	13.5103	1.1	1.8099	3.3	0.1774	3.1	0.94	1052.9	30.2	1049.0	21.7	1041.9	23.0	1041.9	23.0	101.1
Spot 218	170	464334	3.6	13.5013	0.9	1.7867	3.0	0.1750	2.9	0.96	1039.8	27.8	1040.6	19.7	1043.3	17.8	1043.3	17.8	99.7
Spot 173	20	4813	2.8	13.4865	2.3	1.8871	3.7	0.1847	2.9	0.78	1092.4	29.1	1076.6	24.7	1045.5	47.3	1045.5	47.3	104.5
Spot 248	63	5203	3.7	13.4792	1.0	1.8255	2.8	0.1785	2.6	0.93	1059.0	25.6	1054.7	18.4	1046.6	20.2	1046.6	20.2	101.2
Spot 46	87	8637	4.8	13.4680	1.1	1.8965	2.5	0.1853	2.2	0.90	1096.0	22.4	1079.9	16.4	1048.3	21.7	1048.3	21.7	104.6
Spot 191	49	8258	1.0	13.4645	1.2	1.7896	2.8	0.1748	2.5	0.90	1038.7	23.8	1041.7	18.0	1048.8	24.3	1048.8	24.3	99.0
Spot 52	216	62412	3.7	13.4562	1.0	1.7451	3.2	0.1704	3.1	0.95	1014.2	29.0	1025.3	21.0	1050.1	20.2	1050.1	20.2	96.6
Spot 158	25	3907	0.8	13.4553	1.4	1.8120	3.1	0.1769	2.8	0.90	1050.0	27.3	1049.8	20.5	1050.2	27.4	1050.2	27.4	100.0
Spot 216	159	15368	1.9	13.4365	1.1	1.7777	2.8	0.1733	2.6	0.92	1030.3	24.9	1037.3	18.4	1053.0	22.0	1053.0	22.0	97.8
Spot 182	64	13861	2.1	13.4318	1.2	1.8059	2.9	0.1760	2.6	0.90	1045.1	25.5	1047.6	19.1	1053.7	25.2	1053.7	25.2	99.2
Spot 259	80	21202	1.4	13.4194	0.9	1.8069	2.5	0.1759	2.4	0.93	1044.7	22.8	1048.0	16.6	1055.6	18.6	1055.6	18.6	99.0
Spot 283	40	3846	3.3	13.4133	1.4	1.8934	3.2	0.1843	2.9	0.90	1090.3	29.3	1078.8	21.6	1056.5	28.7	1056.5	28.7	103.2
Spot 119	58	38986	4.0	13.3981	1.2	1.8517	3.4	0.1800	3.1	0.93	1067.0	30.6	1064.0	22.1	1058.8	24.9	1058.8	24.9	100.8
Spot 276	121	15470	9.6	13.3939	1.2	1.8682	2.7	0.1816	2.4	0.90	1075.5	24.2	1069.9	17.9	1059.4	23.6	1059.4	23.6	101.5
Spot 308	129	20522	3.1	13.3852	1.1	1.8079	2.7	0.1756	2.5	0.92	1042.8	24.4	1048.3	18.0	1060.7	21.6	1060.7	21.6	98.3
Spot 289	36	9493	1.4	13.3728	1.2	1.9366	3.5	0.1879	3.2	0.94	1110.0	33.0	1093.8	23.2	1062.6	24.6	1062.6	24.6	104.5
Spot 188	63	74628	2.3	13.3707	1.3	1.8388	3.7	0.1784	3.4	0.93	1058.2	33.2	1059.4	24.1	1062.9	27.0	1062.9	27.0	99.6

Spot 190	77	11577	3.8	13.3693	1.2	1.8302	3.2	0.1775	3.0	0.93	1053.5	28.9	1056.4	21.0	1063.1	24.0	1063.1	24.0	99.1
Spot 300	23	5331	1.3	13.3573	1.5	1.9043	2.9	0.1846	2.5	0.85	1091.8	24.9	1082.6	19.3	1064.9	30.3	1064.9	30.3	102.5
Spot 39	115	10011	4.9	13.3565	1.1	1.9187	3.0	0.1860	2.8	0.93	1099.4	28.2	1087.6	20.1	1065.0	22.7	1065.0	22.7	103.2
Spot 32	276	73639	4.0	13.3383	1.0	1.7746	3.3	0.1718	3.2	0.95	1021.8	30.0	1036.2	21.6	1067.8	20.5	1067.8	20.5	95.7
Spot 226	256	139664	21.4	13.3052	1.3	1.8333	3.6	0.1770	3.4	0.94	1050.5	32.6	1057.5	23.6	1072.8	25.1	1072.8	25.1	97.9
Spot 56	169	36431	3.5	13.2934	1.4	1.8454	3.5	0.1780	3.3	0.92	1056.0	31.9	1061.8	23.3	1074.5	27.1	1074.5	27.1	98.3
Spot 14	97	19534	31.9	13.2904	1.2	1.9058	3.1	0.1838	2.9	0.92	1087.6	28.6	1083.1	20.8	1075.0	25.1	1075.0	25.1	101.2
Spot 109	101	15325	6.4	13.2889	1.2	1.9161	3.7	0.1848	3.5	0.94	1092.9	35.0	1086.7	24.7	1075.2	25.0	1075.2	25.0	101.6
Spot 249	33	4738	3.3	13.2825	2.3	1.9549	3.9	0.1884	3.1	0.80	1112.7	32.1	1100.1	26.3	1076.2	46.7	1076.2	46.7	103.4
Spot 211	202	84546	5.7	13.2692	1.2	1.8105	2.9	0.1743	2.6	0.92	1035.9	25.3	1049.3	18.9	1078.2	23.2	1078.2	23.2	96.1
Spot 205	192	24994	4.6	13.2660	0.9	1.7654	2.5	0.1699	2.4	0.93	1011.7	22.1	1032.8	16.5	1078.7	19.0	1078.7	19.0	93.8
Spot 314	14	3300	3.2	13.2592	1.8	1.9535	3.2	0.1879	2.7	0.83	1110.2	27.1	1099.7	21.6	1079.7	36.4	1079.7	36.4	102.8
Spot 166	94	35863	1.7	13.2261	1.0	1.8253	2.8	0.1752	2.6	0.93	1040.5	25.3	1054.6	18.5	1084.7	20.2	1084.7	20.2	95.9
Spot 179	25	5616	3.9	13.1996	1.6	1.8901	2.9	0.1810	2.4	0.83	1072.5	23.5	1077.6	19.0	1088.7	32.2	1088.7	32.2	98.5
Spot 124	47	15873	1.7	13.1990	1.1	1.9213	3.3	0.1840	3.1	0.94	1088.8	31.2	1088.5	22.1	1088.8	22.7	1088.8	22.7	100.0
Spot 237	199	388523	5.1	13.1989	0.9	1.8447	3.4	0.1767	3.3	0.96	1048.7	31.7	1061.5	22.4	1088.8	18.0	1088.8	18.0	96.3
Spot 87	191	23612	6.6	13.1775	1.1	1.8746	3.0	0.1792	2.8	0.93	1062.8	27.0	1072.2	19.6	1092.1	21.9	1092.1	21.9	97.3
Spot 286	9	4552	3.1	13.1272	1.7	2.0330	3.6	0.1936	3.2	0.88	1141.0	33.5	1126.6	24.7	1099.8	33.8	1099.8	33.8	103.8
Spot 1	40	3998	3.1	13.1193	1.7	1.9772	3.4	0.1882	2.9	0.86	1111.7	29.9	1107.8	23.0	1100.9	34.6	1100.9	34.6	101.0
Spot 187	35	35240	18.1	13.1101	1.1	1.8528	3.5	0.1762	3.3	0.94	1046.5	31.4	1064.4	22.8	1102.4	23.0	1102.4	23.0	94.9
Spot 273	18	9405	1.1	13.0856	1.8	1.9148	3.4	0.1818	2.9	0.86	1076.8	29.1	1086.3	22.9	1106.1	35.4	1106.1	35.4	97.4
Spot 113	142	34633	4.8	13.0809	1.4	1.9916	3.4	0.1890	3.1	0.91	1116.1	31.7	1112.7	22.9	1106.8	27.8	1106.8	27.8	100.8
Spot 151	16	4159	2.3	13.0711	2.5	2.0512	4.1	0.1945	3.3	0.80	1145.9	34.9	1132.7	28.3	1108.3	49.4	1108.3	49.4	103.4
Spot 222	69	37214	4.0	13.0491	1.2	2.0197	3.3	0.1912	3.1	0.93	1128.1	31.7	1122.2	22.5	1111.7	24.7	1111.7	24.7	101.5
Spot 177	55	5223	4.9	13.0485	1.2	2.0822	3.5	0.1971	3.2	0.93	1159.9	34.3	1143.0	23.8	1111.8	24.8	1111.8	24.8	104.3

Spot 147	70	87008	3.3	13.0393	1.1	2.0172	3.1	0.1909	2.9	0.93	1126.0	30.0	1121.3	21.1	1113.1	22.3	1113.1	22.3	101.2
Spot 161	60	7569	3.2	13.0302	1.2	2.0721	2.8	0.1959	2.6	0.91	1153.3	27.1	1139.6	19.3	1114.5	23.2	1114.5	23.2	103.5
Spot 80	84	84406	3.8	13.0295	1.1	2.0560	3.2	0.1944	3.0	0.93	1145.0	31.0	1134.3	21.6	1114.6	22.6	1114.6	22.6	102.7
Spot 118	118	28144	2.4	13.0221	0.9	2.0730	2.8	0.1959	2.7	0.95	1153.1	28.5	1139.9	19.5	1115.8	18.0	1115.8	18.0	103.3
Spot 192	27	113888	1.7	13.0205	1.5	1.9132	3.4	0.1807	3.0	0.89	1071.0	30.1	1085.7	22.8	1116.1	30.7	1116.1	30.7	96.0
Spot 112	40	8927	1.4	13.0181	0.9	2.0083	2.9	0.1897	2.7	0.94	1119.7	27.8	1118.3	19.4	1116.4	18.8	1116.4	18.8	100.3
Spot 60	52	5276	2.9	13.0153	1.1	2.0501	3.0	0.1936	2.8	0.94	1140.9	29.6	1132.3	20.6	1116.9	21.1	1116.9	21.1	102.1
Spot 90	9	2408	2.7	12.9940	2.2	2.0444	3.4	0.1928	2.6	0.76	1136.3	27.2	1130.4	23.4	1120.1	44.4	1120.1	44.4	101.4
Spot 266	43	58976	0.6	12.9939	1.2	1.9094	2.7	0.1800	2.4	0.89	1067.1	23.6	1084.4	17.9	1120.1	24.1	1120.1	24.1	95.3
Spot 27	92	15020	3.6	12.9935	1.5	2.0206	3.6	0.1905	3.3	0.92	1124.1	34.2	1122.5	24.6	1120.2	28.9	1120.2	28.9	100.3
Spot 91	30	7624	2.6	12.9932	1.5	2.1064	2.9	0.1986	2.5	0.85	1167.7	26.4	1150.9	20.0	1120.3	30.3	1120.3	30.3	104.2
Spot 172	30	4692	1.0	12.9650	1.6	2.0366	3.0	0.1916	2.6	0.84	1130.0	26.5	1127.8	20.6	1124.6	32.2	1124.6	32.2	100.5
Spot 136	128	39695	3.4	12.9598	1.2	2.0617	3.3	0.1939	3.1	0.93	1142.3	32.0	1136.2	22.4	1125.4	23.3	1125.4	23.3	101.5
Spot 31	100	26729	2.5	12.9426	1.0	2.0134	2.7	0.1891	2.5	0.93	1116.4	26.0	1120.0	18.6	1128.0	20.7	1128.0	20.7	99.0
Spot 285	17	3868	3.8	12.9395	1.4	2.0302	2.7	0.1906	2.3	0.86	1124.7	23.8	1125.7	18.3	1128.5	27.2	1128.5	27.2	99.7
Spot 130	180	73051	5.0	12.9392	1.0	2.0951	3.0	0.1967	2.8	0.94	1157.6	29.6	1147.2	20.4	1128.6	19.7	1128.6	19.7	102.6
Spot 28	36	4738	3.3	12.9376	1.3	2.1261	2.7	0.1996	2.4	0.88	1173.1	25.9	1157.3	19.0	1128.8	26.0	1128.8	26.0	103.9
Spot 61	46	28958	2.7	12.9337	1.1	2.0918	3.0	0.1963	2.8	0.93	1155.5	29.7	1146.1	20.8	1129.4	22.5	1129.4	22.5	102.3
Spot 236	20	26239	1.0	12.9245	1.2	1.8431	3.0	0.1728	2.7	0.91	1027.7	26.0	1061.0	19.7	1130.8	24.4	1130.8	24.4	90.9
Spot 2	215	60904	2.3	12.9229	1.0	2.0718	3.3	0.1943	3.1	0.95	1144.5	33.0	1139.5	22.6	1131.1	20.1	1131.1	20.1	101.2
Spot 11	336	33498	5.2	12.9142	1.0	2.0902	2.7	0.1959	2.5	0.93	1153.0	26.1	1145.6	18.4	1132.4	20.2	1132.4	20.2	101.8
Spot 70	14	6399	2.9	12.9123	2.0	2.0149	4.3	0.1888	3.8	0.89	1114.7	39.0	1120.5	29.1	1132.7	39.3	1132.7	39.3	98.4
Spot 290	286	39017	7.7	12.9064	1.0	2.0494	2.8	0.1919	2.6	0.94	1131.8	27.0	1132.1	19.0	1133.6	19.2	1133.6	19.2	99.8
Spot 134	271	57862	2.8	12.9022	1.2	2.1637	3.4	0.2026	3.2	0.94	1189.0	34.9	1169.5	23.8	1134.2	23.8	1134.2	23.8	104.8
Spot 75	15	9106	3.3	12.8907	1.3	2.1129	2.4	0.1976	2.1	0.86	1162.5	22.3	1153.0	16.9	1136.0	25.2	1136.0	25.2	102.3

Spot 54	29	4584	2.0	12.8855	1.5	2.1063	3.2	0.1969	2.8	0.89	1158.8	30.2	1150.9	22.1	1136.8	29.5	1136.8	29.5	101.9
Spot 279	42	11421	4.6	12.8847	1.0	1.9495	3.3	0.1823	3.2	0.96	1079.3	31.8	1098.3	22.5	1137.0	19.2	1137.0	19.2	94.9
Spot 114	50	6911	3.2	12.8806	1.0	2.0610	2.7	0.1926	2.6	0.93	1135.6	26.6	1136.0	18.7	1137.6	19.7	1137.6	19.7	99.8
Spot 89	290	129933	3.9	12.8748	0.9	2.1163	3.6	0.1977	3.5	0.97	1163.0	37.0	1154.1	24.8	1138.5	18.4	1138.5	18.4	102.2
Spot 313	20	3930	2.3	12.8671	1.2	2.0685	2.6	0.1931	2.3	0.89	1138.2	24.0	1138.4	17.6	1139.7	23.1	1139.7	23.1	99.9
Spot 157	179	178460	7.8	12.8639	1.1	2.1063	2.9	0.1966	2.7	0.93	1157.0	28.4	1150.9	19.9	1140.2	21.6	1140.2	21.6	101.5
Spot 201	30	8977	2.5	12.8622	1.4	2.1254	3.2	0.1984	2.8	0.89	1166.5	30.0	1157.1	21.8	1140.4	28.8	1140.4	28.8	102.3
Spot 104	72	14997	7.8	12.8602	1.2	2.1456	3.0	0.2002	2.8	0.92	1176.5	30.2	1163.6	21.1	1140.7	23.6	1140.7	23.6	103.1
Spot 168	11	6573	0.9	12.8473	1.7	1.9122	3.8	0.1782	3.4	0.89	1057.4	32.7	1085.3	25.1	1142.7	34.1	1142.7	34.1	92.5
Spot 194	73	11558	4.4	12.8417	1.3	2.0836	2.9	0.1941	2.6	0.89	1143.8	27.6	1143.4	20.2	1143.6	26.4	1143.6	26.4	100.0
Spot 292	31	30975	1.4	12.8366	1.2	2.0286	3.1	0.1889	2.8	0.92	1115.7	28.9	1125.2	20.9	1144.4	24.5	1144.4	24.5	97.5
Spot 189	71	21668	2.9	12.8247	1.1	2.1482	2.7	0.1999	2.5	0.92	1174.8	26.8	1164.5	18.9	1146.2	21.7	1146.2	21.7	102.5
Spot 155	326	43204	3.3	12.8233	1.0	2.0990	2.9	0.1953	2.7	0.94	1150.0	28.6	1148.5	19.9	1146.4	19.5	1146.4	19.5	100.3
Spot 30	95	37759	3.5	12.8144	1.2	2.1626	3.1	0.2011	2.9	0.92	1181.1	31.3	1169.1	21.8	1147.8	24.0	1147.8	24.0	102.9
Spot 97	175	20894	3.6	12.8095	1.2	2.1385	3.7	0.1988	3.5	0.95	1168.7	37.6	1161.3	25.7	1148.6	23.9	1148.6	23.9	101.7
Spot 156	27	3239	5.2	12.8038	2.0	2.0185	3.0	0.1875	2.3	0.76	1107.9	23.3	1121.7	20.5	1149.5	39.1	1149.5	39.1	96.4
Spot 149	61	29064	2.8	12.7999	1.1	2.0273	2.8	0.1883	2.5	0.92	1112.1	25.9	1124.7	18.8	1150.1	22.1	1150.1	22.1	96.7
Spot 312	42	9037	0.9	12.7913	1.4	2.1666	3.1	0.2011	2.8	0.89	1181.1	30.1	1170.4	21.8	1151.4	28.6	1151.4	28.6	102.6
Spot 4	86	12128	1.5	12.7855	1.3	2.1551	3.1	0.1999	2.8	0.91	1174.9	29.9	1166.7	21.2	1152.3	25.2	1152.3	25.2	102.0
Spot 93	35	49245	1.8	12.7809	1.2	2.0520	3.5	0.1903	3.3	0.94	1122.9	34.0	1132.9	23.9	1153.0	22.9	1153.0	22.9	97.4
Spot 142	97	37827	5.4	12.7777	1.2	2.0988	3.1	0.1946	2.9	0.92	1146.2	30.1	1148.4	21.5	1153.5	24.4	1153.5	24.4	99.4
Spot 301	81	17474	2.6	12.7688	1.2	2.0134	3.2	0.1865	3.0	0.93	1102.6	30.6	1120.0	22.0	1154.9	23.7	1154.9	23.7	95.5
Spot 293	25	7602	0.9	12.7682	1.3	2.1977	3.2	0.2036	2.9	0.91	1194.7	31.9	1180.3	22.5	1155.0	26.6	1155.0	26.6	103.4
Spot 3	65	34912	5.4	12.7393	1.5	2.2267	3.5	0.2058	3.2	0.90	1206.5	34.9	1189.5	24.6	1159.5	29.8	1159.5	29.8	104.1
Spot 225	45	55084	2.8	12.7383	1.3	2.1305	3.0	0.1969	2.7	0.90	1158.7	28.9	1158.7	20.9	1159.6	26.3	1159.6	26.3	99.9

Spot 195	243	65160	2.9	12.7330	0.9	2.1014	3.1	0.1941	2.9	0.95	1143.8	30.7	1149.3	21.2	1160.5	18.7	1160.5	18.7	98.6
Spot 296	62	9999	1.8	12.7293	1.2	2.2262	3.2	0.2056	3.0	0.93	1205.4	32.8	1189.3	22.6	1161.0	24.1	1161.0	24.1	103.8
Spot 153	78	23991	1.6	12.7238	1.2	2.2025	2.6	0.2033	2.3	0.89	1193.2	25.3	1181.8	18.3	1161.9	23.8	1161.9	23.8	102.7
Spot 165	45	14860	2.4	12.7193	1.2	2.2038	3.0	0.2034	2.8	0.92	1193.5	30.1	1182.3	21.0	1162.6	23.2	1162.6	23.2	102.7
Spot 169	172	12405	4.2	12.7182	1.2	2.0876	3.2	0.1926	3.0	0.93	1135.7	31.1	1144.7	22.1	1162.8	23.9	1162.8	23.9	97.7
Spot 269	29	5013	2.7	12.7171	1.9	2.0968	3.0	0.1935	2.4	0.79	1140.2	24.9	1147.8	20.8	1162.9	37.2	1162.9	37.2	98.0
Spot 38	75	315047	5.7	12.7154	1.4	2.0511	3.5	0.1892	3.2	0.92	1117.2	32.6	1132.7	23.6	1163.2	26.9	1163.2	26.9	96.0
Spot 207	22	31653	2.0	12.7147	1.3	1.9477	3.2	0.1797	3.0	0.92	1065.3	29.2	1097.6	21.7	1163.3	25.3	1163.3	25.3	91.6
Spot 82	40	9499	3.8	12.7109	0.8	2.1386	2.8	0.1972	2.7	0.96	1160.5	28.9	1161.4	19.6	1163.9	15.5	1163.9	15.5	99.7
Spot 5	325	35164	5.7	12.7053	1.2	2.0536	3.0	0.1893	2.8	0.92	1117.7	28.3	1133.5	20.5	1164.8	24.0	1164.8	24.0	96.0
Spot 260	7	4160	4.2	12.7049	1.8	2.0912	3.5	0.1928	3.0	0.86	1136.4	31.0	1145.9	23.8	1164.8	35.1	1164.8	35.1	97.6
Spot 272	116	27492	2.7	12.7005	1.2	2.0538	3.4	0.1893	3.2	0.93	1117.4	32.5	1133.6	23.2	1165.5	24.2	1165.5	24.2	95.9
Spot 88	8	4170	2.5	12.6941	2.7	2.0700	4.2	0.1907	3.2	0.77	1125.0	33.0	1138.9	28.4	1166.5	52.5	1166.5	52.5	96.4
Spot 77	36	7378	0.9	12.6905	1.4	2.0086	3.3	0.1850	3.0	0.91	1094.0	29.9	1118.4	22.2	1167.1	27.5	1167.1	27.5	93.7
Spot 62	36	11185	2.3	12.6881	1.2	2.1698	3.2	0.1998	3.0	0.92	1174.0	31.7	1171.4	22.2	1167.5	24.2	1167.5	24.2	100.6
Spot 310	104	42138	3.8	12.6817	1.1	2.1094	3.3	0.1941	3.1	0.94	1143.6	32.4	1151.9	22.7	1168.5	22.5	1168.5	22.5	97.9
Spot 220	54	10263	1.7	12.6802	1.2	2.0384	3.6	0.1875	3.4	0.94	1108.1	34.2	1128.4	24.4	1168.7	24.6	1168.7	24.6	94.8
Spot 284	47	20112	3.4	12.6784	1.2	2.0156	3.9	0.1854	3.7	0.95	1096.5	37.1	1120.8	26.3	1169.0	24.4	1169.0	24.4	93.8
Spot 73	203	17340	2.7	12.6770	1.1	2.1011	3.3	0.1933	3.1	0.94	1139.0	32.4	1149.2	22.7	1169.2	22.5	1169.2	22.5	97.4
Spot 115	207	43432	3.8	12.6766	1.1	2.1662	3.0	0.1992	2.8	0.93	1171.3	30.1	1170.3	21.1	1169.2	22.8	1169.2	22.8	100.2
Spot 17	22	5479	2.3	12.6752	1.4	2.0298	3.0	0.1867	2.7	0.88	1103.3	27.1	1125.5	20.5	1169.5	27.9	1169.5	27.9	94.3
Spot 53	27	10235	2.5	12.6669	1.3	2.1065	2.9	0.1936	2.6	0.90	1140.9	27.1	1150.9	19.9	1170.8	25.2	1170.8	25.2	97.4
Spot 171	163	159388	2.4	12.6627	1.0	2.1881	2.5	0.2010	2.3	0.92	1180.9	25.2	1177.3	17.7	1171.5	19.9	1171.5	19.9	100.8
Spot 21	117	1125110	2.3	12.6604	1.3	2.2340	3.5	0.2052	3.2	0.92	1203.3	35.5	1191.8	24.6	1171.8	26.6	1171.8	26.6	102.7
Spot 212	30	7705	3.0	12.6559	1.2	2.1131	2.9	0.1940	2.7	0.91	1143.2	28.1	1153.1	20.3	1172.5	24.2	1172.5	24.2	97.5

Spot 203	23	6857	2.2	12.6497	1.5	2.1454	3.0	0.1969	2.5	0.85	1158.7	27.0	1163.6	20.6	1173.5	30.6	1173.5	30.6	98.7
Spot 234	13	3846	1.9	12.6487	1.8	2.1395	3.3	0.1964	2.7	0.83	1155.7	28.5	1161.7	22.5	1173.6	36.2	1173.6	36.2	98.5
Spot 42	233	36746	4.2	12.6410	1.1	2.1415	3.2	0.1964	3.0	0.94	1156.1	31.5	1162.3	21.9	1174.8	20.8	1174.8	20.8	98.4
Spot 102	13	64963	1.8	12.6408	1.9	2.0085	3.7	0.1842	3.2	0.86	1090.0	32.1	1118.4	25.1	1174.9	37.2	1174.9	37.2	92.8
Spot 311	14	11506	2.5	12.6356	1.2	2.0927	3.6	0.1919	3.4	0.94	1131.5	35.2	1146.4	24.7	1175.7	23.9	1175.7	23.9	96.2
Spot 256	32	9885	1.6	12.6299	1.4	2.2533	3.8	0.2065	3.5	0.93	1210.1	38.8	1197.8	26.7	1176.6	28.1	1176.6	28.1	102.8
Spot 26	81	17187	2.1	12.6226	1.2	2.2114	3.1	0.2025	2.9	0.92	1188.9	31.4	1184.6	21.9	1177.7	23.7	1177.7	23.7	100.9
Spot 255	49	17636	4.2	12.6225	1.4	2.1025	3.1	0.1926	2.7	0.89	1135.2	28.5	1149.6	21.3	1177.7	28.4	1177.7	28.4	96.4
Spot 72	255	1448673	4.7	12.6194	0.9	2.1540	2.7	0.1972	2.6	0.94	1160.4	27.1	1166.3	18.8	1178.2	17.9	1178.2	17.9	98.5
Spot 9	313	66101	3.1	12.6151	1.1	2.1006	3.1	0.1923	2.9	0.94	1133.7	30.3	1149.0	21.4	1178.9	21.8	1178.9	21.8	96.2
Spot 33	16	9043	4.0	12.6151	1.6	2.0568	3.0	0.1883	2.6	0.85	1112.0	26.5	1134.6	20.8	1178.9	31.6	1178.9	31.6	94.3
Spot 175	49	14377	3.0	12.6099	0.9	2.1234	3.0	0.1943	2.8	0.95	1144.5	29.7	1156.5	20.6	1179.7	18.7	1179.7	18.7	97.0
Spot 200	32	23558	3.7	12.6077	1.5	2.1582	3.6	0.1974	3.2	0.91	1161.5	34.2	1167.7	24.7	1180.1	29.8	1180.1	29.8	98.4
Spot 96	104	48704	9.8	12.6070	1.1	2.1326	3.1	0.1951	2.9	0.94	1148.8	31.0	1159.4	21.7	1180.2	21.2	1180.2	21.2	97.3
Spot 305	25	64197	3.4	12.5987	1.3	2.0866	3.2	0.1907	3.0	0.91	1125.4	30.6	1144.4	22.3	1181.5	26.1	1181.5	26.1	95.3
Spot 66	40	5756	4.0	12.5933	2.0	2.0594	3.8	0.1882	3.3	0.85	1111.5	33.5	1135.4	26.2	1182.3	39.5	1182.3	39.5	94.0
Spot 221	10	3175	4.3	12.5866	2.3	2.1040	3.6	0.1921	2.8	0.77	1133.0	29.1	1150.1	25.1	1183.4	46.1	1183.4	46.1	95.7
Spot 107	472	75327	5.7	12.5812	0.9	2.0637	3.0	0.1884	2.9	0.96	1112.7	29.3	1136.9	20.5	1184.2	17.3	1184.2	17.3	94.0
Spot 294	113	36366	3.8	12.5763	1.3	2.1454	2.9	0.1958	2.6	0.89	1152.5	27.8	1163.6	20.4	1185.0	25.9	1185.0	25.9	97.3
Spot 22	30	73946	2.6	12.5730	1.5	2.1252	3.1	0.1939	2.7	0.87	1142.3	28.1	1157.0	21.4	1185.5	30.6	1185.5	30.6	96.4
Spot 213	244	37925	3.6	12.5724	0.9	2.1871	2.6	0.1995	2.4	0.93	1172.7	25.6	1177.0	17.8	1185.6	18.4	1185.6	18.4	98.9
Spot 47	118	41847	3.8	12.5662	1.1	2.1850	2.9	0.1992	2.7	0.93	1171.1	28.7	1176.3	20.1	1186.6	21.1	1186.6	21.1	98.7
Spot 198	25	22020	1.3	12.5635	1.2	2.1226	2.6	0.1935	2.3	0.88	1140.3	23.8	1156.2	17.9	1187.0	24.5	1187.0	24.5	96.1
Spot 307	60	11129	1.7	12.5572	1.1	2.1604	3.0	0.1968	2.8	0.93	1158.3	29.9	1168.4	21.1	1188.0	22.4	1188.0	22.4	97.5
Spot 297	65	33874	3.6	12.5498	1.1	2.1836	3.2	0.1988	3.0	0.94	1169.1	32.0	1175.8	22.1	1189.2	20.8	1189.2	20.8	98.3

Spot 58	484	127142	5.7	12.5450	1.0	2.1223	3.3	0.1932	3.2	0.95	1138.6	32.9	1156.1	22.8	1189.9	19.7	1189.9	19.7	95.7
Spot 185	235	87406	4.7	12.5326	1.2	2.1752	2.7	0.1978	2.4	0.89	1163.5	25.3	1173.1	18.5	1191.8	23.6	1191.8	23.6	97.6
Spot 10	58	39184	2.0	12.5215	1.4	2.1643	2.7	0.1966	2.3	0.85	1157.2	24.8	1169.7	19.1	1193.6	28.4	1193.6	28.4	97.0
Spot 35	474	42420	4.3	12.5187	0.9	2.0893	2.6	0.1898	2.5	0.94	1120.2	25.3	1145.3	17.9	1194.0	17.3	1194.0	17.3	93.8
Spot 160	36	6796	6.5	12.5175	1.3	2.0923	3.0	0.1900	2.7	0.90	1121.5	27.8	1146.3	20.6	1194.2	25.6	1194.2	25.6	93.9
Spot 231	117	9119	5.7	12.5147	1.3	2.2605	3.2	0.2053	3.0	0.92	1203.6	32.6	1200.1	22.7	1194.6	24.9	1194.6	24.9	100.7
Spot 43	13	14446	2.4	12.5141	1.5	2.2210	3.8	0.2017	3.5	0.92	1184.3	38.3	1187.7	26.9	1194.8	29.3	1194.8	29.3	99.1
Spot 270	61	13499	1.1	12.5100	1.3	2.2009	3.8	0.1998	3.6	0.94	1174.1	38.6	1181.3	26.8	1195.4	26.2	1195.4	26.2	98.2
Spot 267	199	537563	4.3	12.5062	1.2	2.2182	2.7	0.2013	2.4	0.90	1182.2	25.7	1186.8	18.6	1196.0	23.0	1196.0	23.0	98.8
Spot 111	49	22274	1.8	12.5058	1.0	2.1544	2.6	0.1955	2.4	0.92	1151.0	25.5	1166.5	18.3	1196.1	20.5	1196.1	20.5	96.2
Spot 138	30	171246	3.7	12.4936	1.2	2.1935	2.7	0.1988	2.4	0.89	1169.1	25.5	1179.0	18.7	1198.0	24.2	1198.0	24.2	97.6
Spot 262	44	85926	2.4	12.4922	1.3	2.0896	3.4	0.1894	3.1	0.93	1118.1	32.2	1145.4	23.3	1198.2	25.2	1198.2	25.2	93.3
Spot 100	62	117205	2.8	12.4886	1.1	2.1400	2.2	0.1939	1.9	0.87	1142.6	20.1	1161.8	15.2	1198.8	21.1	1198.8	21.1	95.3
Spot 65	17	10778	3.1	12.4821	1.6	2.2160	2.7	0.2007	2.2	0.82	1179.1	24.2	1186.1	19.1	1199.8	30.7	1199.8	30.7	98.3
Spot 20	65	12018	2.0	12.4734	1.3	2.1593	3.0	0.1954	2.7	0.89	1150.7	28.0	1168.1	20.7	1201.2	26.5	1201.2	26.5	95.8
Spot 298	54	12132	3.2	12.4704	1.0	2.1245	2.9	0.1922	2.7	0.94	1133.4	28.3	1156.8	20.1	1201.7	20.2	1201.7	20.2	94.3
Spot 183	101	1819160	1.5	12.4650	1.0	2.1479	2.6	0.1943	2.4	0.92	1144.4	25.0	1164.4	17.9	1202.5	19.6	1202.5	19.6	95.2
Spot 238	57	11795	7.1	12.4643	1.2	2.1944	2.5	0.1985	2.2	0.87	1167.1	23.4	1179.3	17.5	1202.6	24.3	1202.6	24.3	97.0
Spot 209	180	30762	5.0	12.4629	1.2	2.2364	3.0	0.2022	2.8	0.92	1187.3	30.3	1192.5	21.3	1202.8	23.3	1202.8	23.3	98.7
Spot 48	17	25522	3.3	12.4513	1.3	2.1519	2.9	0.1944	2.6	0.89	1145.2	27.2	1165.7	20.2	1204.7	26.3	1204.7	26.3	95.1
Spot 303	71	34852	2.1	12.4511	1.3	2.1877	3.1	0.1976	2.8	0.91	1162.6	29.6	1177.1	21.3	1204.7	25.2	1204.7	25.2	96.5
Spot 12	64	27772	2.7	12.4500	0.9	2.1956	2.6	0.1983	2.5	0.94	1166.4	26.6	1179.6	18.5	1204.9	17.6	1204.9	17.6	96.8
Spot 217	22	18535	3.5	12.4494	1.6	2.2930	3.5	0.2071	3.1	0.89	1213.5	34.7	1210.1	24.9	1205.0	31.9	1205.0	31.9	100.7
Spot 126	50	42344	1.9	12.4379	1.1	2.2261	2.9	0.2009	2.6	0.92	1180.2	28.5	1189.3	20.0	1206.8	21.4	1206.8	21.4	97.8
Spot 170	384	56442	3.1	12.4353	1.0	2.1612	2.9	0.1950	2.7	0.93	1148.4	28.4	1168.6	20.1	1207.2	20.6	1207.2	20.6	95.1

Spot 180	53	182476	3.9	12.4149	1.1	2.2098	2.7	0.1991	2.4	0.91	1170.3	26.0	1184.1	18.7	1210.4	21.8	1210.4	21.8	96.7
Spot 84	37	19748	1.0	12.4055	1.1	2.2403	3.1	0.2017	2.9	0.94	1184.2	31.5	1193.7	21.8	1212.0	20.8	1212.0	20.8	97.7
Spot 219	41	18141	3.7	12.3932	1.3	2.2256	3.7	0.2001	3.4	0.93	1176.1	36.8	1189.1	25.7	1213.9	26.1	1213.9	26.1	96.9
Spot 128	8	1272931	3.6	12.3898	1.9	2.2954	3.0	0.2064	2.3	0.78	1209.4	25.7	1210.9	21.1	1214.4	36.6	1214.4	36.6	99.6
Spot 71	24	56036	2.5	12.3763	1.4	2.1069	3.9	0.1892	3.7	0.94	1117.0	37.6	1151.1	26.9	1216.6	27.1	1216.6	27.1	91.8
Spot 228	38	75265	2.2	12.3421	1.2	2.2235	3.1	0.1991	2.9	0.92	1170.6	30.6	1188.5	21.8	1222.0	24.2	1222.0	24.2	95.8
Spot 250	8	2222	2.9	12.3277	4.3	2.3017	5.3	0.2059	3.1	0.58	1206.9	33.8	1212.8	37.6	1224.3	85.1	1224.3	85.1	98.6
Spot 235	150	120263	1.8	12.3267	1.0	2.2688	3.2	0.2029	3.0	0.95	1191.0	32.5	1202.6	22.2	1224.4	19.6	1224.4	19.6	97.3
Spot 41	36	3385	2.1	12.2878	1.3	2.3404	3.4	0.2087	3.2	0.92	1221.7	35.2	1224.6	24.4	1230.7	25.6	1230.7	25.6	99.3
Spot 277	45	26491	1.2	12.2638	1.1	2.3453	3.1	0.2087	2.9	0.93	1221.9	31.8	1226.1	21.9	1234.5	22.2	1234.5	22.2	99.0
Spot 55	31	11391	2.9	12.2431	1.5	2.2144	3.8	0.1967	3.5	0.92	1157.6	36.9	1185.6	26.6	1237.8	30.0	1237.8	30.0	93.5
Spot 145	178	172064	0.8	12.2391	0.9	2.3914	3.0	0.2124	2.9	0.95	1241.4	32.3	1240.0	21.6	1238.5	18.4	1238.5	18.4	100.2
Spot 85	16	21821	2.9	12.2084	1.3	2.1884	2.7	0.1939	2.3	0.87	1142.2	24.5	1177.4	18.8	1243.4	26.1	1243.4	26.1	91.9
Spot 261	22	5037	2.8	12.2056	1.7	2.3441	3.5	0.2076	3.1	0.87	1216.0	33.8	1225.8	25.0	1243.8	33.9	1243.8	33.9	97.8
Spot 204	14	10674	2.7	12.1863	1.3	2.2305	3.6	0.1972	3.3	0.93	1160.4	35.5	1190.7	25.2	1246.9	25.9	1246.9	25.9	93.1
Spot 258	81	42782	4.2	12.1574	1.2	2.3714	2.8	0.2092	2.5	0.90	1224.5	28.2	1234.0	20.0	1251.6	23.3	1251.6	23.3	97.8
Spot 49	20	7441	4.0	12.1410	1.7	2.3514	3.2	0.2071	2.8	0.85	1213.6	30.6	1228.0	23.1	1254.2	33.1	1254.2	33.1	96.8
Spot 245	18	8451	3.0	12.0964	1.1	2.2969	2.8	0.2016	2.5	0.91	1183.9	27.6	1211.3	19.7	1261.4	22.2	1261.4	22.2	93.9
Spot 264	27	75316	3.3	12.0471	1.3	2.3141	2.7	0.2023	2.3	0.88	1187.5	25.4	1216.6	18.9	1269.4	24.7	1269.4	24.7	93.6
Spot 302	45	5319	2.5	12.0209	1.3	2.6246	3.0	0.2289	2.7	0.91	1328.9	32.8	1307.6	22.2	1273.6	24.8	1273.6	24.8	104.3
Spot 6	29	15075	3.2	12.0174	1.3	2.4132	2.8	0.2104	2.5	0.89	1231.1	28.2	1246.5	20.2	1274.2	24.7	1274.2	24.7	96.6
Spot 74	108	23000	3.3	11.8997	1.2	2.5139	3.3	0.2171	3.1	0.94	1266.3	35.7	1276.1	24.1	1293.4	22.4	1293.4	22.4	97.9
Spot 295	13	34854	1.6	11.8988	1.5	2.3992	2.9	0.2071	2.5	0.85	1213.5	27.6	1242.4	21.0	1293.5	30.1	1293.5	30.1	93.8
Spot 244	146	27346	2.6	11.8429	1.1	2.5658	2.9	0.2205	2.7	0.93	1284.4	31.1	1291.0	21.0	1302.7	20.7	1302.7	20.7	98.6
Spot 108	53	18344	2.3	11.8406	1.3	2.6678	3.0	0.2292	2.8	0.91	1330.3	33.1	1319.6	22.4	1303.0	24.8	1303.0	24.8	102.1

Spot 197	6	3393	1.8	11.8124	2.7	2.5268	3.9	0.2166	2.9	0.73	1263.7	33.0	1279.8	28.7	1307.7	52.4	1307.7	52.4	96.6
Spot 181	8	5933	2.8	11.7882	1.6	2.4099	3.9	0.2061	3.6	0.92	1208.1	39.2	1245.6	27.9	1311.6	30.1	1311.6	30.1	92.1
Spot 135	59	9890	3.6	11.7867	1.0	2.7300	2.6	0.2335	2.5	0.93	1352.7	30.0	1336.7	19.7	1311.9	18.9	1311.9	18.9	103.1
Spot 154	88	13075626	4.2	11.7427	1.0	2.6655	2.8	0.2271	2.6	0.93	1319.3	31.1	1318.9	20.7	1319.1	20.3	1319.1	20.3	100.0
Spot 51	126	15018	1.8	11.7104	1.1	2.6911	2.9	0.2287	2.7	0.93	1327.5	32.6	1326.0	21.6	1324.5	20.5	1324.5	20.5	100.2
Spot 274	23	6058	2.9	11.6927	1.8	2.6193	3.0	0.2222	2.4	0.81	1293.6	28.7	1306.1	22.3	1327.4	34.7	1327.4	34.7	97.5
Spot 120	33	4903	1.4	11.6503	1.0	2.7989	3.0	0.2366	2.9	0.95	1369.0	35.5	1355.2	22.7	1334.4	19.0	1334.4	19.0	102.6
Spot 63	30	7886	4.3	11.6247	1.4	2.8120	3.4	0.2372	3.1	0.92	1372.0	38.8	1358.7	25.6	1338.7	26.2	1338.7	26.2	102.5
Spot 129	76	39395	3.1	11.6164	1.0	2.6242	3.0	0.2212	2.8	0.94	1288.2	32.6	1307.5	21.8	1340.1	19.1	1340.1	19.1	96.1
Spot 143	23	5227	3.8	11.6145	1.6	2.7061	4.1	0.2281	3.8	0.92	1324.3	45.3	1330.1	30.5	1340.4	30.9	1340.4	30.9	98.8
Spot 152	29	19723	2.4	11.6088	1.3	2.8311	3.3	0.2385	3.1	0.92	1378.7	37.9	1363.8	24.9	1341.3	25.3	1341.3	25.3	102.8
Spot 137	90	411781	2.6	11.5930	1.0	2.8183	2.5	0.2371	2.3	0.92	1371.4	28.8	1360.4	18.9	1344.0	18.7	1344.0	18.7	102.0
Spot 232	37	30466	2.5	11.5443	1.2	2.6719	2.6	0.2238	2.3	0.88	1302.0	26.6	1320.7	18.9	1352.1	23.0	1352.1	23.0	96.3
Spot 241	77	37083	1.7	11.5319	1.0	2.6844	2.7	0.2246	2.5	0.93	1306.2	29.8	1324.2	20.1	1354.2	19.7	1354.2	19.7	96.5
Spot 287	86	212074	2.6	11.5080	1.1	2.6595	3.7	0.2221	3.6	0.96	1292.8	41.9	1317.3	27.6	1358.2	20.9	1358.2	20.9	95.2
Spot 282	38	7950	3.7	11.4581	1.5	2.8861	3.7	0.2399	3.4	0.91	1386.4	41.9	1378.3	27.7	1366.5	28.8	1366.5	28.8	101.5
Spot 186	86	81772	3.0	11.4406	0.9	3.0002	3.0	0.2490	2.8	0.95	1433.6	36.5	1407.7	22.7	1369.5	17.5	1369.5	17.5	104.7
Spot 36	58	19566	2.9	11.4359	0.9	2.8406	2.3	0.2357	2.1	0.91	1364.3	25.3	1366.3	17.0	1370.3	18.2	1370.3	18.2	99.6
Spot 230	97	57757	2.8	11.4173	1.0	2.6939	3.1	0.2232	2.9	0.94	1298.6	34.3	1326.8	22.9	1373.4	19.9	1373.4	19.9	94.6
Spot 227	146	52878	3.5	11.4099	1.0	2.9024	3.4	0.2403	3.2	0.96	1388.2	40.4	1382.5	25.5	1374.7	19.0	1374.7	19.0	101.0
Spot 76	77	32419	3.6	11.3575	1.1	3.0007	3.3	0.2473	3.1	0.94	1424.5	39.9	1407.8	25.3	1383.5	22.0	1383.5	22.0	103.0
Spot 8	79	32712	2.1	11.3326	1.0	2.8405	2.8	0.2336	2.6	0.93	1353.2	31.4	1366.3	20.7	1387.7	19.0	1387.7	19.0	97.5
Spot 40	98	13210	2.5	11.3124	1.3	2.9308	3.4	0.2406	3.2	0.93	1389.6	39.7	1389.9	26.0	1391.2	24.9	1391.2	24.9	99.9
Spot 242	53	344957	4.2	11.3010	1.1	2.8928	2.9	0.2372	2.7	0.92	1372.1	33.5	1380.0	22.2	1393.1	21.7	1393.1	21.7	98.5
Spot 45	51	13217	3.2	11.2897	0.9	2.8638	2.4	0.2346	2.2	0.92	1358.5	27.3	1372.4	18.2	1395.0	17.9	1395.0	17.9	97.4

Spot 125	82	10870	3.0	11.2812	1.3	3.0578	3.1	0.2503	2.9	0.92	1440.0	37.2	1422.2	24.1	1396.4	24.3	1396.4	24.3	103.1
Spot 140	48	10477	1.2	11.2760	1.1	2.9955	2.4	0.2451	2.1	0.89	1413.1	26.8	1406.5	18.0	1397.3	20.3	1397.3	20.3	101.1
Spot 288	72	20978	1.4	11.2407	0.9	2.8524	2.8	0.2326	2.7	0.95	1348.3	32.4	1369.4	21.1	1403.3	16.5	1403.3	16.5	96.1
Spot 133	56	12920	1.1	11.2273	1.1	3.1116	3.1	0.2535	2.9	0.94	1456.4	37.7	1435.6	23.7	1405.6	20.5	1405.6	20.5	103.6
Spot 178	66	24022	2.3	11.2243	1.1	3.0485	2.8	0.2483	2.6	0.92	1429.6	33.3	1419.8	21.5	1406.1	20.6	1406.1	20.6	101.7
Spot 37	143	160903	2.8	11.1969	1.1	2.9106	3.0	0.2365	2.8	0.93	1368.3	34.3	1384.7	22.6	1410.8	20.8	1410.8	20.8	97.0
Spot 13	102	24079	3.0	11.1747	1.0	2.9960	2.7	0.2429	2.5	0.93	1401.9	31.6	1406.6	20.5	1414.6	18.8	1414.6	18.8	99.1
Spot 299	101	256412	2.7	11.1605	1.1	2.8949	3.4	0.2344	3.2	0.94	1357.7	39.0	1380.6	25.5	1417.0	21.6	1417.0	21.6	95.8
Spot 184	36	5922	1.8	11.1370	1.4	3.0697	3.4	0.2481	3.0	0.91	1428.5	39.0	1425.2	25.8	1421.1	27.3	1421.1	27.3	100.5
Spot 69	89	46297	0.6	11.1290	1.0	3.0597	2.5	0.2471	2.3	0.92	1423.3	29.9	1422.7	19.4	1422.4	18.6	1422.4	18.6	100.1
Spot 257	153	723883	2.6	11.1076	1.0	3.1323	2.7	0.2524	2.5	0.93	1451.1	32.4	1440.7	20.6	1426.1	18.5	1426.1	18.5	101.8
Spot 281	47	14162	1.4	11.0330	1.2	3.1581	3.5	0.2528	3.2	0.93	1453.0	41.9	1447.0	26.6	1439.0	23.7	1439.0	23.7	101.0
Spot 199	78	11454	1.7	10.9670	1.1	3.0509	2.4	0.2428	2.1	0.89	1401.1	26.5	1420.5	18.1	1450.4	20.7	1450.4	20.7	96.6
Spot 309	99	86830	2.6	10.9436	1.0	3.1951	3.0	0.2537	2.8	0.95	1457.6	36.5	1456.0	22.9	1454.5	18.3	1454.5	18.3	100.2
Spot 78	36	33177	1.5	10.9393	1.1	3.0059	2.9	0.2386	2.7	0.92	1379.4	33.5	1409.1	22.3	1455.2	21.7	1455.2	21.7	94.8
Spot 304	61	36522	2.8	10.8843	1.1	3.2618	2.7	0.2576	2.4	0.91	1477.6	32.2	1472.0	20.8	1464.8	21.1	1464.8	21.1	100.9
Spot 246	42	43645	1.0	10.8498	1.4	3.0678	2.6	0.2415	2.2	0.85	1394.5	27.7	1424.7	20.0	1470.8	26.5	1470.8	26.5	94.8
Spot 25	27	22295	2.0	10.8261	1.1	3.1714	2.4	0.2491	2.1	0.89	1433.9	27.5	1450.2	18.5	1475.0	20.4	1475.0	20.4	97.2
Spot 253	50	24856	2.4	10.7596	1.4	3.0274	3.5	0.2364	3.3	0.92	1367.7	40.4	1414.6	27.1	1486.7	25.6	1486.7	25.6	92.0
Spot 15	43	6034	1.8	10.7218	1.7	2.8210	3.1	0.2195	2.5	0.82	1279.0	29.1	1361.1	22.9	1493.3	33.0	1493.3	33.0	85.6
Spot 101	95	50232	2.9	10.5111	1.0	3.5774	2.8	0.2728	2.6	0.93	1555.2	35.4	1544.5	21.9	1530.8	19.4	1530.8	19.4	101.6
Spot 86	38	6601	1.2	10.4834	1.7	3.3948	3.3	0.2582	2.8	0.85	1480.8	36.9	1503.2	25.6	1535.8	32.0	1535.8	32.0	96.4
Spot 268	62	159650	2.8	10.1926	1.0	3.5228	2.7	0.2605	2.4	0.92	1492.5	32.6	1532.3	21.0	1588.5	19.1	1588.5	19.1	94.0
Spot 117	33	5639	3.2	10.0937	1.8	3.6717	3.0	0.2689	2.4	0.79	1535.3	32.6	1565.2	24.0	1606.7	34.1	1606.7	34.1	95.6
Spot 252	153	15234	1.8	10.0051	1.0	3.8300	2.9	0.2780	2.7	0.94	1581.5	38.2	1599.1	23.4	1623.1	18.4	1623.1	18.4	97.4

Spot 103	82	172445	2.1	9.9043	1.1	4.1805	3.2	0.3004	3.0	0.94	1693.4	44.3	1670.2	26.0	1641.9	20.2	1641.9	20.2	103.1
Spot 98	30	23422	1.2	9.8061	1.1	4.1449	3.2	0.2949	3.0	0.93	1666.0	43.6	1663.2	26.0	1660.4	20.9	1660.4	20.9	100.3
Spot 64	47	16975	3.9	9.5406	1.2	4.0459	2.7	0.2801	2.4	0.89	1591.7	33.8	1643.5	21.8	1711.1	22.1	1711.1	22.1	93.0
Spot 83	47	27334	1.4	9.5220	1.2	4.2755	2.8	0.2954	2.5	0.91	1668.4	37.4	1688.7	23.1	1714.7	21.7	1714.7	21.7	97.3
Spot 280	30	7022	2.7	9.4924	1.2	4.5471	2.6	0.3132	2.3	0.89	1756.4	34.8	1739.6	21.2	1720.4	21.6	1720.4	21.6	102.1
Spot 251	114	26520	4.2	9.1651	1.0	4.7134	3.2	0.3134	3.1	0.95	1757.6	47.1	1769.6	27.1	1784.6	19.1	1784.6	19.1	98.5
Spot 306	160	35307	2.6	8.6710	1.3	5.3245	3.1	0.3350	2.8	0.91	1862.5	45.0	1872.8	26.2	1885.0	23.1	1885.0	23.1	98.8
Spot 202	58	33875	1.1	6.2229	1.0	8.5243	2.6	0.3849	2.4	0.93	2099.1	43.5	2288.5	23.7	2463.0	16.3	2463.0	16.3	85.2
Spot 159	51	101619	3.6	6.1209	1.0	9.6212	3.0	0.4273	2.8	0.94	2293.5	54.1	2399.2	27.4	2490.9	17.1	2490.9	17.1	92.1
Spot 122	36	9418	0.7	6.0270	1.2	10.3401	3.0	0.4522	2.8	0.92	2405.0	55.6	2465.7	27.9	2516.9	20.1	2516.9	20.1	95.6
Spot 67	22	1785986	1.5	5.7080	1.2	12.5081	3.3	0.5180	3.1	0.93	2690.9	68.3	2643.3	31.3	2607.9	20.0	2607.9	20.0	103.2
Spot 29	18	8565	0.9	5.6729	1.2	12.3844	2.9	0.5098	2.6	0.90	2655.6	56.7	2634.0	27.1	2618.1	20.6	2618.1	20.6	101.4
Spot 208	56	22921	3.8	5.5606	0.9	12.6895	2.6	0.5120	2.5	0.95	2665.1	54.4	2656.9	24.8	2651.4	14.2	2651.4	14.2	100.5
Spot 59	32	26532	2.3	5.4880	1.3	12.9182	3.4	0.5144	3.1	0.92	2675.4	67.8	2673.7	31.8	2673.1	22.2	2673.1	22.2	100.1
Spot 164	21	237478	1.3	5.4805	1.0	12.7670	3.6	0.5077	3.4	0.96	2646.7	74.4	2662.6	33.7	2675.4	17.1	2675.4	17.1	98.9

APPENDIX B: DANBY U-Pb ANALYTICAL RESULTS

Table 2. Danby U-Pb analytical results of sample from Shelburne Falls: 18T 0642154E 4914584N

						Isotope ratios					Apparent ages (Ma)								
Analysis	U (ppm)	206Pb 204Pb	U/Th	206Pb* 207Pb*	± (%)	207Pb* 235U*	± (%)	206Pb* 238U	± (%)	error corr.	206Pb* 238U*	± (Ma)	207Pb* 235U	± (Ma)	206Pb* 207Pb*	± (Ma)	Best age (Ma)	± (Ma)	Conc (%)
Spot 145	481	36987	5.0	14.1298	1.2	1.6085	3.4	0.1649	3.2	0.94	984.0	29.5	973.5	21.5	950.8	23.7	950.8	23.7	103.5
Spot 229	277	72092	1.1	13.9367	1.3	1.6823	3.6	0.1701	3.3	0.93	1012.8	31.3	1001.8	22.8	978.9	26.5	978.9	26.5	103.5
Spot 68	43	3026	1.4	13.9025	2.2	1.7103	4.0	0.1725	3.3	0.84	1026.0	31.5	1012.4	25.4	983.9	43.8	983.9	43.8	104.3
Spot 278	151	17682	1.5	13.8606	1.4	1.6041	3.1	0.1613	2.8	0.90	964.2	24.9	971.8	19.4	990.1	28.0	990.1	28.0	97.4
Spot 169	375	44603	2.0	13.8283	1.2	1.6847	3.3	0.1690	3.1	0.93	1006.8	28.6	1002.8	21.1	994.8	25.2	994.8	25.2	101.2
Spot 38	666	34875	1.1	13.8060	1.0	1.6839	3.3	0.1687	3.2	0.95	1004.9	29.4	1002.5	21.2	998.1	21.3	998.1	21.3	100.7
Spot 90	44	5646	2.0	13.7756	1.4	1.7626	3.0	0.1762	2.6	0.88	1046.0	25.3	1031.8	19.3	1002.6	28.8	1002.6	28.8	104.3
Spot 215	164	17491	0.9	13.7483	1.4	1.5923	4.0	0.1588	3.8	0.94	950.3	33.3	967.2	25.1	1006.6	27.9	1006.6	27.9	94.4
Spot 67	508	27049	2.0	13.7342	1.0	1.7435	2.7	0.1737	2.5	0.92	1032.7	23.9	1024.8	17.5	1008.7	21.0	1008.7	21.0	102.4
Spot 248	107	6780	2.7	13.7334	1.9	1.7882	3.5	0.1782	2.9	0.84	1057.1	28.2	1041.2	22.5	1008.8	38.3	1008.8	38.3	104.8
Spot 214	118	18573	0.3	13.6984	1.4	1.7852	3.4	0.1774	3.1	0.92	1053.0	30.3	1040.1	22.2	1014.0	27.7	1014.0	27.7	103.8
Spot 164	185	12530	1.3	13.6930	1.2	1.7831	4.2	0.1772	4.0	0.96	1051.4	38.9	1039.3	27.2	1014.8	24.1	1014.8	24.1	103.6
Spot 141	504	26002	5.6	13.6745	1.0	1.7940	3.3	0.1780	3.1	0.95	1056.1	30.4	1043.3	21.3	1017.5	19.8	1017.5	19.8	103.8
Spot 2	842	39201	3.0	13.6634	0.9	1.7879	2.7	0.1773	2.6	0.94	1051.9	25.1	1041.1	17.9	1019.2	18.8	1019.2	18.8	103.2
Spot 178	898	86774	1.9	13.6593	1.1	1.7962	3.6	0.1780	3.4	0.95	1056.2	33.4	1044.1	23.5	1019.8	22.6	1019.8	22.6	103.6

Spot 9	135	9542	2.3	13.6249	1.2	1.7430	2.8	0.1723	2.6	0.90	1024.8	24.2	1024.6	18.3	1024.9	24.5	1024.9	24.5	100.0
Spot 313	469	82274	2.6	13.5965	0.9	1.7120	2.5	0.1689	2.3	0.94	1006.0	21.7	1013.0	15.9	1029.1	17.5	1029.1	17.5	97.8
Spot 146	67	3153	2.6	13.5765	1.8	1.7352	3.9	0.1709	3.4	0.88	1017.3	32.3	1021.7	25.0	1032.1	36.6	1032.1	36.6	98.6
Spot 172	60	6233	1.2	13.5754	1.5	1.7291	3.9	0.1703	3.6	0.92	1013.8	34.1	1019.4	25.3	1032.2	30.8	1032.2	30.8	98.2
Spot 10	488	89571	2.7	13.5737	1.0	1.7522	3.4	0.1726	3.2	0.96	1026.3	30.6	1028.0	21.8	1032.5	19.9	1032.5	19.9	99.4
Spot 65	217	30059	1.2	13.5353	1.0	1.8006	2.8	0.1768	2.7	0.94	1049.7	25.8	1045.7	18.5	1038.2	19.6	1038.2	19.6	101.1
Spot 108	236	315599	2.8	13.5263	1.4	1.8591	3.0	0.1825	2.7	0.89	1080.4	26.9	1066.7	20.0	1039.5	27.5	1039.5	27.5	103.9
Spot 255	60	8348	2.3	13.5248	1.5	1.7687	3.8	0.1736	3.5	0.92	1031.7	33.0	1034.0	24.5	1039.8	30.5	1039.8	30.5	99.2
Spot 133	431	306718	4.8	13.5145	0.9	1.7359	2.9	0.1702	2.7	0.95	1013.3	25.7	1022.0	18.7	1041.3	19.0	1041.3	19.0	97.3
Spot 120	225	35229	0.8	13.5051	1.2	1.7135	3.0	0.1679	2.7	0.91	1000.6	24.8	1013.6	18.9	1042.7	25.0	1042.7	25.0	96.0
Spot 123	536	78847	6.0	13.4977	1.2	1.7892	3.4	0.1752	3.2	0.93	1040.9	30.4	1041.6	22.1	1043.8	24.7	1043.8	24.7	99.7
Spot 209	164	12229	0.8	13.4933	1.3	1.7043	4.2	0.1669	4.0	0.95	994.8	36.7	1010.2	26.9	1044.5	27.2	1044.5	27.2	95.2
-Spot 39	206	7253	2.2	13.4929	1.3	1.7584	3.2	0.1721	2.9	0.92	1023.9	27.7	1030.2	20.6	1044.5	25.3	1044.5	25.3	98.0
Spot 211	114	7856	2.4	13.4777	1.3	1.8475	3.6	0.1807	3.4	0.93	1070.6	33.6	1062.5	24.0	1046.8	26.6	1046.8	26.6	102.3
Spot 256	273	83673	2.4	13.4697	1.3	1.7789	3.5	0.1739	3.2	0.93	1033.4	30.6	1037.8	22.4	1048.0	25.9	1048.0	25.9	98.6
Spot 161	229	34567	0.8	13.4670	0.9	1.8574	3.0	0.1815	2.9	0.95	1075.1	28.2	1066.1	19.8	1048.4	18.9	1048.4	18.9	102.5
Spot 288	213	24152	1.9	13.4625	1.3	1.8190	3.1	0.1777	2.8	0.91	1054.3	27.6	1052.3	20.4	1049.1	26.0	1049.1	26.0	100.5
Spot 92	674	25725	3.3	13.4542	1.2	1.7472	4.0	0.1706	3.8	0.95	1015.2	35.6	1026.1	25.6	1050.4	23.9	1050.4	23.9	96.7
Spot 26	183	419572	2.4	13.4409	1.2	1.7324	3.6	0.1690	3.4	0.94	1006.3	31.2	1020.6	23.0	1052.4	24.5	1052.4	24.5	95.6
Spot 284	289	26121	99.5	13.4219	1.1	1.8507	2.5	0.1802	2.2	0.89	1068.3	22.1	1063.7	16.6	1055.2	23.0	1055.2	23.0	101.2
Spot 98	245	38965	0.9	13.4049	1.2	1.8311	2.9	0.1781	2.6	0.91	1056.6	25.5	1056.7	18.9	1057.7	24.1	1057.7	24.1	99.9
Spot 157	113	4463	1.9	13.4019	1.4	1.7875	3.7	0.1738	3.4	0.93	1033.1	32.8	1040.9	24.1	1058.2	28.3	1058.2	28.3	97.6
Spot 204	414	30593	3.3	13.4016	1.4	1.8858	3.4	0.1834	3.1	0.91	1085.4	30.6	1076.1	22.3	1058.2	27.8	1058.2	27.8	102.6
Spot 250	191	20544	1.1	13.3976	1.6	1.9030	3.2	0.1850	2.8	0.87	1094.2	28.1	1082.1	21.3	1058.8	31.8	1058.8	31.8	103.3
Spot 158	458	81686	2.5	13.3898	0.9	1.9063	2.7	0.1852	2.6	0.94	1095.3	25.7	1083.3	18.0	1060.0	17.8	1060.0	17.8	103.3

Spot 143	144	17133	3.0	13.3732	1.3	1.7774	2.6	0.1725	2.2	0.86	1025.7	20.9	1037.2	16.7	1062.5	26.6	1062.5	26.6	96.5
Spot 148	155	40214	1.4	13.3695	1.2	1.8364	3.3	0.1781	3.1	0.94	1056.8	30.2	1058.6	21.8	1063.1	23.6	1063.1	23.6	99.4
Spot 173	325	20850	1.4	13.3677	1.7	1.7926	4.0	0.1739	3.6	0.90	1033.4	34.5	1042.8	26.1	1063.3	34.5	1063.3	34.5	97.2
Spot 59	100	28639	1.9	13.3359	1.3	1.8558	3.3	0.1796	3.0	0.92	1064.6	29.4	1065.5	21.6	1068.1	26.5	1068.1	26.5	99.7
Spot 287	378	25436	3.5	13.3353	1.1	1.8659	2.9	0.1805	2.6	0.92	1070.0	25.8	1069.1	18.9	1068.2	23.0	1068.2	23.0	100.2
Spot 268	90	5483	2.1	13.3296	1.6	1.8890	3.4	0.1827	3.0	0.88	1081.7	29.6	1077.2	22.4	1069.1	32.1	1069.1	32.1	101.2
Spot 267	219	45095	3.0	13.3286	1.4	1.9418	4.2	0.1878	4.0	0.94	1109.4	40.9	1095.6	28.5	1069.2	28.2	1069.2	28.2	103.8
Spot 78	116	12547	1.9	13.3179	1.5	1.8389	4.6	0.1777	4.3	0.94	1054.4	42.1	1059.5	30.2	1070.8	30.9	1070.8	30.9	98.5
Spot 27	454	39091	30.8	13.3175	1.4	1.8433	3.4	0.1781	3.1	0.92	1056.7	30.3	1061.0	22.3	1070.9	27.3	1070.9	27.3	98.7
Spot 263	74	8473	1.0	13.3137	1.2	1.8172	3.3	0.1755	3.1	0.94	1042.6	29.5	1051.7	21.5	1071.5	23.3	1071.5	23.3	97.3
Spot 76	125	28021	1.2	13.3077	1.6	1.8470	3.0	0.1783	2.6	0.85	1057.9	24.9	1062.4	19.8	1072.4	31.9	1072.4	31.9	98.7
Spot 142	361	39823	3.2	13.3039	1.5	1.8378	3.3	0.1774	2.9	0.90	1052.8	28.6	1059.1	21.6	1073.0	29.2	1073.0	29.2	98.1
Spot 188	161	54535	26.8	13.2968	1.1	1.7953	3.2	0.1732	3.0	0.94	1029.8	28.3	1043.7	20.7	1074.0	22.1	1074.0	22.1	95.9
Spot 85	187	27727	0.7	13.2953	1.0	1.6923	3.7	0.1633	3.6	0.96	974.8	32.4	1005.6	23.8	1074.3	20.6	1074.3	20.6	90.7
Spot 69	175	33580	1.5	13.2951	1.4	1.7880	3.9	0.1725	3.6	0.93	1025.8	34.4	1041.1	25.4	1074.3	28.7	1074.3	28.7	95.5
Spot 269	386	18817	3.5	13.2888	1.4	1.8908	4.0	0.1823	3.7	0.94	1079.6	37.3	1077.9	26.5	1075.2	27.5	1075.2	27.5	100.4
Spot 47	129	19701	1.0	13.2872	1.3	1.7889	2.8	0.1725	2.5	0.89	1025.7	23.4	1041.4	18.0	1075.5	25.3	1075.5	25.3	95.4
Spot 35	104	30623	1.5	13.2737	1.3	1.9605	3.2	0.1888	2.9	0.92	1114.9	30.1	1102.0	21.5	1077.5	25.2	1077.5	25.2	103.5
Spot 86	62	4167	3.8	13.2643	2.7	1.9429	4.0	0.1870	3.0	0.74	1105.0	30.0	1096.0	26.7	1078.9	53.5	1078.9	53.5	102.4
Spot 58	258	13745	2.5	13.2534	1.3	1.9659	3.4	0.1891	3.2	0.93	1116.2	32.4	1103.9	22.9	1080.6	25.5	1080.6	25.5	103.3
Spot 91	51	8279	1.3	13.2528	1.5	1.8162	3.6	0.1746	3.3	0.91	1037.7	31.4	1051.3	23.5	1080.7	29.5	1080.7	29.5	96.0
Spot 190	337	18917	22.3	13.2527	1.1	1.9335	3.1	0.1859	2.9	0.94	1099.3	29.7	1092.8	20.9	1080.7	21.4	1080.7	21.4	101.7
Spot 116	170	7963	2.9	13.2523	1.1	1.8559	3.0	0.1785	2.8	0.94	1058.6	27.8	1065.5	20.0	1080.7	21.4	1080.7	21.4	97.9
Spot 202	127	46644	1.6	13.2450	1.5	1.9568	3.3	0.1881	2.9	0.88	1110.8	29.4	1100.8	21.9	1081.9	30.4	1081.9	30.4	102.7
-Spot 44	213	27736	1.6	13.2410	1.0	1.8414	3.4	0.1769	3.2	0.95	1050.1	31.0	1060.3	22.1	1082.5	20.8	1082.5	20.8	97.0

Spot 184	123	7451	2.4	13.2405	1.8	1.8699	3.3	0.1796	2.8	0.85	1065.0	27.8	1070.5	22.1	1082.5	35.3	1082.5	35.3	98.4
Spot 201	452	89507	2.0	13.2395	1.2	1.9735	3.4	0.1896	3.2	0.93	1119.1	32.8	1106.5	23.1	1082.7	24.7	1082.7	24.7	103.4
Spot 302	413	4244305	11.5	13.2307	1.2	1.8559	3.5	0.1782	3.3	0.94	1056.9	32.1	1065.5	23.2	1084.0	24.9	1084.0	24.9	97.5
Spot 311	158	40648	5.7	13.2301	1.2	1.7454	3.5	0.1676	3.3	0.94	998.6	30.4	1025.5	22.7	1084.1	24.6	1084.1	24.6	92.1
Spot 300	160	16327	1.5	13.2282	1.7	1.8832	3.3	0.1808	2.8	0.85	1071.1	27.7	1075.2	21.9	1084.4	34.7	1084.4	34.7	98.8
-Spot 55	231	43814	3.7	13.2166	1.5	1.8613	3.9	0.1785	3.6	0.92	1058.7	35.1	1067.4	25.7	1086.1	29.9	1086.1	29.9	97.5
Spot 135	1384	105274	2.7	13.2069	1.3	1.8185	3.4	0.1743	3.1	0.93	1035.5	30.0	1052.1	22.2	1087.6	25.3	1087.6	25.3	95.2
Spot 177	233	127638	1.6	13.2018	1.2	1.7997	2.9	0.1724	2.6	0.92	1025.3	25.0	1045.3	18.8	1088.4	23.1	1088.4	23.1	94.2
Spot 109	50	2824	4.4	13.1967	3.2	1.9625	4.7	0.1879	3.5	0.74	1110.1	35.5	1102.7	31.6	1089.2	63.3	1089.2	63.3	101.9
Spot 308	115	120921	2.6	13.1948	1.1	1.8096	3.1	0.1733	2.9	0.94	1030.0	27.9	1048.9	20.4	1089.5	21.8	1089.5	21.8	94.5
Spot 104	94	7871	1.0	13.1865	1.7	1.6907	3.4	0.1618	2.9	0.87	966.6	26.3	1005.0	21.5	1090.7	33.4	1090.7	33.4	88.6
Spot 223	106	10976	1.5	13.1822	1.3	1.8438	3.3	0.1764	3.0	0.91	1047.0	28.7	1061.2	21.4	1091.4	26.6	1091.4	26.6	95.9
Spot 234	164	11436	2.0	13.1699	1.1	1.8788	3.8	0.1795	3.6	0.96	1064.4	35.6	1073.6	25.0	1093.2	21.3	1093.2	21.3	97.4
Spot 36	189	38518	1.0	13.1686	0.9	1.8133	3.0	0.1733	2.9	0.95	1030.0	27.2	1050.3	19.6	1093.5	18.6	1093.5	18.6	94.2
Spot 6	71	32182	1.1	13.1637	1.3	1.7783	3.3	0.1699	3.0	0.92	1011.3	28.3	1037.6	21.4	1094.2	25.8	1094.2	25.8	92.4
Spot 243	345	20327	2.2	13.1513	1.3	1.9993	2.5	0.1908	2.1	0.84	1125.6	21.6	1115.3	16.8	1096.1	26.9	1096.1	26.9	102.7
Spot 57	216	165987	1.2	13.1502	1.0	1.9066	2.2	0.1819	1.9	0.88	1077.4	19.1	1083.4	14.6	1096.2	20.6	1096.2	20.6	98.3
Spot 45	407	30692	1.9	13.1499	0.9	2.0268	2.9	0.1934	2.7	0.95	1139.7	28.4	1124.5	19.5	1096.3	18.2	1096.3	18.2	104.0
Spot 22	72	33918	1.4	13.1471	1.6	1.7369	3.3	0.1657	2.8	0.87	988.3	26.1	1022.3	21.0	1096.7	31.7	1096.7	31.7	90.1
Spot 275	168	49597	5.0	13.1448	1.3	1.9295	3.5	0.1840	3.2	0.93	1089.0	32.3	1091.4	23.2	1097.1	25.4	1097.1	25.4	99.3
Spot 274	367	189709	3.9	13.1211	1.2	1.9154	3.0	0.1824	2.7	0.92	1079.8	27.2	1086.5	19.8	1100.7	23.0	1100.7	23.0	98.1
Spot 299	94	34028	0.6	13.1114	1.2	1.8067	3.0	0.1719	2.8	0.93	1022.5	26.7	1047.9	19.9	1102.2	23.0	1102.2	23.0	92.8
Spot 103	151	7830	3.1	13.0956	1.2	2.0181	2.5	0.1918	2.2	0.89	1130.9	23.1	1121.6	17.1	1104.6	23.4	1104.6	23.4	102.4
Spot 128	46	10170	2.1	13.0909	1.7	1.7651	4.1	0.1677	3.7	0.91	999.2	34.5	1032.7	26.7	1105.3	34.7	1105.3	34.7	90.4
-Spot 11	71	13979	1.4	13.0906	1.3	1.7325	3.4	0.1646	3.1	0.92	982.1	28.4	1020.7	21.8	1105.3	26.3	1105.3	26.3	88.8

Spot 175	68	7673	0.8	13.0896	1.5	1.7825	3.2	0.1693	2.8	0.89	1008.2	26.2	1039.1	20.6	1105.5	29.0	1105.5	29.0	91.2
Spot 207	165	35544	2.7	13.0575	1.3	1.9381	4.1	0.1836	3.9	0.95	1086.7	39.4	1094.3	27.7	1110.4	25.6	1110.4	25.6	97.9
Spot 277	134	11560	2.1	13.0381	1.2	1.8421	4.2	0.1743	4.0	0.96	1035.6	38.4	1060.6	27.6	1113.3	24.3	1113.3	24.3	93.0
Spot 222	197	12369	2.8	13.0358	1.1	2.0988	3.0	0.1985	2.8	0.93	1167.3	29.5	1148.4	20.6	1113.7	22.6	1113.7	22.6	104.8
Spot 254	71	6475	2.8	13.0330	1.3	1.9377	2.5	0.1832	2.1	0.85	1084.6	21.1	1094.2	16.7	1114.1	26.7	1114.1	26.7	97.4
Spot 185	144	23888	1.8	13.0316	1.4	1.9207	3.0	0.1816	2.6	0.89	1075.8	26.0	1088.3	19.8	1114.3	27.2	1114.3	27.2	96.5
Spot 73	104	9659	1.7	13.0229	1.5	1.9653	4.0	0.1857	3.7	0.93	1098.1	37.7	1103.7	27.0	1115.7	29.8	1115.7	29.8	98.4
Spot 180	107	33624	2.2	13.0161	1.2	1.8885	4.2	0.1784	4.0	0.96	1058.0	38.8	1077.1	27.7	1116.7	24.6	1116.7	24.6	94.7
Spot 51	228	197693	1.7	13.0133	1.1	1.9510	4.0	0.1842	3.9	0.96	1090.0	39.0	1098.8	27.1	1117.2	21.8	1117.2	21.8	97.6
Spot 232	77	32995	1.0	13.0006	1.6	1.7989	4.0	0.1697	3.6	0.92	1010.4	33.9	1045.0	25.9	1119.1	31.9	1119.1	31.9	90.3
Spot 64	1066	251644	3.4	12.9889	1.1	1.8601	3.4	0.1753	3.2	0.94	1041.3	30.9	1067.0	22.5	1120.9	22.4	1120.9	22.4	92.9
Spot 193	61	7900	1.1	12.9881	1.7	1.9011	3.7	0.1792	3.3	0.89	1062.4	32.7	1081.5	24.8	1121.0	33.4	1121.0	33.4	94.8
Spot 4	184	39018	1.2	12.9844	1.4	2.1205	2.9	0.1998	2.5	0.88	1174.1	27.3	1155.5	19.9	1121.6	27.3	1121.6	27.3	104.7
Spot 33	68	5424	5.2	12.9626	1.7	1.9707	3.7	0.1854	3.3	0.89	1096.2	33.4	1105.5	25.1	1124.9	34.1	1124.9	34.1	97.4
Spot 264	73	8662	0.9	12.9597	1.7	2.0300	3.4	0.1909	2.9	0.86	1126.2	30.4	1125.6	23.2	1125.4	34.4	1125.4	34.4	100.1
Spot 94	185	13446	1.7	12.9563	1.5	2.0586	3.2	0.1935	2.8	0.89	1140.4	29.6	1135.1	21.8	1125.9	29.1	1125.9	29.1	101.3
Spot 66	88	8740	2.6	12.9550	1.2	2.0059	2.8	0.1886	2.6	0.90	1113.5	26.1	1117.5	19.1	1126.1	24.0	1126.1	24.0	98.9
Spot 24	490	33601	3.6	12.9464	0.7	2.0388	2.5	0.1915	2.4	0.96	1129.6	25.4	1128.5	17.4	1127.4	14.2	1127.4	14.2	100.2
Spot 289	125	8134	3.1	12.9281	1.3	2.1447	3.4	0.2012	3.1	0.92	1181.7	33.4	1163.4	23.2	1130.3	25.7	1130.3	25.7	104.5
Spot 208	177	9018	4.0	12.9250	1.2	2.0183	2.8	0.1893	2.5	0.90	1117.5	26.0	1121.7	19.0	1130.7	23.7	1130.7	23.7	98.8
Spot 40	185	170628	2.5	12.9175	1.1	2.0990	3.2	0.1967	3.0	0.94	1157.7	31.9	1148.5	22.0	1131.9	21.7	1131.9	21.7	102.3
Spot 114	270	114246	5.0	12.9120	1.1	2.0801	3.6	0.1949	3.5	0.95	1147.7	36.3	1142.3	24.9	1132.7	22.2	1132.7	22.2	101.3
Spot 272	260	146782	8.1	12.9056	1.3	1.9358	3.1	0.1813	2.8	0.90	1073.9	27.6	1093.5	20.7	1133.7	26.3	1133.7	26.3	94.7
Spot 102	632	298056	3.1	12.9051	1.2	1.9129	4.0	0.1791	3.9	0.95	1062.2	37.7	1085.6	26.9	1133.8	23.9	1133.8	23.9	93.7
Spot 1	214	33841	2.2	12.9018	1.3	2.0189	3.4	0.1890	3.1	0.92	1115.9	32.2	1121.9	23.2	1134.3	26.5	1134.3	26.5	98.4

Spot 262	547	23170	2.5	12.8978	1.2	2.1342	3.3	0.1997	3.0	0.93	1173.8	32.6	1159.9	22.6	1134.9	23.7	1134.9	23.7	103.4
Spot 81	129	22739	4.1	12.8929	1.3	2.0826	3.7	0.1948	3.4	0.94	1147.5	36.0	1143.1	25.1	1135.7	25.5	1135.7	25.5	101.0
Spot 165	203	13770	2.4	12.8916	1.0	1.8882	2.6	0.1766	2.4	0.92	1048.5	23.5	1076.9	17.5	1135.9	20.7	1135.9	20.7	92.3
Spot 130	160	16889	1.6	12.8771	1.4	2.0889	3.9	0.1952	3.6	0.93	1149.4	37.8	1145.2	26.5	1138.1	28.1	1138.1	28.1	101.0
Spot 150	65	8914	1.7	12.8748	1.4	2.0317	3.1	0.1898	2.8	0.89	1120.3	28.4	1126.2	21.1	1138.5	27.8	1138.5	27.8	98.4
Spot 293	246	15456	3.1	12.8743	1.2	2.0358	2.9	0.1902	2.6	0.90	1122.3	26.9	1127.6	19.7	1138.6	24.8	1138.6	24.8	98.6
Spot 187	65	17717	1.8	12.8688	1.7	2.0201	3.6	0.1886	3.1	0.87	1113.9	31.7	1122.3	24.2	1139.4	34.6	1139.4	34.6	97.8
Spot 224	143	6177	1.9	12.8562	1.3	2.1599	2.8	0.2015	2.5	0.90	1183.3	27.3	1168.3	19.6	1141.3	24.9	1141.3	24.9	103.7
Spot 72	162	18695	2.4	12.8491	1.3	2.0588	3.4	0.1919	3.2	0.92	1131.9	33.0	1135.2	23.6	1142.4	26.7	1142.4	26.7	99.1
Spot 52	222	12648	2.0	12.8417	1.2	2.0715	2.8	0.1930	2.6	0.91	1137.7	26.9	1139.4	19.4	1143.6	23.1	1143.6	23.1	99.5
Spot 238	342	22059	3.5	12.8298	1.1	2.0490	3.2	0.1907	3.0	0.94	1125.4	31.0	1131.9	21.8	1145.4	21.1	1145.4	21.1	98.2
Spot 231	300	1109788	1.9	12.8225	0.9	2.1565	2.8	0.2006	2.6	0.95	1178.7	28.5	1167.1	19.4	1146.6	17.5	1146.6	17.5	102.8
Spot 281	237	66873	2.3	12.8199	0.9	2.0579	2.7	0.1914	2.5	0.94	1129.1	26.1	1134.9	18.4	1147.0	18.5	1147.0	18.5	98.4
Spot 115	171	24730	3.0	12.8178	1.2	2.0017	3.3	0.1862	3.1	0.93	1100.6	31.3	1116.1	22.6	1147.3	24.6	1147.3	24.6	95.9
Spot 239	359	51408	5.0	12.8142	1.1	2.0380	2.7	0.1895	2.5	0.92	1118.6	25.5	1128.3	18.5	1147.9	21.6	1147.9	21.6	97.5
Spot 195	201	21698	5.0	12.8141	1.3	2.0413	3.8	0.1898	3.5	0.94	1120.2	36.3	1129.4	25.6	1147.9	25.4	1147.9	25.4	97.6
Spot 282	54	39209	1.8	12.8057	1.4	2.0145	3.9	0.1872	3.7	0.94	1106.1	37.6	1120.4	26.8	1149.2	27.0	1149.2	27.0	96.2
Spot 279	638	87860	1.2	12.7994	0.8	2.1202	3.1	0.1969	3.0	0.96	1158.7	31.6	1155.4	21.3	1150.1	16.4	1150.1	16.4	100.7
Spot 226	265	35742	2.0	12.7904	1.0	2.1548	3.8	0.2000	3.6	0.96	1175.2	38.9	1166.6	26.1	1151.5	19.8	1151.5	19.8	102.1
Spot 28	626	64295	1.3	12.7895	1.2	2.1242	3.4	0.1971	3.2	0.94	1159.9	34.3	1156.7	23.8	1151.7	24.1	1151.7	24.1	100.7
Spot 20	401	33987	4.6	12.7881	1.1	2.1582	3.2	0.2003	3.1	0.94	1176.7	33.0	1167.7	22.5	1151.9	21.1	1151.9	21.1	102.2
Spot 122	125	33997	0.9	12.7832	1.4	2.0303	3.4	0.1883	3.1	0.92	1112.2	31.5	1125.7	22.9	1152.6	26.8	1152.6	26.8	96.5
Spot 138	524	24137	2.0	12.7796	1.3	2.0496	3.6	0.1901	3.3	0.93	1121.7	34.2	1132.2	24.4	1153.2	26.2	1153.2	26.2	97.3
Spot 80	251	19212	2.0	12.7666	1.2	2.0312	2.7	0.1882	2.5	0.91	1111.4	25.3	1126.0	18.6	1155.2	23.0	1155.2	23.0	96.2
Spot 305	127	12571	2.4	12.7610	1.6	2.0960	3.6	0.1941	3.3	0.90	1143.4	34.5	1147.5	25.0	1156.1	30.9	1156.1	30.9	98.9

Spot 96	606	51140	6.4	12.7539	1.0	2.1288	3.5	0.1970	3.3	0.96	1159.2	35.4	1158.2	23.9	1157.2	18.9	1157.2	18.9	100.2
Spot 101	130	39397	2.0	12.7511	1.3	2.1105	3.6	0.1953	3.3	0.93	1149.8	34.8	1152.3	24.6	1157.6	26.6	1157.6	26.6	99.3
Spot 168	194	27010	36.9	12.7508	1.4	2.0277	3.6	0.1876	3.3	0.92	1108.3	33.3	1124.8	24.2	1157.7	28.1	1157.7	28.1	95.7
Spot 121	333	18350	1.4	12.7489	1.2	2.0981	2.9	0.1941	2.7	0.91	1143.4	28.1	1148.2	20.2	1158.0	24.2	1158.0	24.2	98.7
Spot 95	115	10805	1.5	12.7461	1.3	1.9737	3.2	0.1825	2.9	0.91	1080.8	29.2	1106.6	21.7	1158.4	25.8	1158.4	25.8	93.3
Spot 233	163	118895	1.8	12.7390	1.3	2.0427	3.3	0.1888	3.1	0.92	1114.9	31.4	1129.9	22.7	1159.5	25.8	1159.5	25.8	96.2
Spot 245	300	54559	4.4	12.7339	0.8	2.1594	3.7	0.1995	3.6	0.97	1172.7	38.6	1168.1	25.7	1160.3	16.7	1160.3	16.7	101.1
Spot 25	340	24346	1.6	12.7322	1.0	2.1725	3.5	0.2007	3.3	0.96	1179.1	36.1	1172.3	24.2	1160.6	19.2	1160.6	19.2	101.6
Spot 225	86	13607	2.2	12.7274	1.4	2.0927	3.2	0.1933	2.8	0.89	1139.0	29.5	1146.4	21.7	1161.3	28.0	1161.3	28.0	98.1
Spot 89	52	4032	5.6	12.7273	2.0	1.9692	3.8	0.1819	3.2	0.84	1077.1	31.4	1105.1	25.4	1161.3	40.6	1161.3	40.6	92.7
Spot 236	358	31732	2.1	12.7234	1.0	2.0963	3.6	0.1935	3.5	0.96	1140.5	36.4	1147.6	24.9	1162.0	19.6	1162.0	19.6	98.2
Spot 249	147	43034	3.7	12.7224	1.2	2.0802	3.0	0.1920	2.8	0.92	1132.3	28.7	1142.3	20.7	1162.1	23.9	1162.1	23.9	97.4
Spot 181	259	83913	3.9	12.7211	1.3	2.0681	3.1	0.1909	2.8	0.91	1126.2	29.1	1138.3	21.1	1162.3	25.1	1162.3	25.1	96.9
Spot 134	211	89720	1.9	12.7200	1.1	2.0874	3.0	0.1927	2.8	0.93	1135.8	28.9	1144.7	20.5	1162.5	21.9	1162.5	21.9	97.7
Spot 154	199	20475	1.2	12.7193	1.1	2.1373	3.7	0.1972	3.5	0.95	1160.5	37.0	1160.9	25.4	1162.6	22.4	1162.6	22.4	99.8
Spot 261	422	22260	1.8	12.6967	1.2	2.1704	3.9	0.1999	3.7	0.95	1175.0	39.6	1171.6	26.9	1166.1	23.0	1166.1	23.0	100.8
Spot 48	323	19543	2.0	12.6913	1.1	2.1926	3.5	0.2019	3.3	0.95	1185.6	35.9	1178.7	24.4	1166.9	22.0	1166.9	22.0	101.6
Spot 166	496	56146	2.7	12.6775	0.8	2.0847	3.2	0.1918	3.1	0.97	1130.9	32.2	1143.8	22.0	1169.1	15.9	1169.1	15.9	96.7
Spot 167	46	30625	1.7	12.6683	1.6	2.2700	3.9	0.2087	3.5	0.91	1221.6	38.9	1203.0	27.2	1170.6	32.1	1170.6	32.1	104.4
Spot 54	1412	59669	2.5	12.6453	1.1	2.0319	2.9	0.1864	2.7	0.92	1102.0	27.0	1126.3	19.6	1174.2	21.8	1174.2	21.8	93.9
Spot 280	643	35191	3.3	12.6313	1.1	2.1595	2.7	0.1979	2.4	0.91	1164.1	25.9	1168.1	18.6	1176.4	22.6	1176.4	22.6	99.0
Spot 5	251	50497	3.0	12.6248	1.2	2.0750	3.2	0.1901	3.0	0.93	1121.8	30.7	1140.6	21.9	1177.4	23.1	1177.4	23.1	95.3
Spot 297	186	176403	1.6	12.6146	1.1	2.1024	2.7	0.1924	2.5	0.91	1134.5	26.0	1149.6	18.9	1179.0	22.4	1179.0	22.4	96.2
Spot 151	108	14757	3.1	12.6115	1.3	2.1282	3.8	0.1947	3.6	0.94	1147.0	38.0	1158.0	26.5	1179.5	25.4	1179.5	25.4	97.3
Spot 219	56	5478	0.9	12.6112	1.5	2.0470	3.5	0.1873	3.1	0.90	1106.8	31.8	1131.3	23.8	1179.5	30.5	1179.5	30.5	93.8

Spot 246	491	19827	4.7	12.6066	1.1	2.0583	3.4	0.1883	3.2	0.95	1112.0	32.7	1135.0	23.0	1180.2	20.9	1180.2	20.9	94.2
Spot 119	111	24077	2.0	12.6043	1.5	1.8364	3.5	0.1679	3.1	0.90	1000.8	29.2	1058.6	22.9	1180.6	29.7	1180.6	29.7	84.8
Spot 19	27	2933	1.6	12.6013	3.5	2.2506	4.6	0.2058	2.9	0.64	1206.3	32.3	1197.0	32.0	1181.1	68.9	1181.1	68.9	102.1
Spot 60	131	29855	1.6	12.5882	1.2	2.0908	3.1	0.1910	2.9	0.92	1126.6	29.8	1145.8	21.4	1183.1	23.6	1183.1	23.6	95.2
Spot 46	275	28204	4.3	12.5863	1.5	2.2050	3.3	0.2014	3.0	0.90	1182.7	31.9	1182.6	23.0	1183.4	28.9	1183.4	28.9	99.9
Spot 110	337	48526	1.5	12.5820	1.1	2.0642	3.2	0.1884	3.0	0.93	1113.0	30.4	1137.0	21.8	1184.1	22.7	1184.1	22.7	94.0
Spot 182	304	50095	2.8	12.5801	1.0	2.1973	3.0	0.2006	2.8	0.95	1178.4	30.3	1180.2	20.8	1184.4	19.1	1184.4	19.1	99.5
Spot 259	211	10208	3.3	12.5741	1.3	2.2401	3.1	0.2044	2.8	0.91	1198.8	31.1	1193.7	21.9	1185.3	25.4	1185.3	25.4	101.1
Spot 186	207	22922	2.1	12.5699	1.0	2.2168	3.1	0.2022	3.0	0.95	1187.1	32.2	1186.4	21.9	1186.0	20.0	1186.0	20.0	100.1
Spot 291	94	11558	1.8	12.5644	1.3	2.1727	3.2	0.1981	2.9	0.91	1164.9	31.2	1172.3	22.4	1186.9	26.5	1186.9	26.5	98.2
Spot 257	171	53326	5.4	12.5621	1.1	2.1094	3.1	0.1923	2.9	0.94	1133.7	30.3	1151.9	21.4	1187.2	21.5	1187.2	21.5	95.5
Spot 217	66	37068	1.3	12.5573	1.7	2.1230	3.8	0.1934	3.4	0.90	1139.9	35.4	1156.3	26.1	1188.0	33.2	1188.0	33.2	96.0
Spot 273	390	28888	1.0	12.5364	1.1	2.0883	3.6	0.1900	3.4	0.96	1121.1	35.3	1145.0	24.6	1191.2	20.9	1191.2	20.9	94.1
Spot 129	136	53253	1.8	12.5221	1.2	2.1155	3.1	0.1922	2.9	0.93	1133.3	30.3	1153.9	21.7	1193.5	23.6	1193.5	23.6	95.0
Spot 12	127	993806	2.1	12.5068	1.2	2.1166	3.6	0.1921	3.4	0.95	1132.6	35.8	1154.2	25.1	1195.9	23.3	1195.9	23.3	94.7
Spot 176	345	108810	1.9	12.5040	1.2	2.2176	3.9	0.2012	3.7	0.95	1181.8	40.2	1186.6	27.4	1196.3	24.2	1196.3	24.2	98.8
Spot 285	1424	174114	1.8	12.5013	1.1	2.1139	2.9	0.1917	2.7	0.93	1130.8	28.2	1153.3	20.2	1196.8	21.3	1196.8	21.3	94.5
Spot 220	307	34420	1.8	12.4993	1.2	2.2325	3.8	0.2025	3.7	0.95	1188.6	39.7	1191.3	27.0	1197.1	23.6	1197.1	23.6	99.3
Spot 198	488	125945	2.7	12.4861	0.9	2.2512	2.9	0.2039	2.8	0.95	1196.5	30.1	1197.1	20.4	1199.2	18.0	1199.2	18.0	99.8
Spot 251	67	28882	3.4	12.4839	1.0	2.0467	3.1	0.1854	2.9	0.95	1096.4	29.5	1131.2	21.0	1199.5	19.3	1199.5	19.3	91.4
Spot 212	93	24992	2.7	12.4725	1.3	2.0403	3.2	0.1846	2.9	0.91	1092.3	28.9	1129.1	21.5	1201.3	25.4	1201.3	25.4	90.9
Spot 117	193	33808	1.2	12.4457	1.2	2.1536	3.0	0.1945	2.7	0.92	1145.6	28.8	1166.2	20.7	1205.5	23.1	1205.5	23.1	95.0
Spot 147	166	481756	1.4	12.4441	1.3	2.0679	3.3	0.1867	3.1	0.92	1103.6	31.2	1138.3	22.9	1205.8	26.1	1205.8	26.1	91.5
Spot 30	189	22097	2.8	12.4073	1.0	2.0938	2.9	0.1885	2.7	0.94	1113.2	27.6	1146.8	19.8	1211.6	19.5	1211.6	19.5	91.9
Spot 237	73	4443	1.5	12.4005	2.4	2.4092	4.0	0.2168	3.3	0.81	1264.8	37.4	1245.4	28.9	1212.7	46.6	1212.7	46.6	104.3

Spot 139	236	800271	1.4	12.3959	1.2	2.2232	3.0	0.2000	2.7	0.91	1175.1	29.2	1188.4	20.8	1213.5	23.6	1213.5	23.6	96.8
Spot 8	132	11993	2.1	12.3908	1.2	2.2992	3.6	0.2067	3.4	0.95	1211.3	37.6	1212.0	25.5	1214.2	22.9	1214.2	22.9	99.8
Spot 171	418	70660	2.1	12.3722	1.3	2.2565	3.4	0.2026	3.2	0.92	1189.1	34.3	1198.8	24.1	1217.2	25.9	1217.2	25.9	97.7
Spot 271	70	755322	1.4	12.3664	1.5	2.0554	3.1	0.1844	2.8	0.88	1091.1	27.9	1134.1	21.5	1218.1	29.0	1218.1	29.0	89.6
Spot 160	143	254447	1.9	12.3567	1.0	2.1787	3.2	0.1953	3.1	0.95	1150.2	32.1	1174.3	22.3	1219.7	19.4	1219.7	19.4	94.3
Spot 314	219	27934	4.9	12.3456	1.0	2.1711	2.9	0.1945	2.7	0.94	1145.6	28.1	1171.8	19.9	1221.5	19.6	1221.5	19.6	93.8
Spot 50	127	49694	2.3	12.3122	1.3	2.2463	3.1	0.2007	2.9	0.92	1179.0	31.1	1195.6	22.1	1226.8	24.9	1226.8	24.9	96.1
Spot 118	78	173281	2.0	12.2887	1.4	2.1615	3.7	0.1927	3.4	0.92	1136.1	35.7	1168.7	25.7	1230.5	27.7	1230.5	27.7	92.3
Spot 34	63	7125	3.0	12.2476	1.6	2.2793	3.8	0.2026	3.5	0.91	1189.0	38.2	1205.9	27.1	1237.1	30.6	1237.1	30.6	96.1
Spot 156	194	24191	7.5	12.2075	1.0	2.2614	3.4	0.2003	3.2	0.95	1176.9	34.4	1200.3	23.7	1243.5	20.4	1243.5	20.4	94.6
Spot 286	50	7983	2.8	12.1995	1.5	2.4400	3.2	0.2160	2.8	0.88	1260.6	31.7	1254.5	22.7	1244.8	29.3	1244.8	29.3	101.3
Spot 111	85	14141	1.9	12.1784	1.1	2.2676	2.9	0.2004	2.7	0.92	1177.3	29.2	1202.3	20.8	1248.2	22.4	1248.2	22.4	94.3
Spot 159	47	5778	0.9	12.1557	1.9	1.9558	3.8	0.1725	3.3	0.88	1025.9	31.8	1100.4	25.7	1251.9	36.2	1251.9	36.2	81.9
Spot 163	47	4598	1.9	12.1451	1.6	2.5442	3.3	0.2242	2.9	0.88	1304.0	34.5	1284.8	24.2	1253.5	30.6	1253.5	30.6	104.0
Spot 290	248	91652	2.9	12.1406	1.1	2.3731	3.2	0.2090	3.0	0.94	1223.7	33.9	1234.5	23.0	1254.3	21.0	1254.3	21.0	97.6
Spot 276	141	185983	1.8	12.1304	1.1	2.2295	3.4	0.1962	3.2	0.95	1155.1	33.6	1190.4	23.5	1255.9	20.8	1255.9	20.8	92.0
Spot 241	338	31469	1.6	12.1262	1.4	2.4253	3.5	0.2134	3.3	0.92	1246.9	37.0	1250.1	25.5	1256.6	27.0	1256.6	27.0	99.2
Spot 61	104	22319	1.9	12.1180	1.5	2.3065	4.0	0.2028	3.7	0.93	1190.3	40.0	1214.3	28.1	1257.9	29.0	1257.9	29.0	94.6
Spot 100	166	9410	1.1	12.1072	1.5	2.3716	3.0	0.2083	2.6	0.87	1220.0	29.4	1234.1	21.7	1259.7	29.3	1259.7	29.3	96.8
Spot 74	102	19490	1.9	12.0834	1.3	2.4312	3.8	0.2132	3.6	0.94	1245.6	40.7	1251.9	27.5	1263.5	25.1	1263.5	25.1	98.6
Spot 183	353	1167902	2.9	12.0759	1.3	2.3934	4.0	0.2097	3.8	0.95	1227.3	42.1	1240.6	28.6	1264.7	25.4	1264.7	25.4	97.0
Spot 105	99	5430	2.3	12.0371	1.5	2.4217	3.3	0.2115	2.9	0.89	1236.8	32.4	1249.0	23.4	1271.0	29.5	1271.0	29.5	97.3
Spot 16	85	12226	3.6	12.0288	1.6	2.3874	3.5	0.2084	3.1	0.89	1220.1	34.7	1238.8	25.1	1272.3	31.2	1272.3	31.2	95.9
Spot 303	92	18189	1.6	11.9821	1.3	2.4054	3.8	0.2091	3.6	0.94	1224.1	40.0	1244.2	27.3	1279.9	24.7	1279.9	24.7	95.6
Spot 77	268	31499	1.5	11.9698	1.1	2.4645	3.0	0.2140	2.8	0.93	1250.3	32.0	1261.7	21.9	1281.9	21.7	1281.9	21.7	97.5

Spot 235	160	14199	1.8	11.9176	1.2	2.4528	3.5	0.2121	3.3	0.94	1240.0	37.0	1258.2	25.1	1290.4	22.7	1290.4	22.7	96.1
Spot 206	178	260765	2.6	11.8905	1.1	2.2949	3.1	0.1980	2.9	0.94	1164.5	30.5	1210.7	21.6	1294.9	20.8	1294.9	20.8	89.9
Spot 132	121	9925	4.6	11.8882	1.4	2.2991	3.6	0.1983	3.3	0.92	1166.3	35.5	1212.0	25.7	1295.2	28.0	1295.2	28.0	90.0
Spot 253	756	170812	4.1	11.8669	1.4	2.3799	3.5	0.2049	3.2	0.92	1201.7	35.3	1236.6	25.1	1298.7	27.2	1298.7	27.2	92.5
Spot 13	127	66040	2.5	11.8657	0.9	2.5684	3.0	0.2211	2.9	0.96	1287.8	33.6	1291.7	22.0	1298.9	17.3	1298.9	17.3	99.1
Spot 43	241	593552	1.4	11.8322	1.3	2.5398	3.0	0.2181	2.8	0.91	1271.6	31.8	1283.5	22.1	1304.4	24.7	1304.4	24.7	97.5
Spot 191	180	82410	2.9	11.8182	1.2	2.5781	3.4	0.2211	3.2	0.93	1287.6	36.9	1294.5	24.8	1306.7	23.6	1306.7	23.6	98.5
Spot 304	129	53450	2.5	11.7832	1.3	2.7704	3.0	0.2369	2.7	0.90	1370.4	33.0	1347.6	22.1	1312.5	25.0	1312.5	25.0	104.4
Spot 170	243	39007	3.8	11.7216	0.9	2.5890	3.0	0.2202	2.9	0.95	1282.9	33.7	1297.5	22.3	1322.6	18.0	1322.6	18.0	97.0
Spot 49	177	32963	2.4	11.6977	1.3	2.6411	3.0	0.2242	2.7	0.89	1303.9	31.3	1312.2	21.9	1326.6	26.0	1326.6	26.0	98.3
Spot 203	100	903542	1.7	11.6906	1.2	2.6357	3.1	0.2236	2.8	0.92	1300.7	33.2	1310.7	22.6	1327.8	23.3	1327.8	23.3	98.0
Spot 228	196	22870	1.2	11.6767	1.3	2.5960	3.7	0.2199	3.5	0.94	1281.6	40.1	1299.5	27.1	1330.1	25.2	1330.1	25.2	96.4
Spot 298	336	20098	2.8	11.6588	1.0	2.6916	2.8	0.2277	2.6	0.93	1322.4	30.9	1326.2	20.5	1333.0	19.6	1333.0	19.6	99.2
Spot 79	326	35860	1.4	11.6500	1.2	2.7544	3.1	0.2328	2.9	0.92	1349.3	35.0	1343.3	23.3	1334.5	23.9	1334.5	23.9	101.1
Spot 153	504	254788	6.1	11.6433	0.9	2.5666	3.8	0.2168	3.7	0.97	1265.1	42.0	1291.2	27.6	1335.6	18.2	1335.6	18.2	94.7
Spot 41	137	57304	2.4	11.6149	1.4	2.7042	4.0	0.2279	3.8	0.94	1323.5	45.3	1329.6	29.9	1340.3	26.9	1340.3	26.9	98.7
Spot 196	260	14768	2.2	11.6125	1.4	2.7495	3.0	0.2317	2.7	0.88	1343.2	32.3	1341.9	22.5	1340.7	27.5	1340.7	27.5	100.2
Spot 23	95	7266	3.3	11.5490	1.6	2.6791	3.4	0.2245	3.0	0.88	1305.6	35.4	1322.7	25.3	1351.3	31.8	1351.3	31.8	96.6
Spot 260	381	37814	2.1	11.5454	1.1	2.6259	3.3	0.2200	3.1	0.94	1281.7	36.0	1307.9	24.2	1351.9	21.1	1351.9	21.1	94.8
Spot 82	181	22760	2.1	11.5240	1.1	2.8704	3.5	0.2400	3.3	0.95	1386.8	41.3	1374.2	26.3	1355.5	21.2	1355.5	21.2	102.3
Spot 14	153	12754	2.1	11.5122	0.8	2.8666	2.5	0.2395	2.4	0.94	1383.8	29.7	1373.2	19.0	1357.5	15.9	1357.5	15.9	101.9
Spot 174	194	49208	2.7	11.5009	1.1	2.8128	3.3	0.2347	3.1	0.95	1359.2	38.4	1358.9	24.8	1359.4	20.4	1359.4	20.4	100.0
Spot 155	70	9505	1.9	11.4834	1.6	2.6951	3.5	0.2246	3.2	0.89	1305.9	37.2	1327.1	26.2	1362.3	30.7	1362.3	30.7	95.9
Spot 213	372	39132	4.2	11.4834	1.2	2.7445	3.5	0.2287	3.3	0.94	1327.5	40.0	1340.6	26.4	1362.3	23.1	1362.3	23.1	97.4
Spot 295	193	24420	2.6	11.4563	1.2	2.7346	2.7	0.2273	2.4	0.90	1320.4	28.6	1337.9	19.8	1366.8	22.5	1366.8	22.5	96.6

Spot 140	101	5252	2.4	11.4189	1.2	2.9204	3.1	0.2420	2.9	0.93	1396.9	36.2	1387.2	23.6	1373.1	22.5	1373.1	22.5	101.7
Spot 240	419	38047	1.9	11.4056	1.1	2.8117	3.6	0.2327	3.4	0.96	1348.6	41.8	1358.7	26.9	1375.4	20.3	1375.4	20.3	98.1
Spot 210	678	210086	1.3	11.3701	1.0	2.6875	3.3	0.2217	3.2	0.95	1290.9	36.9	1325.0	24.6	1381.4	20.0	1381.4	20.0	93.5
Spot 7	130	9601	3.0	11.3271	1.3	2.5937	3.2	0.2132	2.9	0.91	1245.7	33.1	1298.9	23.5	1388.6	25.6	1388.6	25.6	89.7
Spot 75	31	616482	1.8	11.3194	1.6	2.7243	3.5	0.2238	3.1	0.88	1301.7	36.8	1335.1	26.2	1390.0	31.6	1390.0	31.6	93.6
Spot 315	319	39696	2.6	11.2953	1.2	2.8360	3.2	0.2324	3.0	0.92	1347.2	35.9	1365.1	24.0	1394.0	23.3	1394.0	23.3	96.6
Spot 247	94	4886	2.4	11.2786	1.3	3.0784	3.0	0.2519	2.7	0.89	1448.4	34.4	1427.3	22.8	1396.9	25.6	1396.9	25.6	103.7
Spot 126	64	7371	1.2	11.2428	1.1	2.8350	3.1	0.2313	2.9	0.94	1341.2	35.7	1364.9	23.6	1403.0	21.0	1403.0	21.0	95.6
Spot 244	234	79680	2.2	11.2415	1.4	2.8355	3.5	0.2313	3.3	0.92	1341.2	39.4	1365.0	26.6	1403.2	26.8	1403.2	26.8	95.6
Spot 270	116	37395	1.2	11.2082	1.3	2.9974	3.3	0.2438	3.0	0.92	1406.2	38.3	1407.0	25.1	1408.9	24.7	1408.9	24.7	99.8
Spot 137	37	7684	3.1	11.1796	1.2	2.8696	3.3	0.2328	3.1	0.93	1349.0	37.5	1374.0	24.9	1413.8	22.8	1413.8	22.8	95.4
Spot 252	138	13119	1.4	11.1794	1.3	3.0252	3.9	0.2454	3.7	0.94	1414.7	47.2	1414.0	30.1	1413.8	25.4	1413.8	25.4	100.1
Spot 31	120	2175	3.3	11.1781	1.7	2.4174	3.3	0.1961	2.8	0.86	1154.2	29.6	1247.8	23.4	1414.0	32.0	1414.0	32.0	81.6
Spot 99	52	10609	2.3	11.1294	1.6	2.6963	3.5	0.2177	3.1	0.89	1269.9	36.2	1327.5	26.1	1422.4	30.3	1422.4	30.3	89.3
Spot 179	247	34017	1.5	11.1244	1.4	3.1442	2.7	0.2538	2.3	0.85	1458.0	29.8	1443.6	20.6	1423.2	26.6	1423.2	26.6	102.4
Spot 112	129	12226	1.4	11.1178	1.1	2.8818	2.8	0.2325	2.6	0.92	1347.4	31.2	1377.2	21.1	1424.4	21.4	1424.4	21.4	94.6
Spot 218	126	37168	2.2	11.1176	1.1	3.0745	3.7	0.2480	3.5	0.96	1428.2	45.1	1426.4	28.2	1424.4	20.5	1424.4	20.5	100.3
Spot 17	301	24349	1.1	11.0828	1.2	3.0043	2.8	0.2416	2.5	0.91	1395.0	31.6	1408.7	21.2	1430.4	22.4	1430.4	22.4	97.5
Spot 306	287	36409	2.1	11.0738	1.3	2.9958	3.3	0.2407	3.1	0.92	1390.4	38.3	1406.5	25.5	1431.9	25.7	1431.9	25.7	97.1
Spot 87	497	431856	1.9	11.0539	0.9	3.0536	3.5	0.2449	3.3	0.96	1412.2	42.2	1421.1	26.4	1435.4	17.6	1435.4	17.6	98.4
Spot 149	86	25051	2.5	10.9983	1.1	2.9702	3.9	0.2370	3.7	0.96	1371.2	46.1	1400.0	29.6	1445.0	20.9	1445.0	20.9	94.9
Spot 266	577	33639	133.2	10.9621	1.3	3.0014	4.1	0.2387	3.9	0.95	1380.1	48.1	1408.0	31.2	1451.3	24.9	1451.3	24.9	95.1
Spot 124	602	54837	2.4	10.9567	1.2	3.1066	3.0	0.2470	2.8	0.92	1422.9	35.9	1434.3	23.4	1452.2	22.2	1452.2	22.2	98.0
Spot 3	299	131691	2.4	10.9512	1.0	3.1159	2.7	0.2476	2.5	0.93	1426.0	32.3	1436.6	20.9	1453.1	19.2	1453.1	19.2	98.1
Spot 227	1027	96536	4.0	10.8841	1.1	3.1217	3.7	0.2465	3.5	0.95	1420.6	45.0	1438.1	28.5	1464.8	21.2	1464.8	21.2	97.0

Spot 197	146	78776	2.7	10.8772	1.0	3.1621	2.6	0.2496	2.4	0.92	1436.2	31.1	1448.0	20.3	1466.0	19.7	1466.0	19.7	98.0
Spot 307	114	19128	0.9	10.8378	1.2	3.1436	3.2	0.2472	2.9	0.92	1424.0	37.0	1443.4	24.3	1472.9	23.7	1472.9	23.7	96.7
Spot 136	86	26311	1.6	10.8311	1.2	3.2348	3.3	0.2542	3.1	0.93	1460.2	40.7	1465.5	25.9	1474.1	23.1	1474.1	23.1	99.1
-Spot 21	56	12920	1.9	10.8040	1.4	3.0318	3.2	0.2377	2.9	0.90	1374.6	35.5	1415.7	24.3	1478.8	26.0	1478.8	26.0	92.9
Spot 312	141	200702	2.4	10.7985	1.2	3.0188	3.7	0.2365	3.5	0.95	1368.6	43.1	1412.4	28.1	1479.8	22.5	1479.8	22.5	92.5
Spot 296	62	7481	2.1	10.7659	1.4	2.9467	3.2	0.2302	2.9	0.90	1335.5	34.6	1394.0	24.3	1485.5	26.8	1485.5	26.8	89.9
Spot 62	296	46896	7.1	10.7512	0.9	3.2634	3.0	0.2546	2.9	0.95	1462.0	37.7	1472.4	23.6	1488.1	17.9	1488.1	17.9	98.2
Spot 152	190	67247	0.9	10.5334	1.2	3.3521	3.3	0.2562	3.1	0.93	1470.3	40.3	1493.3	25.9	1526.8	23.5	1526.8	23.5	96.3
Spot 221	45	5783	2.3	10.4421	1.3	3.1164	3.6	0.2361	3.3	0.93	1366.5	40.8	1436.7	27.3	1543.2	23.9	1543.2	23.9	88.5
Spot 63	39	1950	0.9	10.3270	1.4	3.6906	3.6	0.2765	3.3	0.92	1573.9	45.8	1569.3	28.4	1564.0	26.0	1564.0	26.0	100.6
Spot 192	209	187772	1.9	10.0265	1.2	3.7584	2.8	0.2734	2.5	0.90	1558.2	34.4	1583.9	22.2	1619.1	23.0	1619.1	23.0	96.2
Spot 15	69	6289	2.1	10.0174	1.3	4.0556	3.0	0.2948	2.7	0.90	1665.4	39.4	1645.4	24.3	1620.8	24.1	1620.8	24.1	102.7
Spot 242	207	30203	1.4	9.9247	1.1	3.7685	3.0	0.2714	2.7	0.93	1547.8	37.7	1586.1	23.7	1638.1	20.4	1638.1	20.4	94.5
Spot 283	127	30509	1.3	9.8812	1.3	3.8644	3.6	0.2771	3.4	0.93	1576.6	47.4	1606.3	29.3	1646.3	24.4	1646.3	24.4	95.8
Spot 309	77	10942	1.7	9.7739	1.1	4.0954	2.8	0.2904	2.5	0.92	1643.7	36.7	1653.4	22.5	1666.5	20.2	1666.5	20.2	98.6
Spot 301	307	26093	1.3	9.7267	0.9	4.0843	3.2	0.2883	3.1	0.96	1632.8	44.9	1651.2	26.5	1675.4	17.0	1675.4	17.0	97.5
Spot 93	262	31938	3.3	9.6620	1.2	3.8579	3.8	0.2705	3.6	0.95	1543.1	49.0	1604.9	30.4	1687.8	22.5	1687.8	22.5	91.4
Spot 310	78	57509	1.6	9.6575	1.2	3.9232	3.6	0.2749	3.4	0.94	1565.7	46.8	1618.5	28.9	1688.6	21.7	1688.6	21.7	92.7
Spot 194	905	313565	2.7	9.5988	1.0	3.9665	2.7	0.2763	2.5	0.93	1572.5	35.2	1627.4	22.1	1699.9	19.0	1699.9	19.0	92.5
Spot 53	108	39440	1.6	9.5454	1.2	4.3200	2.9	0.2992	2.7	0.91	1687.3	39.7	1697.2	24.2	1710.1	22.1	1710.1	22.1	98.7
Spot 32	119	12615	1.6	9.5233	1.1	4.2767	2.9	0.2955	2.7	0.92	1669.1	39.3	1688.9	23.8	1714.4	20.6	1714.4	20.6	97.4
Spot 199	206	47510	0.9	8.8981	1.3	5.0600	3.2	0.3267	2.9	0.91	1822.3	45.8	1829.4	26.9	1838.3	24.1	1838.3	24.1	99.1
Spot 127	243	66046	1.0	8.6757	0.9	5.2999	2.9	0.3336	2.7	0.95	1855.9	44.2	1868.9	24.6	1884.0	15.9	1884.0	15.9	98.5
Spot 107	80	10069	0.7	7.3075	2.3	7.6260	4.3	0.4043	3.6	0.84	2189.0	66.8	2187.9	38.2	2187.6	39.6	2187.6	39.6	100.1
Spot 97	149	12159	1.2	7.0223	1.1	6.7793	3.5	0.3454	3.4	0.95	1912.7	55.5	2083.0	31.2	2256.6	19.1	2256.6	19.1	84.8

Spot 200	54	7061	0.9	6.1819	1.6	8.8355	3.3	0.3963	2.9	0.88	2152.1	52.6	2321.2	29.9	2474.2	26.4	2474.2	26.4	87.0
Spot 56	212	22541	3.8	5.9883	1.6	9.7302	3.4	0.4228	2.9	0.88	2273.1	56.5	2409.6	31.0	2527.7	27.1	2527.7	27.1	89.9
Spot 106	234	202032	2.2	5.9014	0.9	10.6723	2.6	0.4570	2.4	0.93	2426.2	48.4	2495.0	23.8	2552.2	15.3	2552.2	15.3	95.1
Spot 230	36	37337	1.7	5.7450	1.2	10.0243	3.2	0.4179	3.0	0.93	2250.7	56.8	2437.0	29.8	2597.1	20.1	2597.1	20.1	86.7
Spot 83	138	36640	1.3	5.7322	1.3	11.8530	3.1	0.4930	2.9	0.91	2583.6	60.8	2592.9	29.3	2600.8	21.3	2600.8	21.3	99.3
Spot 29	188	149060	1.8	5.6543	1.0	11.5569	3.5	0.4741	3.4	0.96	2501.7	69.7	2569.2	32.7	2623.6	16.0	2623.6	16.0	95.4
Spot 37	235	89074	1.2	5.6008	1.2	11.7074	3.9	0.4758	3.7	0.95	2508.8	76.2	2581.3	36.1	2639.4	20.1	2639.4	20.1	95.1
Spot 18	89	186925	2.2	5.5431	1.3	12.2545	3.3	0.4929	3.0	0.92	2583.1	64.0	2624.1	30.8	2656.6	21.9	2656.6	21.9	97.2